PHYSIOLOGICAL PARAMETER SENSING WITH WEARABLE DEVICES AND NON-CONTACT DOPPLER RADAR

A THESIS SUBMITTED TO THE GRADUATE DIVISION OF THE UNIVERSITY OF HAWAII AT MANOA IN PARTIAL FULFILLMENT OF THE REQUIREMENTS FOR THE DEGREE OF

MASTER OF SCIENCE

IN

ELECTRICAL ENGINEERING

MAY 2017

By

Alexander G.S.K. Lee

Thesis Committee:
Olga Boric-Lubecke, Chairperson
Victor Lubecke
Aaron Ohta

Keywords: Doppler Radar, Wearable Devices, Vital Sign Sensing

Table of Contents

Abstract

Vital sign measurement with wearable devices is an important need in the paradigm shift occurring with health care. The Internet of things (IoT) is a concept that will allow healthcare providers to keep up to date continuously on the health of their patients through accurate wearable sensors and non-contact sensing in their homes. In order to meet this growing need for robust sensors, there are currently many devices that sense physiological parameters through photo-plethysmography (PPG) and piezoelectric methods. These methods of sensing have their own inherent limitations which include low flexibility, inaccuracy at higher rates, and susceptibility to motion artifact. Elastomeric sensors are another material being explored because of it's potential for higher flexibility than piezoelectric pressure sensors. A wearable elastomeric arm sensor, that was designed and tested on the upper arm of 3 subjects, showed capability of measuring respiratory and heart rate with a low voltage DC power source.

In addition to wearable sensors, there is a need for non-contact sensing in home health monitoring. Previous research with Doppler radar physiological sensing has focused mostly on measuring respiratory rate and displacement accurately. Recent work with radar cross-section (RCS) measurements, have shown that it is possible to determine body position of a subject based on the RCS. A study was done to investigate the dynamic RCS of a human subject during varying respiration depth. Measurement with a retro-reflective infrared camera marker on the sternum of the subject was used as a reference and compared with a 2.4GHz continuous wave Doppler radar system. Results showed that the RCS of a subject facing the radar changed between deep and shallow breathing. A further study with 13 reference markers revealed that there were two main areas, sternum and abdomen, that contributed to the overall dynamic RCS. The implications of this study are important for accurately determining subject position, medical diagnosis, and unique identification with Doppler radar.

Chapter 1. Introduction

1.1 Overview

The respiratory signal of a person includes the rate and depth of breathing. This information can be used to make quick assessments about a person's immediate health status. In sleep studies and hospitals, a chest belt is often used to monitor a person's respiration, but these are obtrusive and can become uncomfortable to wear over time. Currently, there are many wearable fitness devices that use a method called photo---plethysmography (PPG) to sense heart rate when worn on the wrist. Respiration can be also extracted from the PPG signal using principal component analysis (PCA) [1]. In a previous paper [2], it was shown that the PPG signal contains features such as pulse wave variability and pulse amplitude variability, which can be used to determine the respiratory rate. It has also been shown that pulse wave velocity in arteries is significantly affected by respiration [3]. Pulse wave velocity is the velocity of the arterial pulse and can also be used as a measure of arterial stiffness. Increased arterial stiffness can indicate occluded arteries due to plaque or aging and is associated with myocardial infarctions and strokes. A wearable device that could sense these detailed changes from the respiratory signal would be valuable as an early warning system for heart disease and strokes.

In addition to the growing interest in wearable devices, there is also a need for home health monitoring systems that are non---invasive and non---contact. Doppler radar vital sign monitoring is one of the viable options that could be developed to meet this need. In particular, Doppler radar has been shown to be capable of monitoring respiratory and heart rates of stationary human targets. Advantages of using non-contact sensing include being more sanitary and comfortable than the current devices used for monitoring patient vital signs. However, there are also many challenges involved in utilizing this in a healthcare environment, where a robust system is needed. Some issues that are currently being addressed include removing internal and external DC offset [4]-[5], compensating for motion artifact of targets [6,7,8], monitoring multiple targets [9], recognizing body position [10]-[11], and identifying targets based on unique features of baseline vital sign

measurements [12]. This study aims to investigate the dynamic cardiopulmonary radar cross--section changes during varying respiration depth. This could lead to several applications including improving recognition of body position changes, utilization as a feature in unique identification and correlation with physiological parameters in medical diagnosis.

1.2 Contribution

In this study, design of an elastomeric based wearable sensor for the upper arm and method of cardiopulmonary radar cross-section measurement with non-contact Doppler radar is proposed. An elastomeric material will be tested to determine whether a low cost and minimal power wearable device can be used to measure vital signs on the upper arm. To investigate cardiopulmonary radar cross-section changes with Doppler radar during varying respiration depth, an infrared camera marker system will be used to calibrate and investigate the dynamic changes in a human subject's radar cross section while the subject is breathing with varied depth or fidgeting.

1.3 Thesis Organization

This thesis is organized into chapters as follows. Chapter 1 serves as a basic overview, chapter 2 contains a review of the latest literature on the related topics, and chapter 3 focuses on the development of the wearable device for measuring respiration and heart vital signs. Chapter 4 goes over the fundamentals of radar cross-section measurements and Chapter 5 covers the fundamentals of continuous wave radar for physiological monitoring. Chapter 6 contains the development of a method of calibration for improved accuracy in radar cross-section measurement with continuous wave radar on human subjects.

Chapter 2. Literature Review

2.1. Contact Sensing with Textile and Elastomer Based Sensors

A study [13] investigating the design of electro-textiles for elasticity, response time, and other requirements for target applications was done and focused on the production methods in addition to selection of suitable raw materials. [14] found that elasticity could be increased by knitting conductive yarns with elastomeric yarns, but led to a small working sensor range as well as decreased responsivity and reliability over time, due to necessary deformation from repeated usage. Other methods of sensing that can be embedded in textiles [14] include pyroelectric, piezoelectric, piezoresistive, capacitive, and thermistors. These contact based sensing methods have a wide range of applications in healthcare [14] and could eventually be combined to effectively sense many physiological parameters of a subject through sensors embedded in clothing. For example, strain sensors have been used to measure posture of the body and degree of ease of movement of the hand in elderly [14]. Pressure sensors are capable of measuring heart rate from a patch or band on the wrist and respiratory rate from a patch on the front of the nostrils [14]. A pressure based sensor used in a patch or band on the neck has also been shown to capable of measuring jugular venous pulses [14]. A summary of the research done on designing the active materials for piezoelectric, piezoresistive and capacitive strain and pressure sensors is included in [14] with the range and sensitivity for each type of sensor.

An elastomer-based sensor was designed in [15] for measuring respiratory rate and kinetic activity through a chest belt and accelerometer. The material used in [15] was Xilor rubber and had a resistivity of $7 \cdot 10{-}5\ \Omega \cdot \mathrm{m}$ with moderate sensitivity to stress. It was found that the resistivity of the material increased tenfold within a few hours [15] and a study on the compression effects of rubber conductivity was suggested for future work.

2.2. Radar-Based Non Contact Sensing

2.2.1. Non-Contact Physiological Sensing

The Doppler effect has been used in many applications, which include vehicle speed monitoring, storm tracking and physiological parameter sensing. Doppler radar has been shown to be capable of measuring respiratory and heart rate of human subjects [16]. Previous work has been done to increase the accuracy of displacement measurement by increasing gain through introduction of a phase shifter, which works to cancel local oscillator (LO) leakage [4] and also IQ imbalance compensation in direct conversion quadrature radar systems [5]. Recent work in [17] focused on achieving sub-mm displacement accuracy with CW Doppler radar and comparing to an infrared camera marker reference. [18] showed how incorrect radius estimation lead to error propagation in displacement accuracy.

2.2.2. Cardiopulmonary Radar Cross Section Measurements

Ultra-wide band (UWB) experiments have shown that the human body radar cross-section changes with frequency [19]. In addition to this, the human body RCS has been simulated and measured experimentally for a wide range of center frequencies [20]. Characterizing physical changes of a human subject during vital sign monitoring with CW radar has been previously studied in regard to body orientation. By modeling the front of the body as a cylinder and the back as a flat surface, it was found that the RCS was much greater in back of the torso than the front [21]. Measurements of subjects with 2.4GHz CW radar at 2 meters distance from the antenna yielded an RCS of $0.24m^2$ in supine position and $2.15m^2$ in prone position [22].

2.3. Summary

Recent work in physical sensing platforms show a trend towards embedded textile sensors that have elastomeric properties of stretching and flexing [23]. Research into the types of raw materials that yield the optimal dynamic range, response time, and elasticity for pressure and strain sensors is also being done [14]. Successful sensors have been designed by combining conductive and elastomeric yarns together to create a flexible and sensitive physical sensor [13].

Improving accuracy with CW Doppler radar has been focused on in recent research by compensating for IQ imbalance inherent in direct conversion quadrature radar [5] and also cancelling LO leakage [4] to increase gain and signal to noise ratios (SNR). In addition to hardware improvements, there is also signal processing research

that has shown error propagation occurs in displacement accuracy if an incorrect radius is estimated [18].

Radar cross section studies have been done with UWB and CW Doppler radar for the human body in [19]-[22]. In these studies [19]-[22], it was shown that the human body RCS changes with frequency for UWB and also with body position for CW 2.4 GHz Doppler radar. It was noted in [22] that a subject lying in prone position had a decreased respiration depth compared to supine position, due to the nature of the experiment design, but a study on RCS changes caused by varying respiration depth was not investigated.

Chapter 3. Elastomer and Textile Sensor Based Physiological Monitoring

3.1. Introduction to Elastomer and Textile Sensors

Conductive elastomers are elastic polymers designed to conduct electricity and have the properties of a rubber in terms of deformation from physical pressure. The elastomer is made conductive by distributing carbon or other conductive particles throughout the material during the manufacturing process. These conductive elastomers are mainly used as flexible seals and gaskets or as conductive mats to prevent electrostatic damage to electronic devices [24]. The properties of this material lend well towards pressure sensors and as potential transducers for embedded physiological textile sensors. The elasticity of a physical sensor is important since repeated usage can lead to permanent deformation of the material and reduced sensitivity range due to increased resistivity. Current manufacturing capabilities allow designers to control minute details about the raw materials and how they are distributed to optimize for requirements of the target application. For example, some sensors are designed to be sensitive within a medium pressure range and for others, a high pressure range is desired.

3.2. Respiratory Measurement on Upper Arm Principle

During respiration, there are changes in blood volume that occur in the arteries. Upon inspiration, the blood volume in the lungs increases and in the artery of the arm it decreases. On expiration, blood volume in the artery of the arm increases since the volume in the lungs decrease. This effect on pulse measurement in the arm could be used to extract the respiratory rate during normal breathing [25].

3.3. Measurement Design System

A Wheatstone bridge with variable resistors is useful for sensing small changes in resistance. When a resistive element is used to measure displacement of a physiological parameter, the other resistors in the bridge are balanced and the resistance related to displacement can be sensed. For one element sensing configurations, a voltage VCC is placed in series with R1+R4|| R2+R3 resistances. As shown in figure 1., R3 represents the variable resistance that changes with displacement. If the bridge is balanced, the output, Vout, is measured as 0 volts. This balance is achieved by setting the ratio of R1/R2 equal to R4/R3. Once there is a change in the resistance of R3, the output will increase proportionally to the value of x, where R3=Ro(1+x). Ro corresponds to the baseline resistance of the sensing element when the displacement is zero.

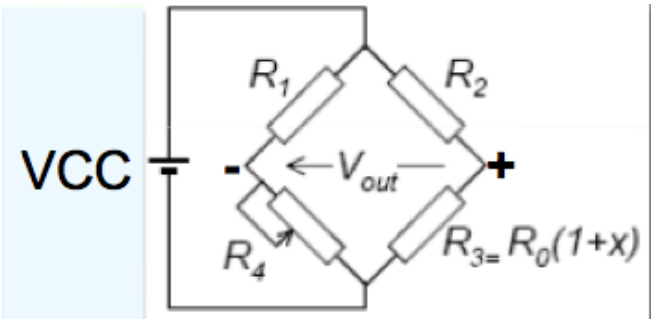

Figure 1. A one element sensing, Wheatstone bridge configuration, with R3 representing the variable resistance changing with displacement.

3.4. Experiment Setup

To determine whether it was possible to obtain the respiration signal from the upper arm, a preliminary experiment was run with an infrared PPG device. An inductive plethysmography chest belt was used synchronously as a reference to verify that the PPG device was accurately measuring respiration. Figure 2 shows that the infrared watch was capable of sensing the respiration signal from the upper left arm.

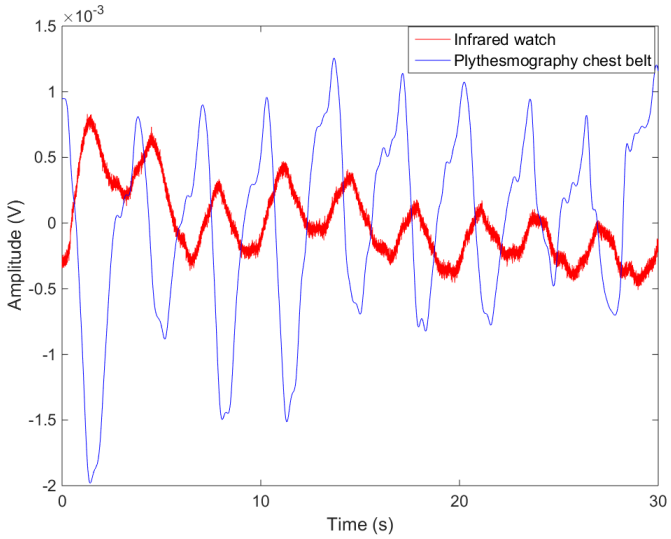

Figure 2. Infrared PPG device on upper left arm compared with inductive plethysmography reference chest belt.

The design for the elastomeric sensor required a DC voltage source, Wheatstone bridge, amplifier, filter, analog to digital converter (ADC), and a program for data acquisition. Figure 3 illustrates the general design of the setup from the sensor to data acquisition.

Figure 3. Block diagram of general setup showing required components, for experiment with elastomeric sensor on upper arm. Note that the resistors used in the Wheatstone

bridge were dependent on the nominal resistance of the elastomeric resistance of the sensor on the human subject's upper arm. Amplification and filtering were done with a low noise amplifier and data acquisition was done with LABVIEW.

Testing on a breadboard design was implemented next with a low noise amplifier (LNA) set to have 1000V/V gain, 0.3-3Hz bandpass filtering, and AC coupling initially. The LNA output was connected to an analog to digital converter (ADC) and sampled at a rate of 1kHz with LABVIEW data acquisition program. An AC voltage source was used first, but it was found that a DC voltage source yielded better measurements. The Wheatstone bridge was designed with potentiometers to adjust for the nominal resistance of the elastomer material, which was dependent on the subject's arm circumference.

3.5. Human Testing Results and Wearable Device Design Fabrication

The first preliminary test with the elastomer sensor, realized with the breadboard circuit, was done in sync with an inductive plethysmography chest belt reference only. From the previous preliminary test with the PPG infrared sensor, it appeared that the heart beat signal was not being measured on the arm. Three human subjects were tested with the elastomer and chest belt for 60 seconds each and the output was sampled at a rate of 1kHz through the LABVIEW data acquisition program. Figure 4 and 5 show the results for subject 1 in the time and frequency domain respectively. Figures 6 and 7 show subject 2 results, while figures 8 and 9 are measurement results for subject 3. These preliminary results from the breadboard testing clearly prove that respiration is capable of being sensed with the elastomeric material on the upper arm. Figure 10 shows the actual setup of the sensors on the human subject.

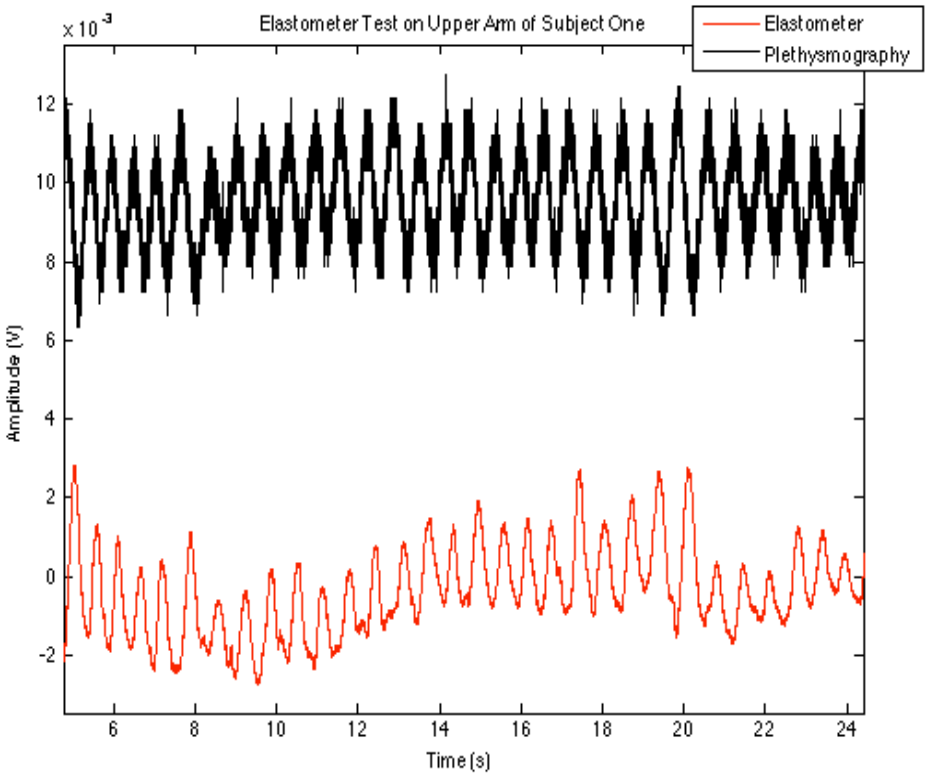

Figure 4. Elastomeric sensor test measurement on upper arm with respiration reference conducted on subject 1.

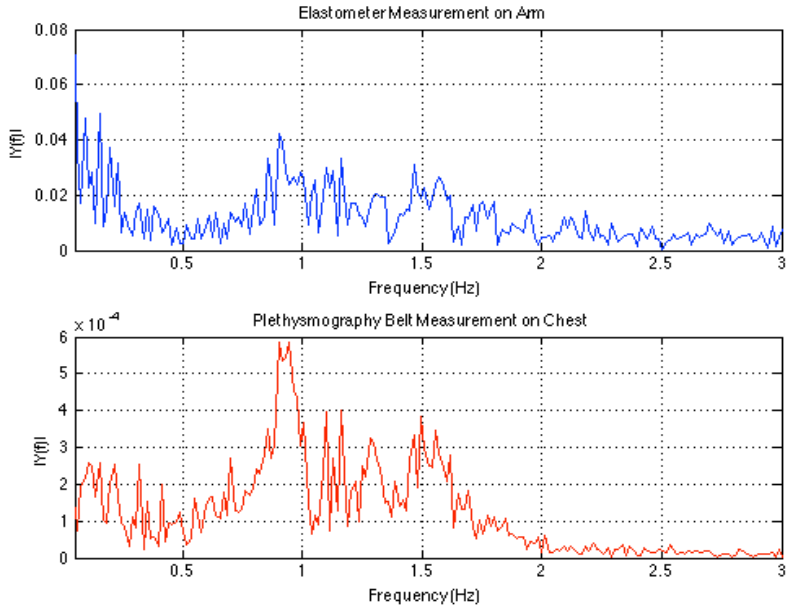

Figure 5. Fast Fourier transform (FFT) of the 60 second test of subject 1 processed in MATLAB. From the time domain plot, the rate appears to be around 1Hz, which corresponds to the FFT plot's results.

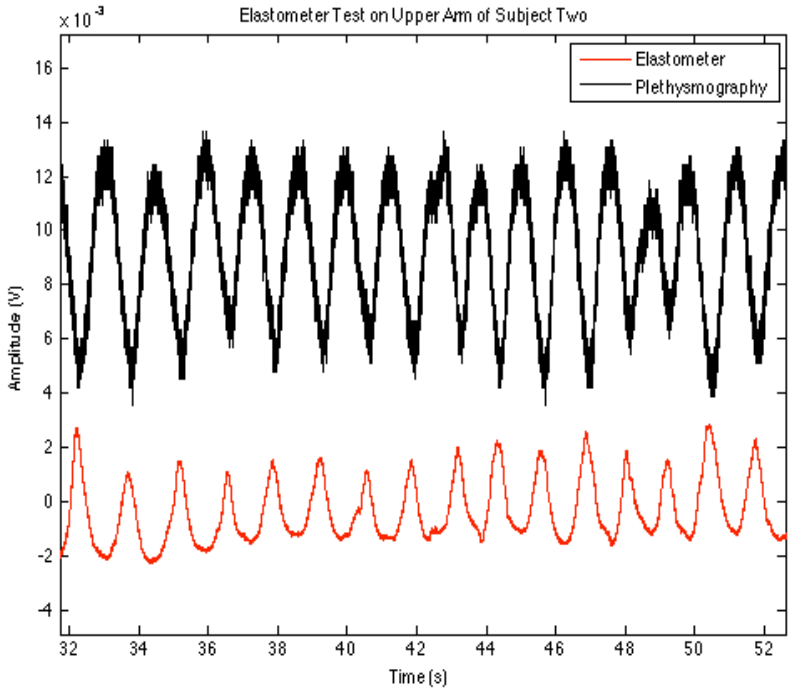

Figure 6. Time domain plot of elastomer sensor test on subject 2 with reference

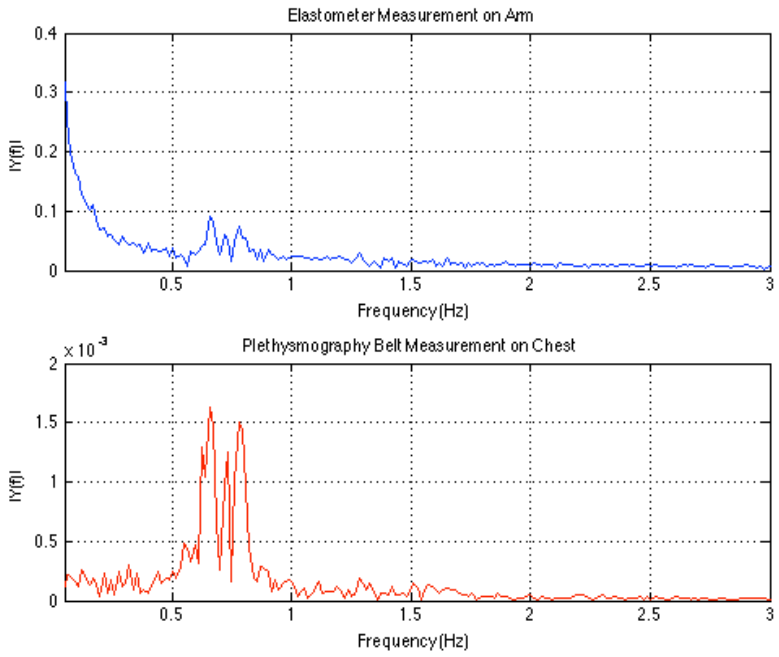

Figure 7. FFT plot of subject 2's 60 second test with elastomer sensor and reference.

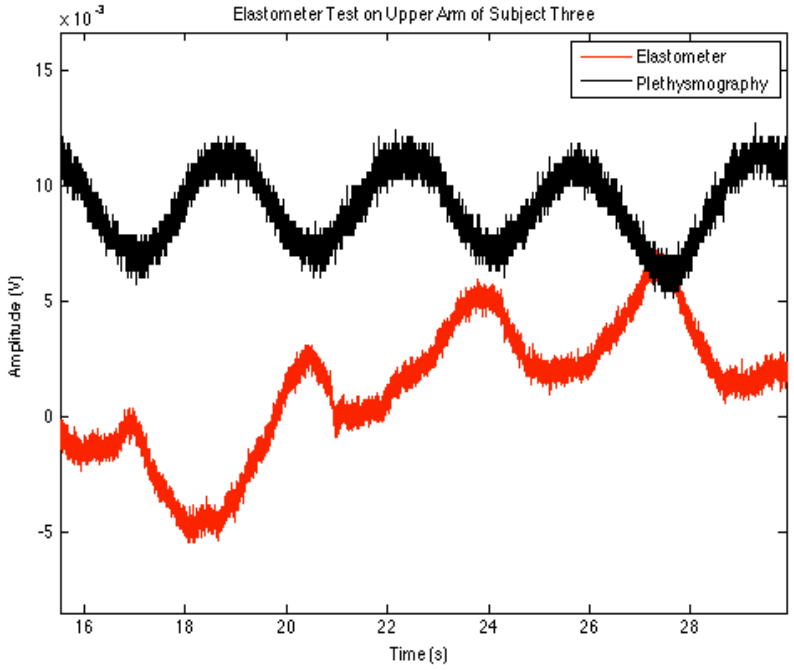

Figure 8. Time domain plot of elastomer sensor test on subject 3 with reference.

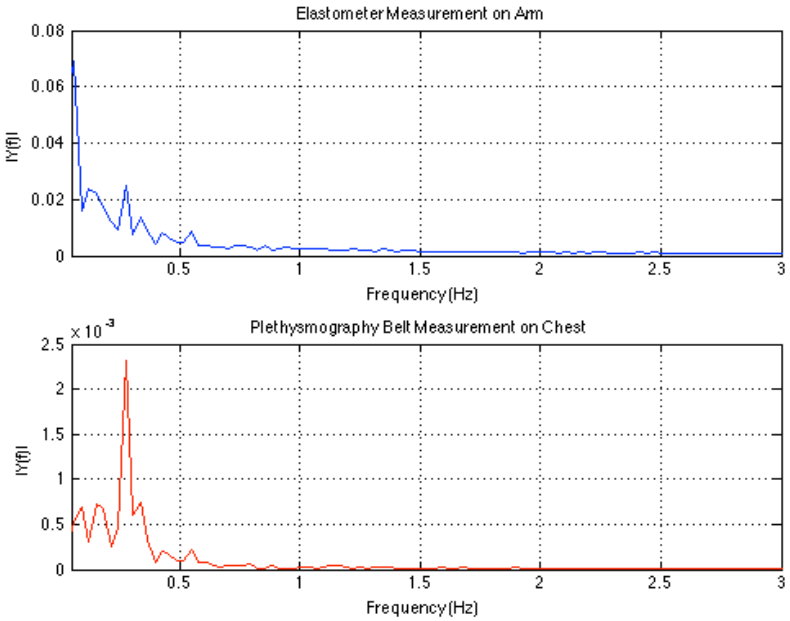

Figure 9. FFT plot of subject 3's elastomer sensor test with reference.

Figure 10. Elastomer sensor on upper arm and inductive plethysmography chest belt reference setup on subject 1.

In order to achieve a small form factor, the DC voltage source and Wheatstone

bridge were realized through a PCB with potentiometers to adjust for variability in testing human subjects. Figure 11 shows the design of the PCB used for testing with human subjects. The fabricated PCB is shown in figure 12 with the parts soldered and ready for testing. Table 1 is a list of the parts ordered and used for the final design of the wearable arm sensor device.

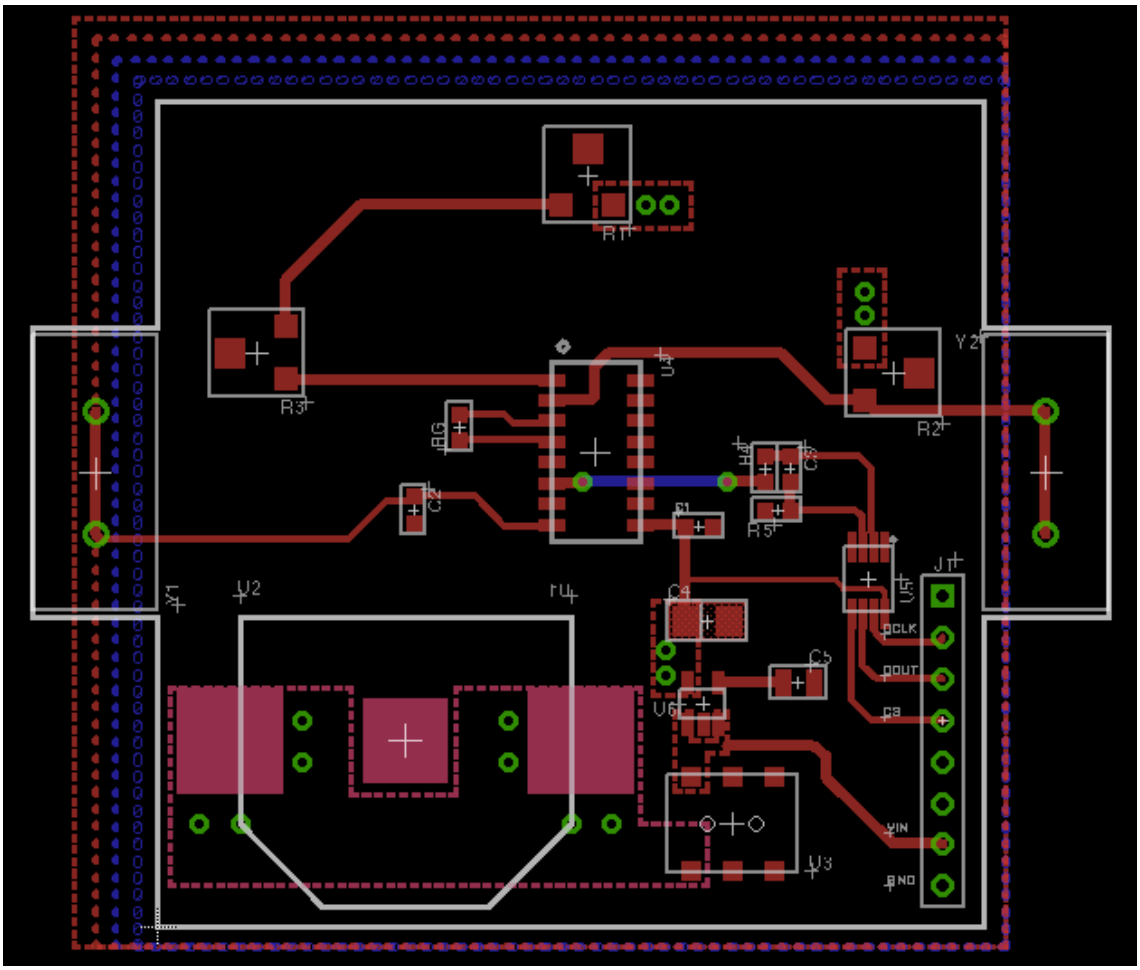

Figure 11. Proposed PCB design of wearable elastomer armband sensor. PCB design includes two 3V DC coin cell batteries, potentiometers for Wheatstone bridge, instrumentation amplifier, on/off switch, and ADC. The output from the PCB goes directly to the data acquisition program on a laptop where it can be recorded. Output of the elastomer sensor signal after being amplified, filtered and converted to digital, is measured from the output pin on J1 part.

Table 1. Parts list for elastomeric wearable armband sensor

Pic	Part #	Manufacturer	Price	Description	Voltage Range	Power Consumption	Capacity
	INA2126	Texas Instruments	$1.91	Micropower Instrumentation Amplifier	±1.35V-±18V		
	277-1317-ND	Phoenix Contact	$0.70	Connection Terminal Block End	N/A	N/A	N/A
	TC33X-2-202E	Bourne Inc.	$0.27	2kΩ Trimmer Potentiometer	N/A	0.1W	N/A
	P189-ND	Panasonic-BSG	$0.28	Battery Lithium 3V Coin 20mm	N/A	N/A	225mAh
	ADS7816	Texas Instruments	$2.29	12 Bit High Speed Micro Power Sampling Analog to Digital Converter	N/A	1.9mW	N/A
	AYZ0202AG RLC	C&K Components	$1.22	Slide Switch DPDT	Contact Current Rating 100mA	Voltage Rating 12VDC	N/A

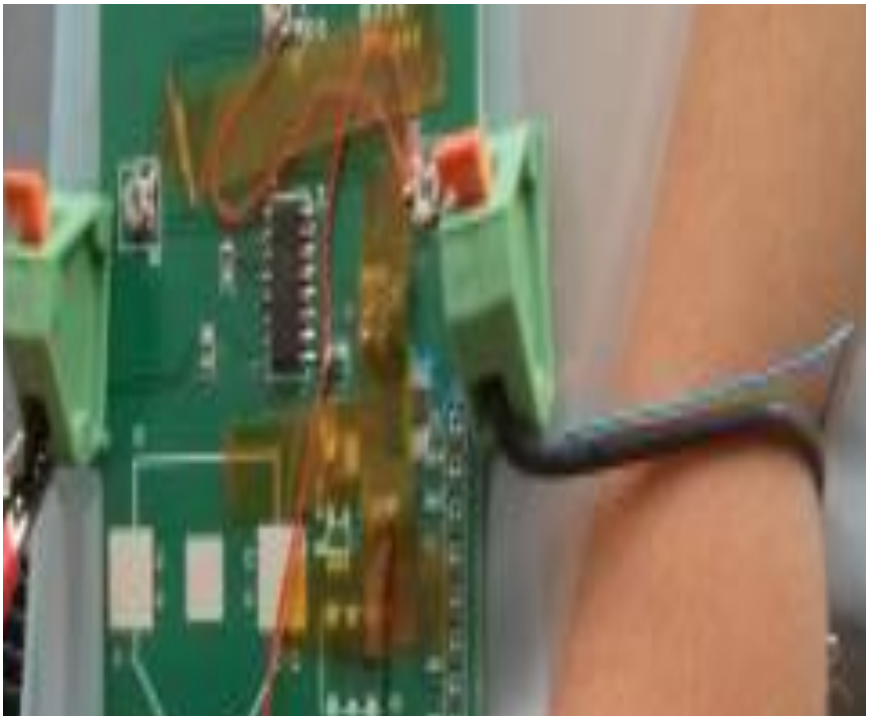

Figure 12. Fabricated PCB with parts soldered and ready for testing on human subjects.

After fabrication of the PCB and assembly of components, the wearable device was tested again with three human subjects on the left upper arm. Piezoelectric finger pulse sensor and inductive plethysmography chest belt were used as heartbeat and respiration references respectively. Figures 13 and 14 are the results for subject one with the time domain plot and FFT.

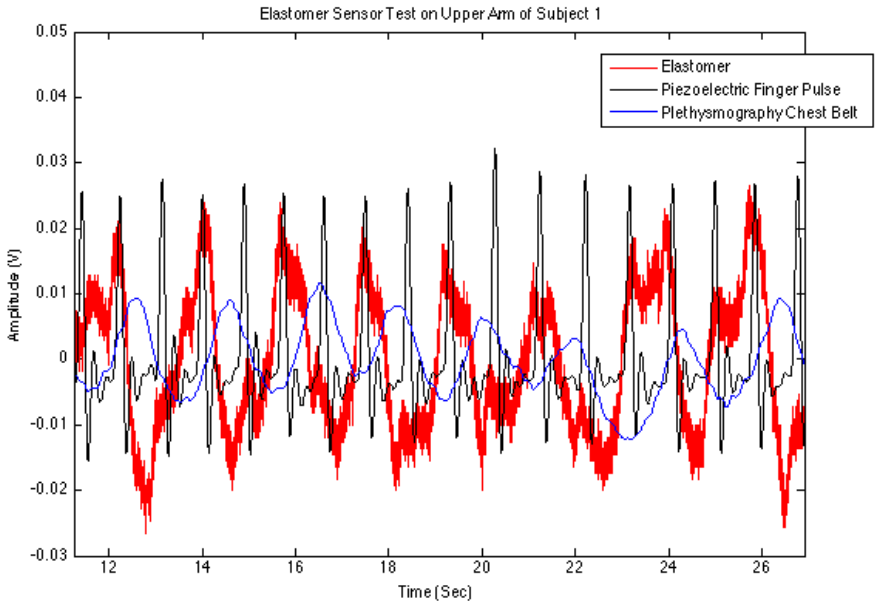

Figure 13. Elastomer sensor test on subject 1 with heartbeat and respiration references.

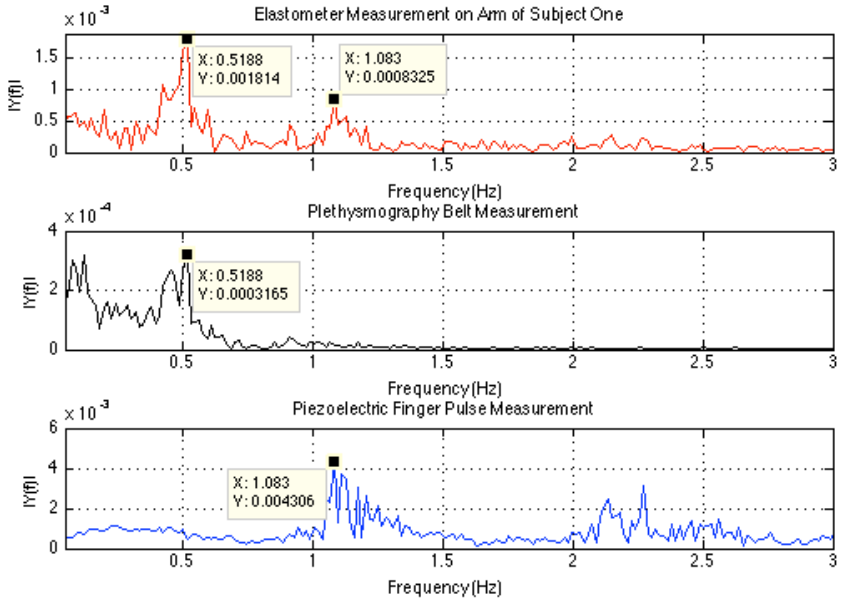

Figure 14. FFT plot of subject 1 testing with references to verify heartrate and respiration were measured with the elastomeric sensor.

Figures 15, 16 and 17 are results for subject 2, while figures 18 and 19 show measurement results for subject 3. Table 2 summarizes testing results with the fabricated

PCB wearable sensor device in comparison with heart rate and respiration references.

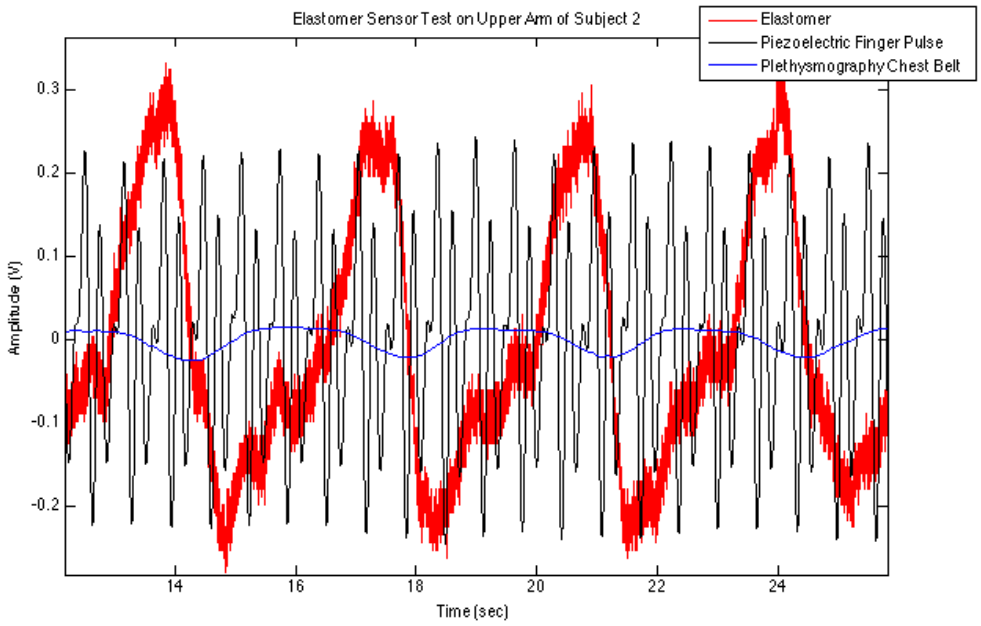

Figure 15. Time domain plot of subject 2's elastomer sensor test with references.

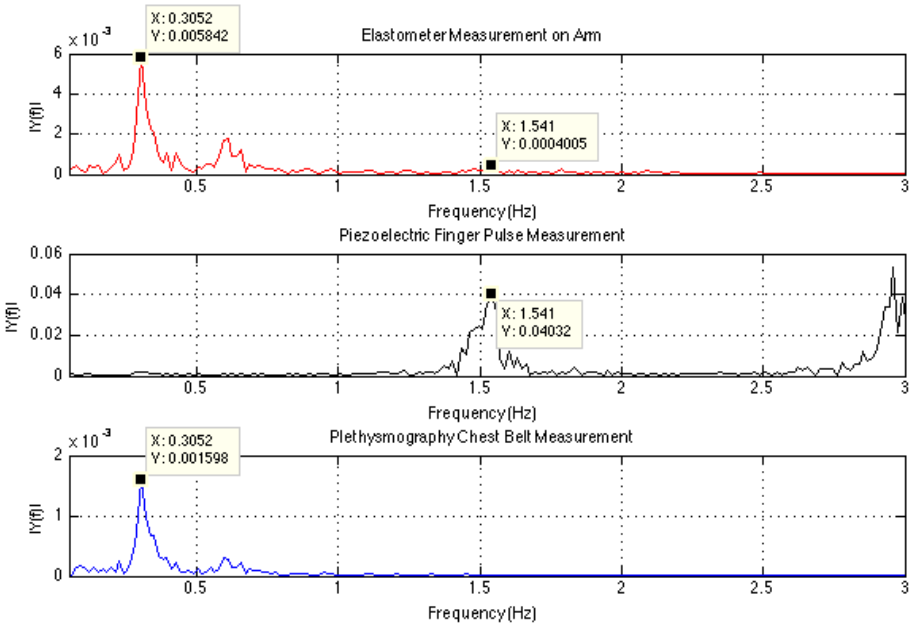

Figure 16. FFT plot of subject 2 testing with references to verify heartrate and respiration were measured with the elastomeric sensor.

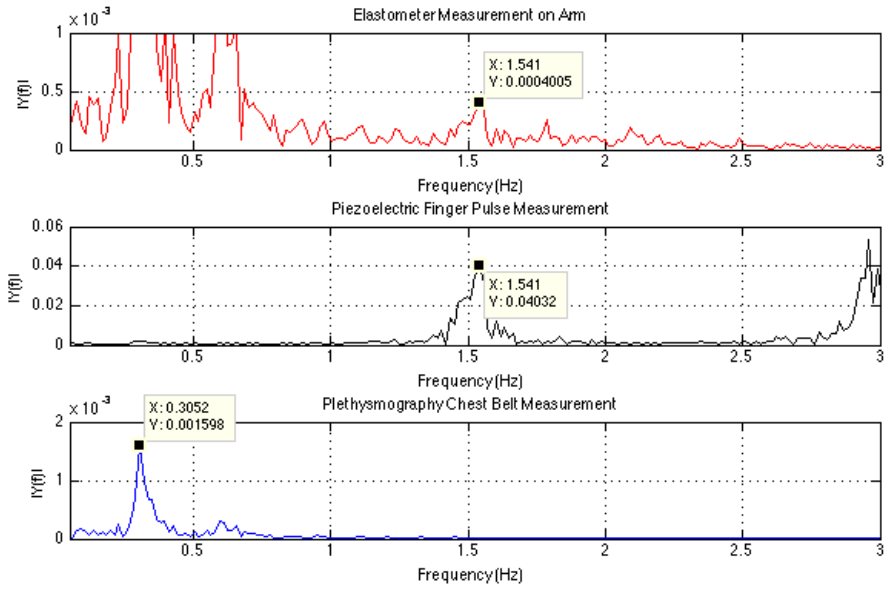

Figure 17. Scaling changed on elastomer sensor FFT plot of subject 2 to verify that heartrate was measured.

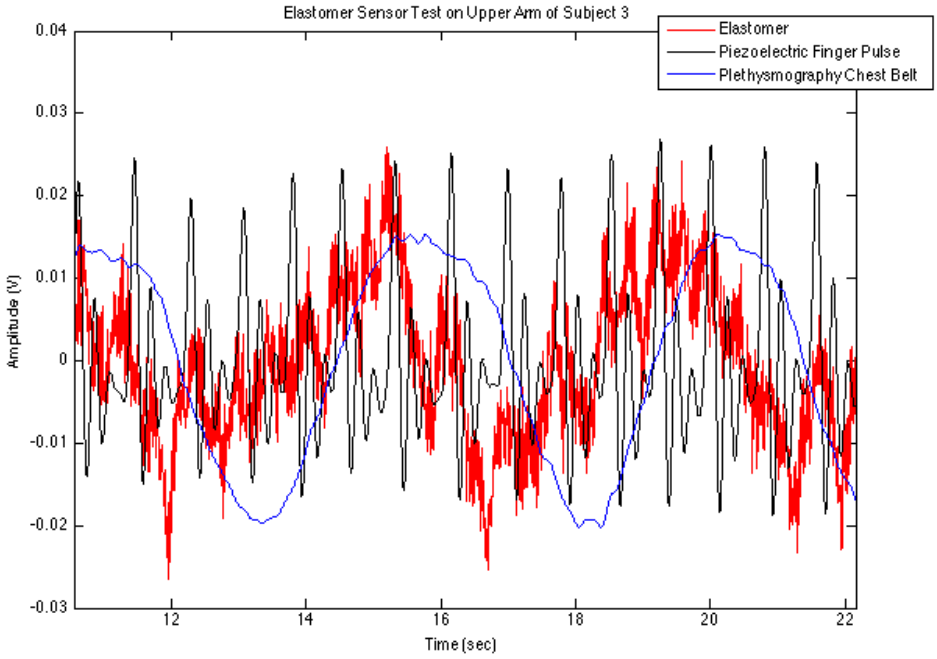

Figure 18. Time domain plot for subject 3's elastomer sensor tests with references.

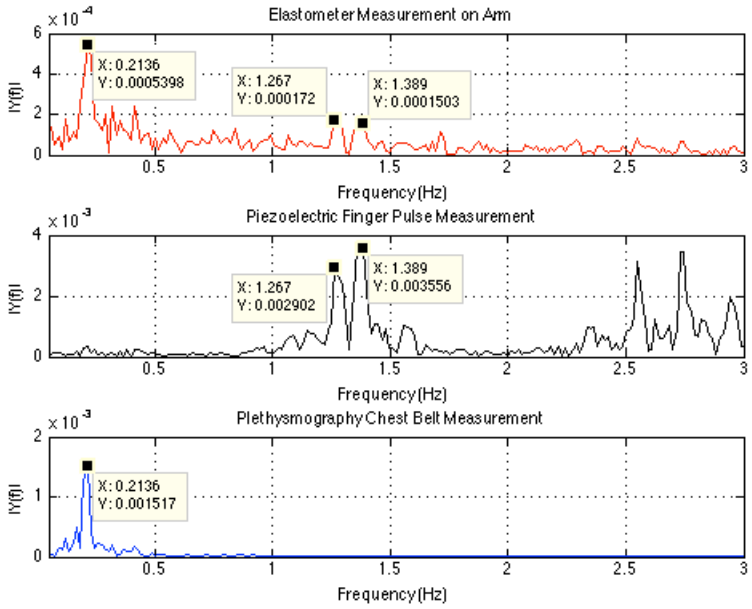

Figure 19. FFT plot of subject 3 testing with references to verify heartrate and respiration were measured with the elastomeric sensor.

Figures 13-19 show that heart and respiration rate were capable of being measured with the fabricated PCB wearable elastomeric sensor. Table 2 is a summary of the results from the testing of the three subjects.

Table 2. Summary of results for testing with fabricated PCB elastomeric sensor

Subject #	Measurement Results	
	Elastomer Measured (Respiration-Top Row, Heartrate-Bottom Row)	Reference (Respiration-Top Row, Heartrate-Bottom Row)
1	0.5188 Hz	0.5188 Hz
	1.083 Hz	1.083 Hz
2	0.3052 Hz	0.3052 Hz
	1.541 Hz	1.541 Hz
3	0.2136 Hz	0.2136 Hz
	1.389 Hz	1.389 Hz

3.6. Summary

Preliminary testing with a PPG infrared sensor on the upper arm showed that respiration could be measured. Further preliminary testing on a breadboard circuit with an elastomeric sensor armband showed that respiration could also be measured through this method of sensing also. After verification of accurate respiration measurement when compared with an inductive plethysmography chest belt, a PCB design for a wearable elastomeric sensor device was proposed and fabricated. Results from testing of three human subjects on the left upper arm revealed that heart and respiratory rate are capable of being measured with the elastomeric sensor device.

Chapter 4. Radar Cross-Section Measurements

4.1. Measurement Overview

The radar cross section (RCS) of an object is defined as the ratio between the power reflected by a target and the incident power density. It is essentially a property of the target's reflectivity. For a rectangular flat plate in the far field region, the effective area used to calculate the RCS, is equal to the physical area of the plate [22]. When measurements are done to measure the movement of the rectangle plate target, all reflected components are in phase and the effective area of the target does not change with movement. For the measurement of human vital signs, the radar cross section cannot be simplified to a rectangular plate where all transmitted power is reflected equally and in phase.

4.2. RCS Measurement of Cardiopulmonary Target

4.2.1. Calibration From Targets with Known RCS

In order to do proper calibration, the IQ imbalance must be determined by measuring with a linear stage target. Since there are phase and amplitude imbalances that are introduced from non-ideal circuit components, compensation must be done to recover the output for arc radius and subsequent displacement estimation. Once the imbalances are known and the radar output can be recovered accurately, measurements must be done with a moving target that has a known RCS. A rectangular flat plate has physical dimensions equal to its effective RCS (Area that reflects the most power) since all transmitted power is reflected in phase with the same amplitude due to total reflection of the metal material. If another type of material is used, some of the power will not reflect and instead transmit through the dielectric depending on the frequency being used. For the human body, it can be approximated that half of the power is reflected due to the dielectric of the torso. If subjects with the same body type are tested, it can be assumed that this approximation will hold. For body types that are outside the norm of testing, proper simulation must be done to determine the difference in dielectric due to fat tissue.

The movement of the human torso during respiration varies from person to person

and also changes with depth. When there is an obstruction in the airway, paradoxical breathing occurs and different parts of the torso move out of phase. Since it is difficult to simulate the cardiopulmonary torso movement, it is often assumed that the movement is similar to a machine target mover instead of the more complicated reality. To simulate paradoxical breathing, two separate targets moving out of phase are commonly used to model the chest and abdomen. These approaches assume that the power reflected from the torso is a constant with the same effective RCS throughout respiration for each segment of the body.

4.2.2. Effective RCS Calculation for Cardiopulmonary Target

To determine the effective RCS for a cardiopulmonary target, it will be necessary to observe the movement of the torso and measure displacement at different points. When a subject changes respiration depth, there is a change in movement and displacement. The effective area that is reflecting power is also changing when depth of respiration varies. In the following chapter, experiments designed to determine the effective area, which contributes to the cardiopulmonary RCS and to the displacement estimation from radar will be described. It has been shown that 2.4GHz CW Doppler radar has higher accuracy for sub-mm measurements on a metal plate mover [17], but in order to apply this finding to human subject monitoring, it should be determined exactly what displacement is being measured on a cardiopulmonary target. It will be investigated how respiration depth variation affects the displacement that is being measured with radar.

4.2.3. Biomechanics of Cardiopulmonary Target Movement

Movement during respiration involves multiple muscles and bones that work together to allow the lungs to inhale or exhale air. There are two ways inhalation can occur and they affect the type of displacement that occurs on the torso. In the first method, inhalation begins when scalene muscles pull the first and second ribs up. These ribs then pull on the successive ribs via intercostal muscles. The ribs move up and out similar to bucket handles, which causes the thoracic cavity to increase in volume. This increase in volume of the thoracic cavity creates a decrease in pressure, which causes air

to be drawn inside the lungs. The second method uses the diaphragm and is known as abdominal breathing. When the diaphragm contracts, it flattens the dome like shape and causes an increase in thoracic cavity volume. This subsequently creates a decrease in pressure of the cavity, which draws air into the lungs. Inhalation can be increased by increasing the movement of the ribs through the scalene muscles or through the movement of the diaphragm. In both methods, however, the volume of the thoracic cavity increases. This volume in the lungs is important for determining tidal volume, which is a valuable parameter for diagnosis in people with respiratory diseases.

4.3. Summary

Previous studies that measured displacement and RCS of human subjects have assumed that the cardiopulmonary movement can be simplified to a two-target (chest and abdomen) plate mover that reflects power uniformly. However, the biomechanics of human subject respiration must be taken into account if more useful parameters such as tidal volume are to be extracted. Even displacement being measured on human subjects is not clear and requires further investigation to determine precisely what displacement the radar based estimation corresponds to in a physical sense.

Chapter 5. Continuous Wave Radar for Physiological Measurement

5.1. Doppler Radar Measurement System

5.1.1. Measurement Principle

Doppler radar measurements are based on the Doppler effect that uses the shift in frequency, which occurs when a signal is reflected from a moving object. The frequency shift of the reflected signal can be used to determine the speed of moving object. For the purposes of cardiopulmonary movement measurement, the parameter of interest is displacement, which can be used to extract the rate and depth of respiration. Since the frequency of the transmitter is known, the frequency that is reflected by the chest to the receiver can be compared and used to determine the speed and subsequently the displacement.

5.1.2. Doppler Radar Fundamentals

For continuous wave narrowband radar, a single frequency is transmitted continuously over time. The frequency that is used will determine the wavelength, which must be much larger than the displacement being measured. When a single receiver system design is used, there is a problem with decreased sensitivity due to null points. The quadrature receiver design overcomes the null point issue by splitting the transmitted signal into components that are offset by 90 degrees from each other. These components are known as the in-phase and quadrature components (I and Q respectively). At the receiver, the components are mixed with the input RF signal and filtered with a high pass filter to yield the baseband signals of each component. From these baseband components, the radar output can be plotted on the complex plane where I corresponds to the real axis and Q represents the imaginary axis. When the Doppler radar is used to monitor a human subject, the sinusoidal displacement movement of the chest draws an arc on the IQ complex plot. The position of the arc on the plot is related to the total constant phase, φ_{tot}, which determines which component is in a null or optimum point. When a component is at the optimum point, the sensitivity of measurement will be greatest. The advantage of the quadrature receiver design over a single receiver lies in

the ability to still recover the signal of interest regardless of target range when the wavelength is much larger than the displacement being measured.

5.1.3. Displacement Estimation using Circle Fitting Algorithms on Radar Data

When the displacement of the human respiratory motion is measured with a quadrature Doppler radar system, there is an arc drawn on the IQ complex plot, whose length is correlated to the displacement of the torso. For shallow breathing, where displacement is in the order of a few millimeters, the shorter arc length makes it difficult to estimate the circle that fits to that arc. [Reference] compares the best performing center estimation algorithms, which are needed to accurately estimate radius and displacement from the arc transcribed on the IQ plot.

5.1.4. Summary

Accurate displacement estimation with radar is dependent on correctly estimating the radius of the arc drawn on the IQ plot during measurement of respiratory motion. Prior to human testing, IQ imbalance calculation must be done by testing a flat rectangular plate in order to determine the amount of amplitude and phase imbalance inherent in the non ideal circuit components of the radar system. Before IQ imbalance is done, a phase shifter can be used to maximally increase the gain of the LNA as described in [Reference]. This is done to increase the signal to noise ratio (SNR) and allow accurate measurement of the subject. Arc tangent demodulation is the preferred method for vital sign measurement with radar because

5.2. Doppler Radar RCS Measurements and Improved Physiological Displacement Estimation

5.2.1. 1 IR Marker Reference Tested with Radar

An infrared (IR) camera marker was placed on the sternum of a subject seated 2 meters away from the radar transceiver. The LNA gain was increased to 200 V/V with the phase shifter added as shown in figure x. A 10Hz low pass filter (LPF) and DC coupling were used to further obtain a clean vital sign measurement. The IR camera was synced with the radar through a third channel on the ADC. The power and frequency of

the transmitter were 10dBm and 2.4GHz respectively. Subjects were tested for deep and shallow breathing in 30 second time segments. To maintain consistency, the subject was asked to breath deeply for 30 seconds and then shallow for 30 seconds after that. This was done to pair up each set of deep/shallow breathing tests and minimize motion artifact between measurements.

5.2.2. Measurement Results and Discussion for 1 IR Marker Experiment

Signal processing, radius and displacement estimation of radar were calculated with arc tangent demodulation and a circle fitting algorithm. The IR marker data was first synced to the radar by comparing the overall signal for the three channels on the ADC as shown in figure 20. After the correct time stamp was found to sync the radar and camera data, the marker data was plotted to see the physical path of displacement as seen in figure 21.

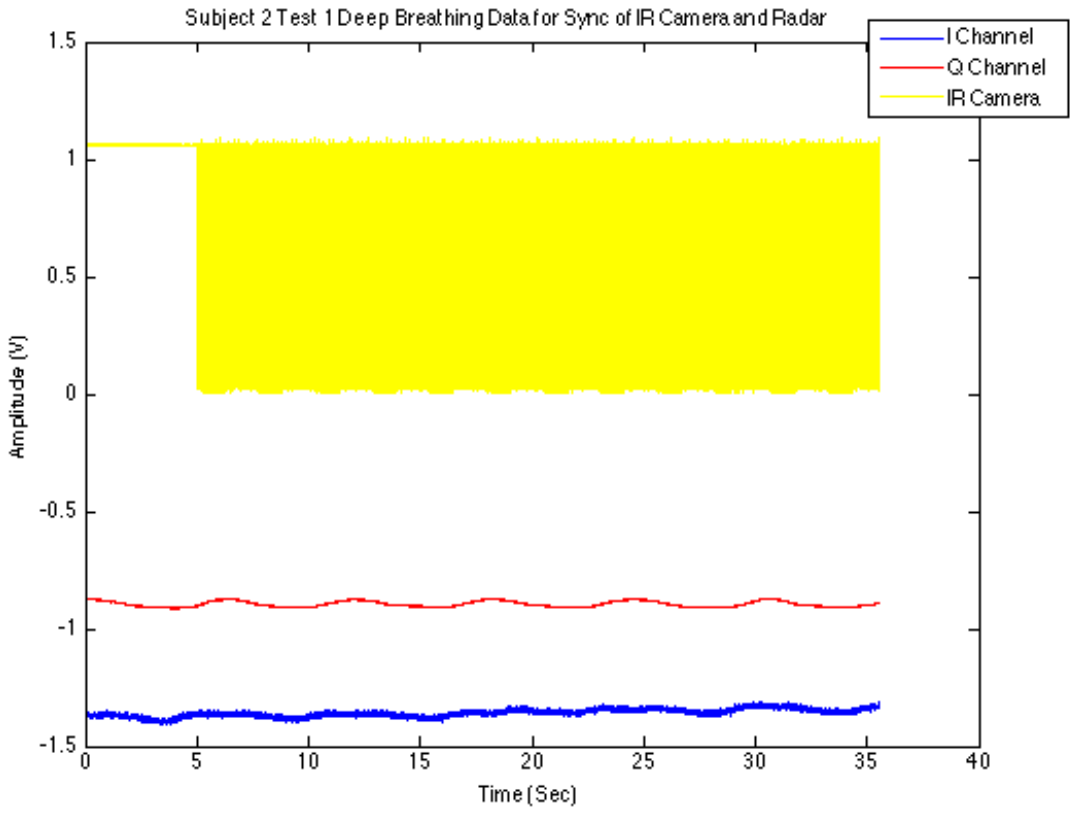

Figure 20. IR camera starts recording when signal drops to 0V for the first time. Data from radar is used from the same point in time that IR camera started recording. Note that radar was sampled at rate of 1kHz with LABVIEW data acquisition.

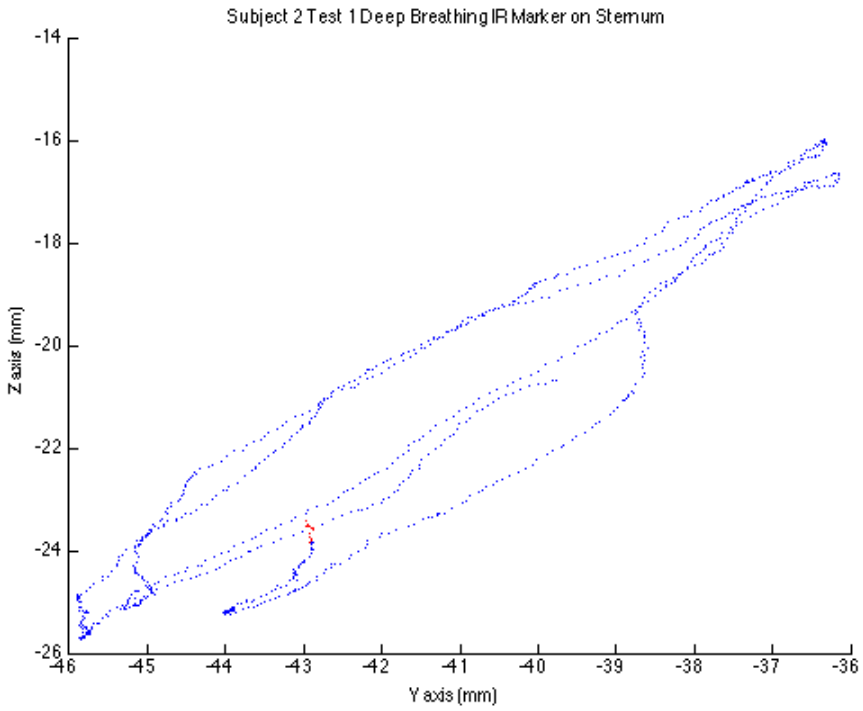

Figure 21. Start of recording marked by the red plotted points. Y-axis is perpendicular to radar and Z-axis is the vertical axis.

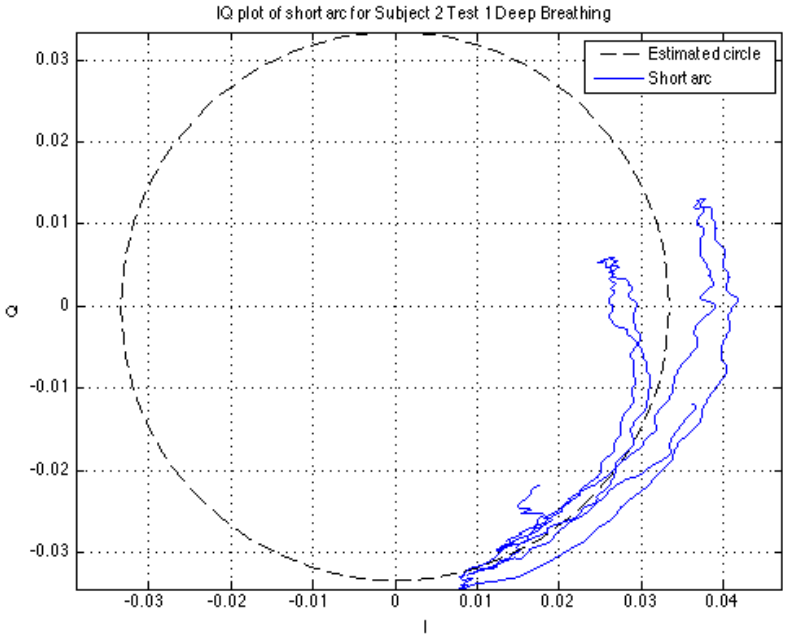

Figure 22. IQ plot of subject 2's deep breathing radar data synced with IR reference. Note that the circle-fitting algorithm is estimating the radius off of the average of the entire test time. Based on this test, the radius of the circle was estimated to be 0.0334 and average displacement estimated at 15.3 mm. For the 2.4 GHz frequency, the entire circle in the IQ plot corresponds to 62.5 mm. The arc drawn on the IQ plot for subject 2's first deep breathing test is 24% of the entire circle estimated by the algorithm and the displacement estimated matches the ratio for the frequency used.

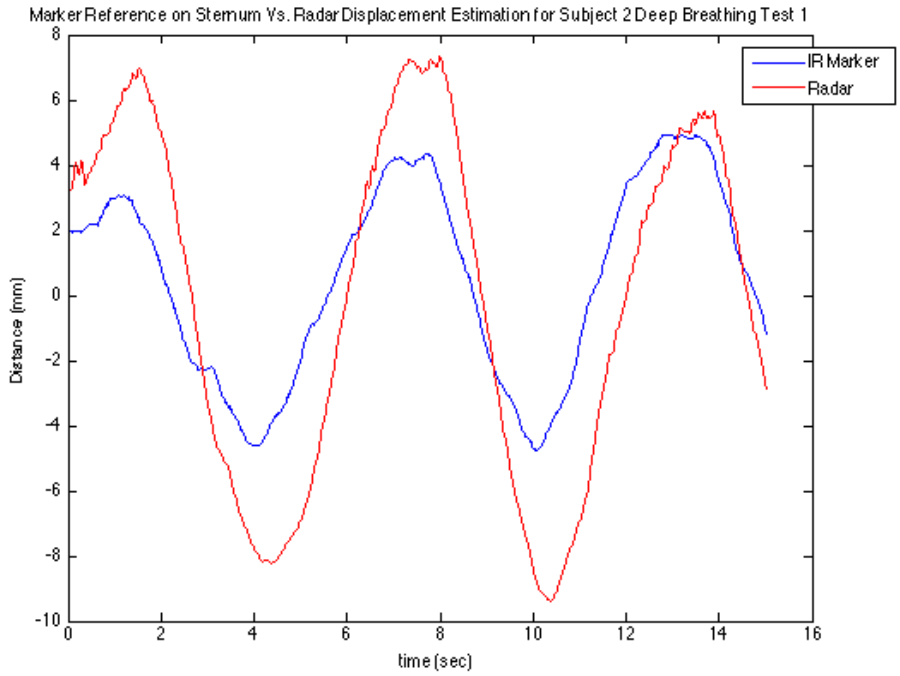

Figure 23. Comparison of displacement measured from IR marker on sternum with displacement estimated from radar output. Radar displacement estimate is based on overall signal average radius.

The main focus of these tests with one IR marker and radar was to investigate the difference in radius and RCS when respiration depth is varied. In order to compare the RCS of human subjects for deep and shallow breathing, it is necessary to confirm that the radius being estimated by the circle-fitting algorithm on the radar data is accurate. Due to inherent noise from motion artifact of subjects and other factors, it was not possible to use all of the experiment data. One pair of deep and shallow breathing tests was compared for each of the two subjects and the radii were used to calculate the RCS. Figure 24 is the IR camera plot for subject 2's shallow breathing test. The corresponding IQ plot for subject 2 is shown in figure 25 and radius was estimated to be 0.0223. Figure 28 compares the circles estimated for subject 2's deep and shallow breathing tests based on radar data only (not segmented, overall average was used to estimate circle).

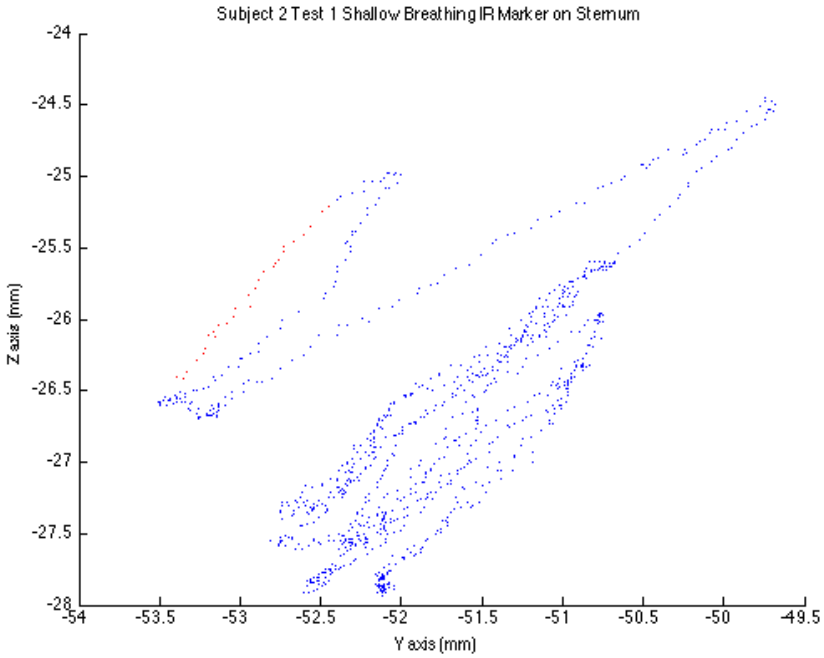

Figure 24. Subject 2 Test 1 IR marker on sternum for shallow breathing. Note that red plot points mark the beginning of test recording.

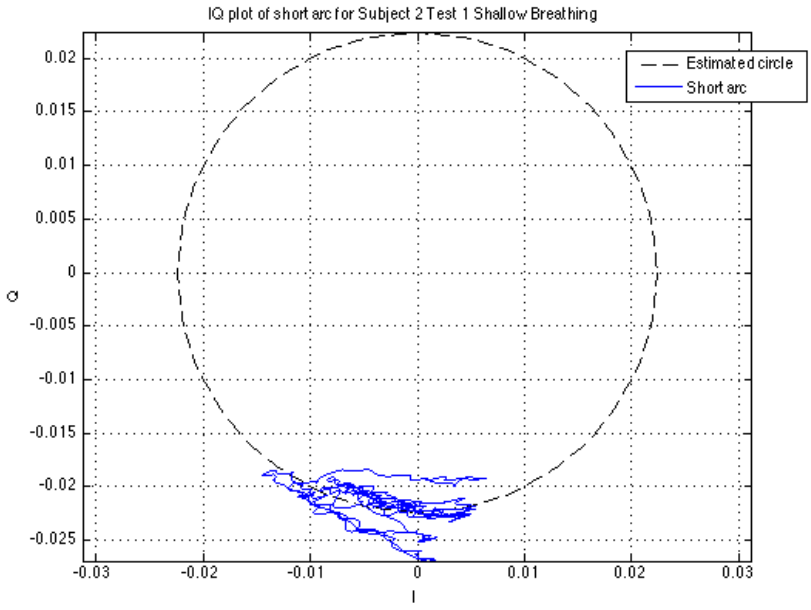

Figure 25. IQ plot for Subject 2 Test 1 Shallow breathing radar data. Radius was estimated to be 0.0223 and displacement estimated at 5.1mm. Based on 2.4GHz frequency, the arc should be approximately 8% of the entire circle estimated by the algorithm.

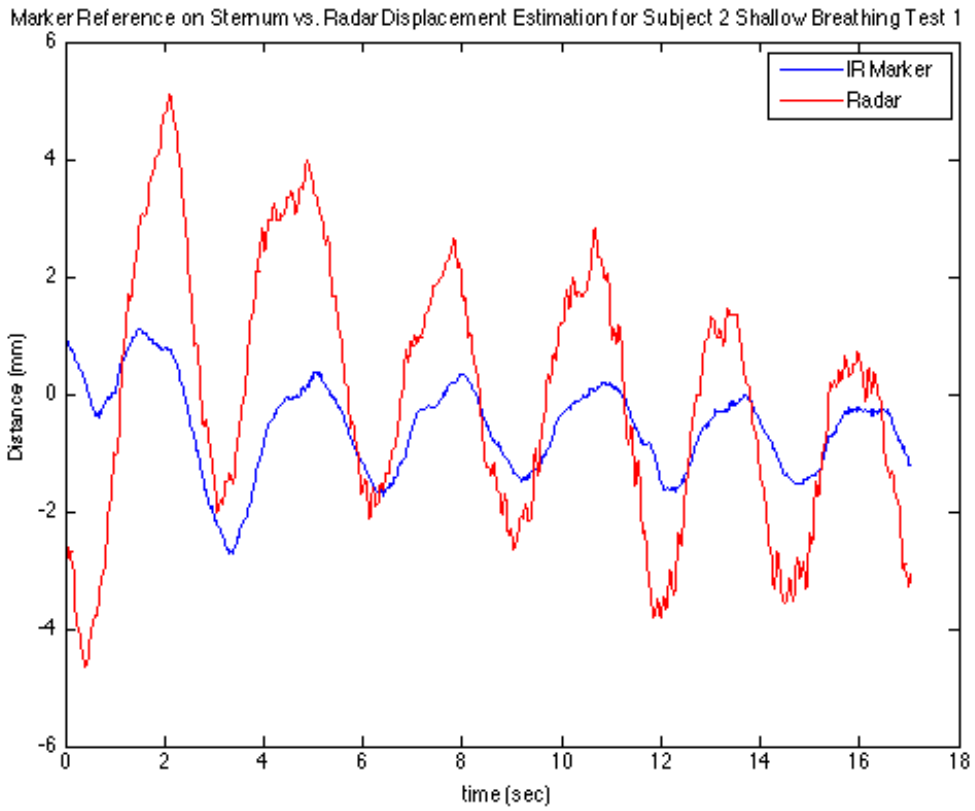

Figure 26. Comparison of displacement estimated by radar and IR marker reference on sternum of subject 2 for shallow breathing test 1. Displacement estimated by radar is approximately twice as large as the displacement measured by the IR marker reference on the subject's sternum.

The angle of the marker displacement on the sternum was seen to be changing during shallow breathing tests. This is also a factor that could affect radar measurements if the subject is not aligned with the antenna (e.g. at a different height).

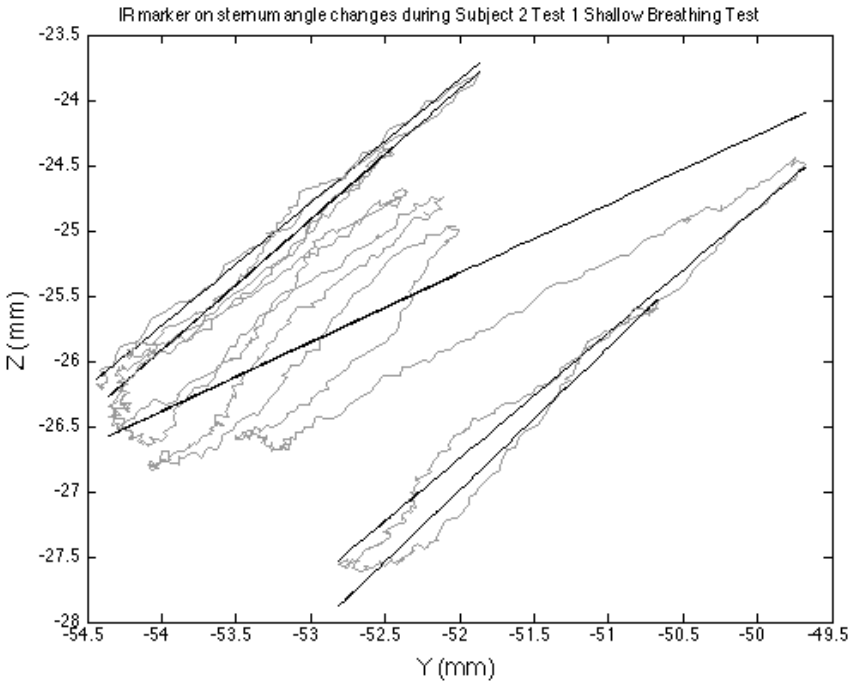

Figure 27. Plot showing that angle of the displacement tracked by IR marker on the sternum changes even during shallow breathing.

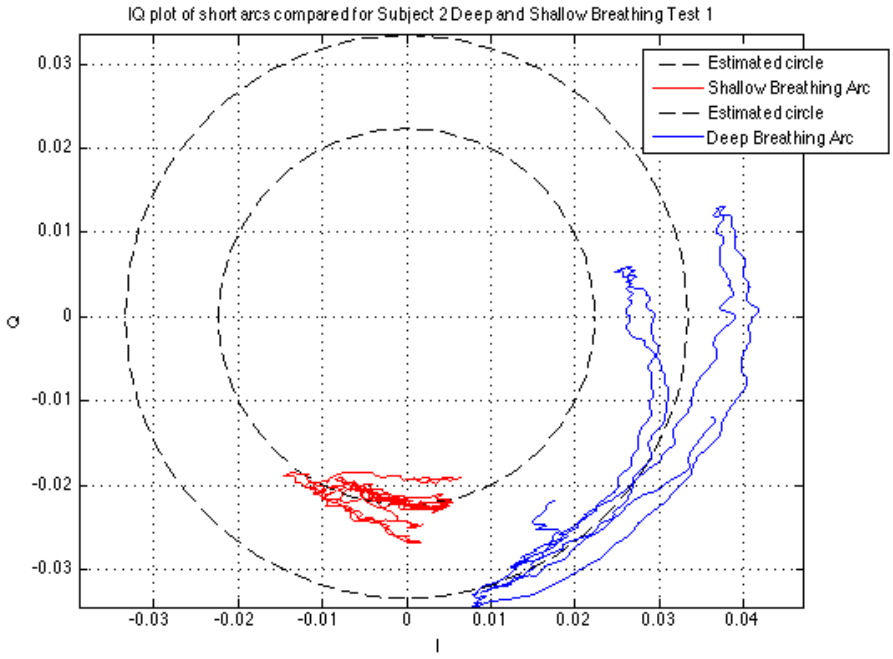

Figure 28. IQ plot comparing the circles estimated for deep and shallow breathing tests on subject 2. Radii for deep and shallow breathing tests were estimated to be 0.0334 and

0.0223 respectively. Ratio of arc to estimated circles based on circle fitting and displacement match the corresponding 2.4GHz frequency used for testing.

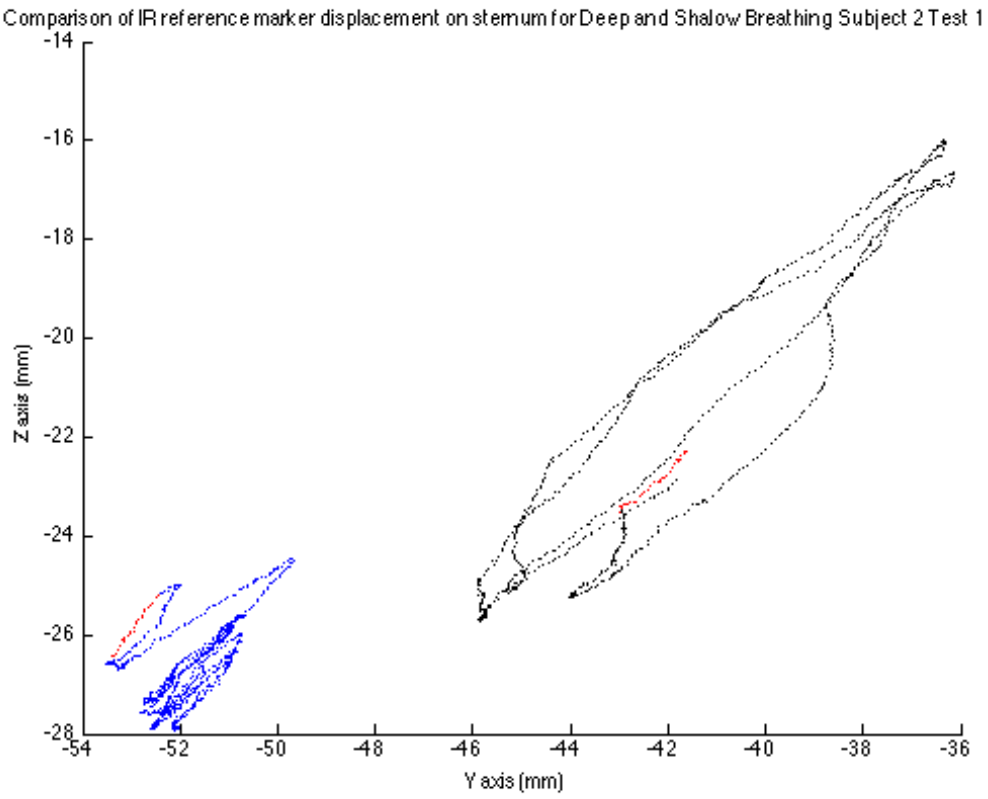

Figure 29. IR marker reference comparison for deep breathing (black) and shallow breathing (blue) with marker on sternum of subject 2. Red plot points for mark the start of marker camera recording for each test.

In figure 26, it can be seen that the radar displacement estimation is nearly twice the displacement measured with the IR marker on the subject's sternum. Based on this result, it was theorized that the sternum is not be the only contribution to the displacement that the radar measures. In addition, the radar displacement was based on the overall signal average radius and the radius could be more accurately calculated if the radar output was segmented into breathing cycles. Figure 27 shows that the IR marker did not follow the same trajectory for the entire test time. This deviation from linear

motion due to normal human breathing mechanics could affect the radius that is being calculated.

The radar cross section is directly related to the radius estimated and can be calculated by first finding the constant gain value (R) with a known target. A rectangular flat metal plate with dimensions 20cm by 15cm was used to do calibration. With input power of 10dBm, range of 2 meters (200cm), and LNA gain (G_{LNA}) of 200 V/V, the constant gain value was calculated from **(1)**. Figure 30 shows the circle estimated after IQ imbalance compensation. The effective radar cross section (σ_{cal}) of the known target is calculated using the effective area, which is equal to the physical area since the rectangular flat metal plate was used.

$$\Re = \frac{R^4}{\sigma_{cal}} \cdot \frac{1}{P_{in}} \left(\frac{A}{G_{LNA}} \right)^2 \quad \textbf{(1)}$$

The radius (A) estimated with the calibration target moving with displacement of 40mm was 0.0856. Based on these parameters, the constant gain value was calculated to be [$0.000405\Omega m^2$]. Since the range of the target was in the far field ($R>>\lambda$), the effective RCS was calculated with **(2)** to do calibration.

$$\sigma = \frac{4\pi \cdot A_{ph}^{\ 2}}{\lambda^2} \quad \textbf{(2)}$$

$$\sigma_{eff} = \frac{R^4}{\Re} \cdot \frac{IL_{add}}{P_{in}} \left(\frac{A}{G_{LNA}} \right)^2 \quad \textbf{(3)}$$

To calculate the effective RCS of human subjects, **(3)** was used, where IL_{add} was set to 1, P_{in} set to 10dBm, G_{LNA}=200V/V, R=2 meters, and *A* is replaced with the radius estimated by the circle fitting algorithm for each test.

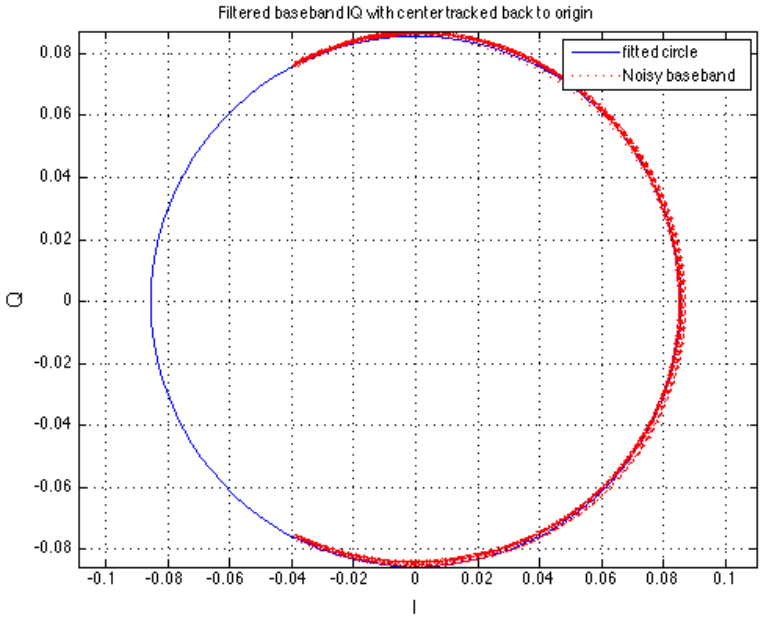

Figure 30. Fitted circle for calibration target measured at range of 2 meters and with displacement of 40mm. Plot shows estimated radius of 0.0856 after filtering and IQ imbalance (amplitude imbalance measured to be 1.0186 and phase imbalance measured to be -16.3223). IQ imbalance measurements were done with the same experiment setup and directly before human subject testing for deep and shallow breathing.

After calibration with the rectangular flat plate, the constant gain factor of [0.000405 Ωm^2] was used to calculate all future RCS measurements with human subjects (where R=2 meters, G_{LNA}=200V/V, P_{in}=10dBm, etc). For subject 2's first deep and shallow breathing tests, the RCS values calculated from the estimated radii were 0.11 and 0.049 respectively. These RCS values were based on the radius estimated by the average of the arcs that were drawn on the IQ plot over multiple breathing cycles. Using the IR marker reference data for the displacement of the sternum, a corrected radius was calculated with (4), in order to determine a more accurate RCS associated with the sternum area.

$$R_1^2 = R_2^2 \frac{\left(\frac{1}{\tan^2(\frac{2\pi D_1}{\lambda})}\right)+1}{\left(\frac{1}{\tan^2(\frac{2\pi D_2}{\lambda})}\right)+1} \quad (4)$$

Utilizing the relationship between the estimated radius of the arc (R_2) and displacement from radar data (D_1) with the displacement from the IR marker (D_2) on the sternum, a calibrated radius for the sternum area (R_1) was calculated. For subject 2's first deep and shallow breathing tests, the calibrated sternum marker radius was determined to be 0.0017 for shallow and 0.0132 for deep breathing. It is important to note that these corrected radii and the resulting RCS measurements for different respiration depth are only based on a small area (sternum marker) of the entire cardiopulmonary target.

5.2.3. 13 IR Marker Experiment Setup

Using the same experiment setup as the 1 marker experiment, a 13 IR marker configuration was tested with two concentric circles of IR markers around the original sternum IR marker reference. One human subject was tested while seated 2 meters from the radar with 10dBm power, 200 V/V gain, and 10Hz LPF. The 13 IR marker configuration is shown in figure 31 below.

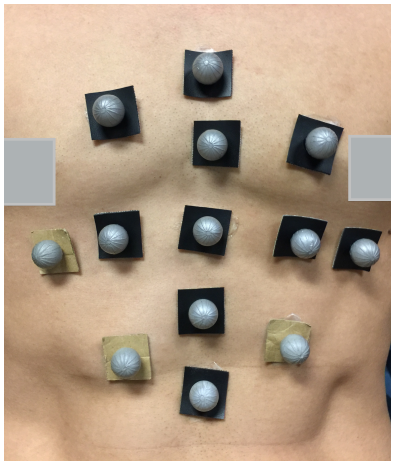

Figure 31. 13 IR marker reference configuration used for testing with one of subjects from the first experiment with 1 IR marker on sternum.

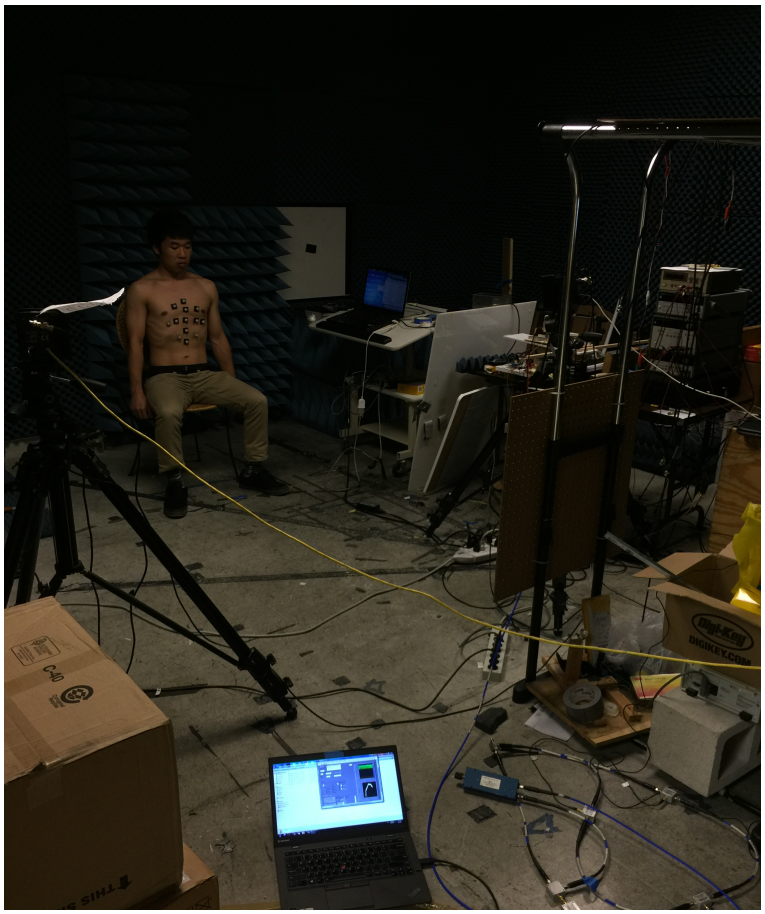

Figure 32. Experiment setup with subject seated 2 meters from radar transceiver with 13 marker configuration. Note that the same setup was used for the 1 marker tests with same range of subject to the radar.

In order to do accurate circle fitting for the radar data, IQ imbalance compensation needed to be performed again to measure amplitude and phase imbalances. A rectangular flat plate with dimensions of 20cm by 15cm was tested again and the amplitude imbalance was measured to be 1.06113 and phase imbalance measured at -12.26839. Figure 33 below shows the circle fitted for the 40mm displacement of the rectangular flat plate target.

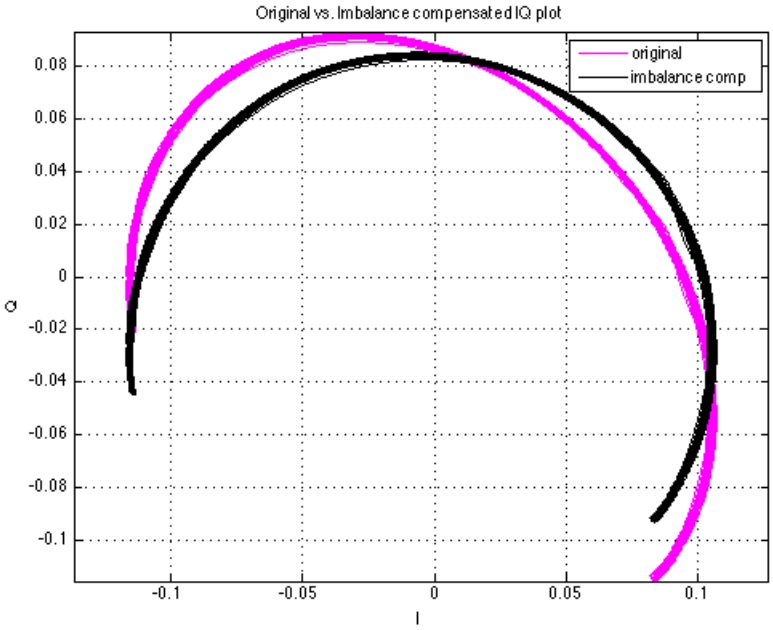

Figure 33. IQ imbalance compensation for rectangular flat plate with 40mm displacement at a 2 meter range from radar. Amplitude imbalance was 1.06113 and phase imbalance was -12.26839.

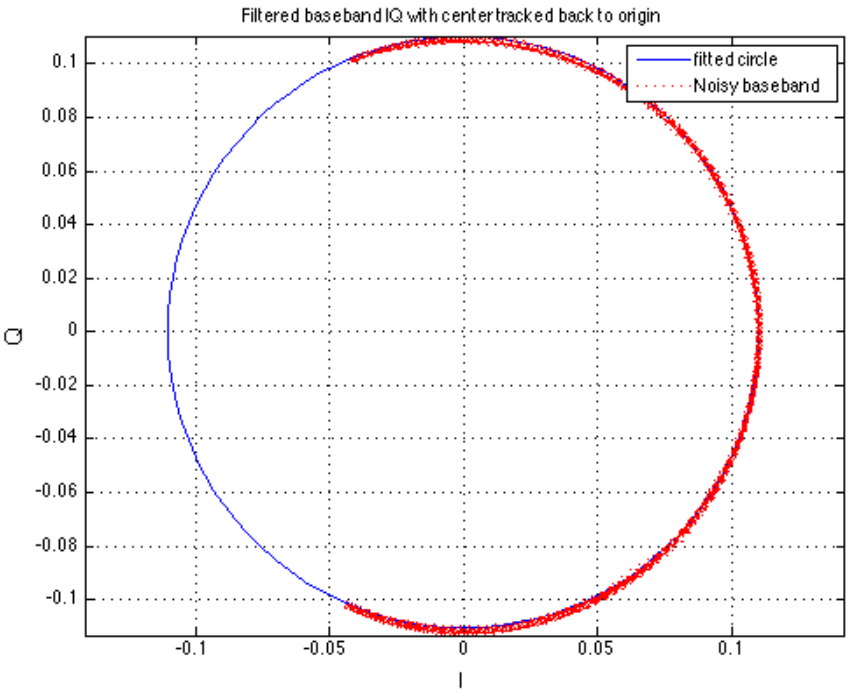

Figure 34. Circle fitted for IQ imbalance compensated radar data taken before 13 IR marker reference and radar tests.

5.2.4. 13 IR Marker Measurement Results and Discussion

After IQ imbalance compensation was done with the 40mm displacement tests of the rectangular flat plate, the human subject with 13 IR markers was tested. Figure 35 shows the 13 markers plotted in the X-Z plane of the subject over the 60 second period.

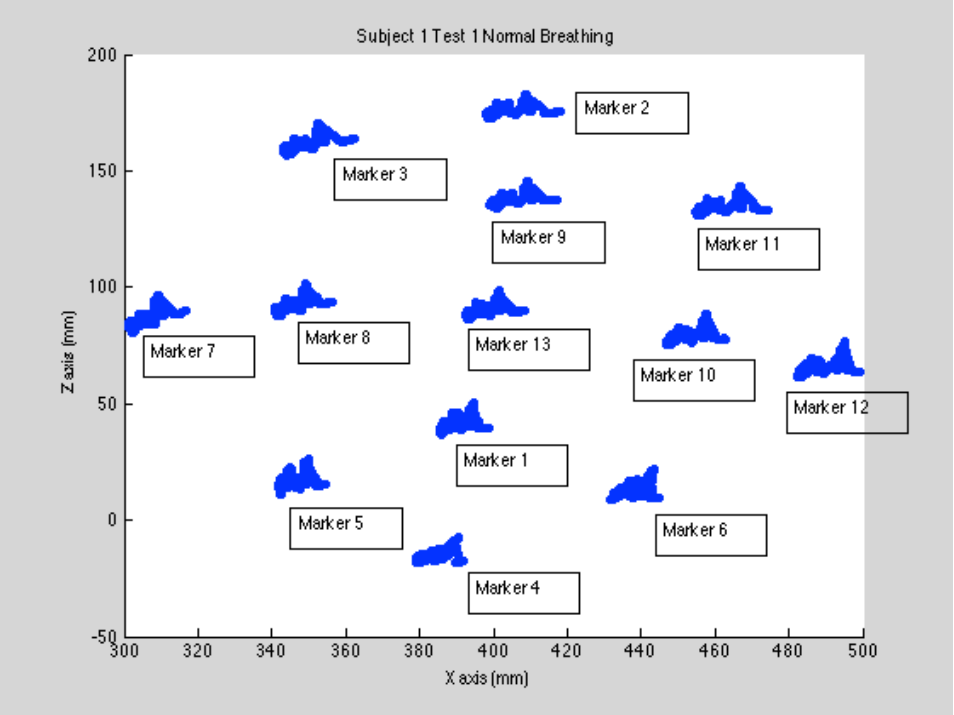

Figure 35. X-Z plane showing minimal movement in the X and Z axis directions for shallow/normal breathing. Marker numbers in the plot are used to match with subsequent displacement plots since the IR camera records data in the order that the markers are recognized. Each of the following tests will include documentation as seen in this figure for each test to match the markers with their corresponding displacement in the Y axis.

The procedure of syncing the radar with the IR marker reference data was followed as in the 1 IR marker tests. Once the data was synced, the displacement was plotted for each of the 13 markers as shown in figure 36.

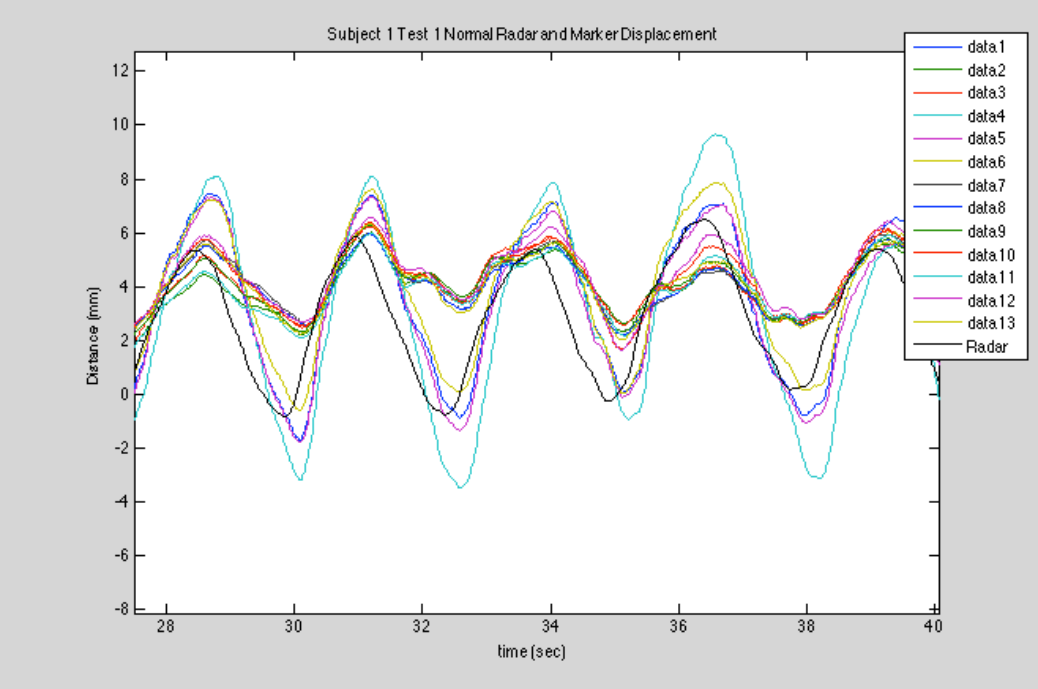

Figure 36. 13 IR markers plotted for subject's first test of shallow/normal breathing and compared to average radar estimate displacement (shown in black). Each data color in the legend corresponds to the marker number in figure 35 (e.g. data 1 is marker 1, data 2 is marker 2, etc.).

To simplify the processing of data from the markers, two of the markers with the greatest displacement difference were chosen to compare to radar estimates. After processing all of the marker data, it was noted that the sternum marker had a much smaller displacement than the lowest marker (on abdomen). For the subject's first shallow breathing test, figure 37 shows the comparison with these markers and the radar displacement estimated from the overall test time (i.e. average radius calculated from entire test). The arc drawn on the IQ plot from the radar data of the first test of shallow breathing is also included in figure 38.

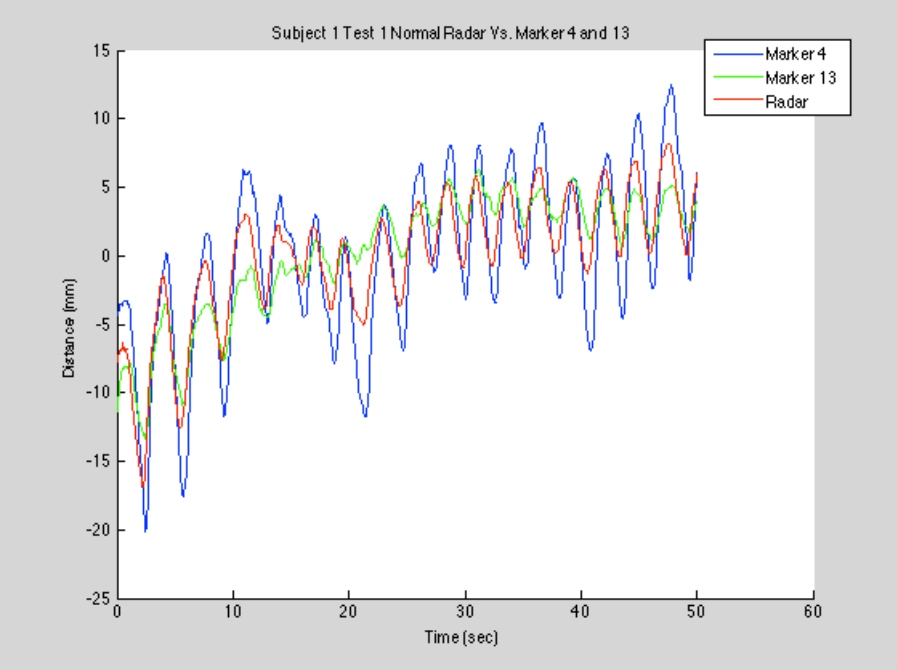

Figure 37. Subject test 1 shallow breathing displacement results comparing sternum marker (marker 13), abdomen marker (marker 4) and radar estimated displacement from average radius of entire test time (~52 seconds).

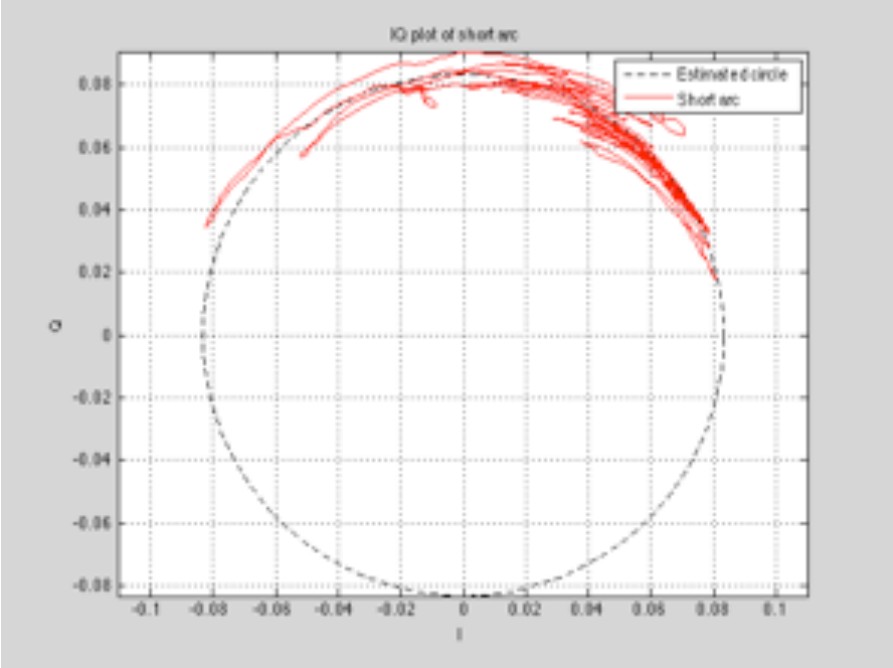

Figure 38. IQ plot of the arc drawn during radar measurement and the circle fitted to the average radius (~0.08).

Deep breathing was tested immediately following the shallow breathing test and results are included in figure 39 below.

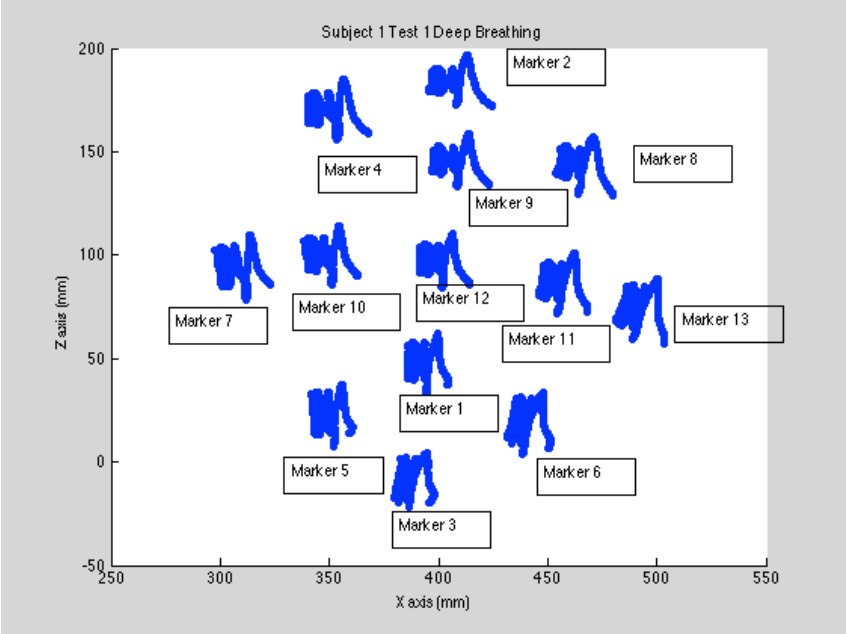

Figure 39. IR marker notation for use with subsequent plots of test 1 deep breathing displacement results. Note that marker 12 (sternum) and marker 3 (abdomen) are used to compare to radar.

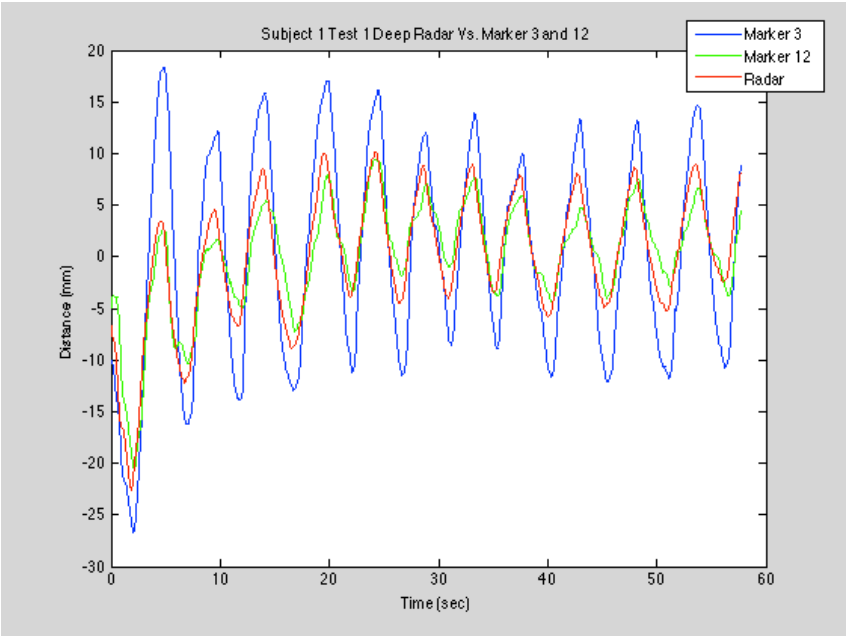

Figure 40. Displacement results of sternum (marker 12) and abdomen (marker 3) markers compared with estimated radar displacement.

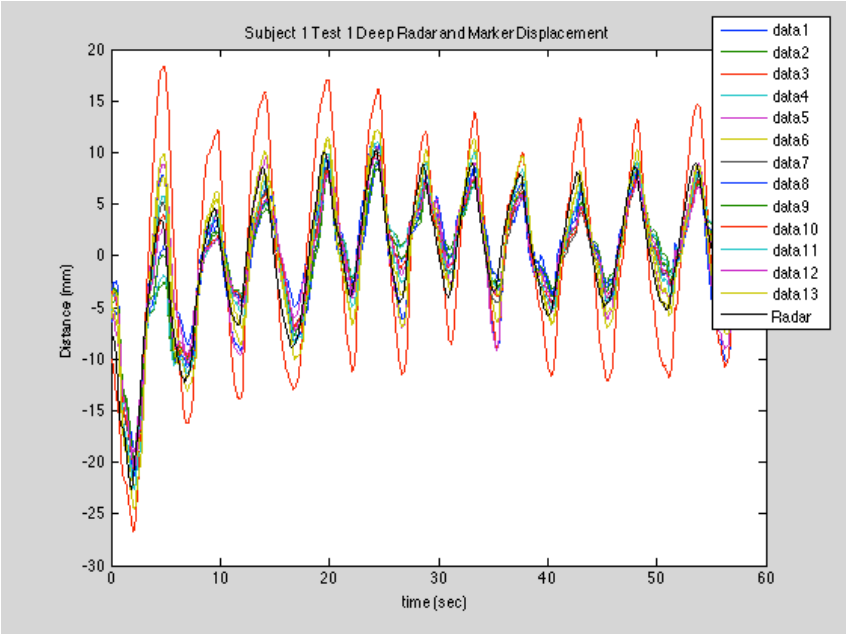

Figure 41. 13 IR markers and radar displacement of test 1 deep breathing plotted for comparison.

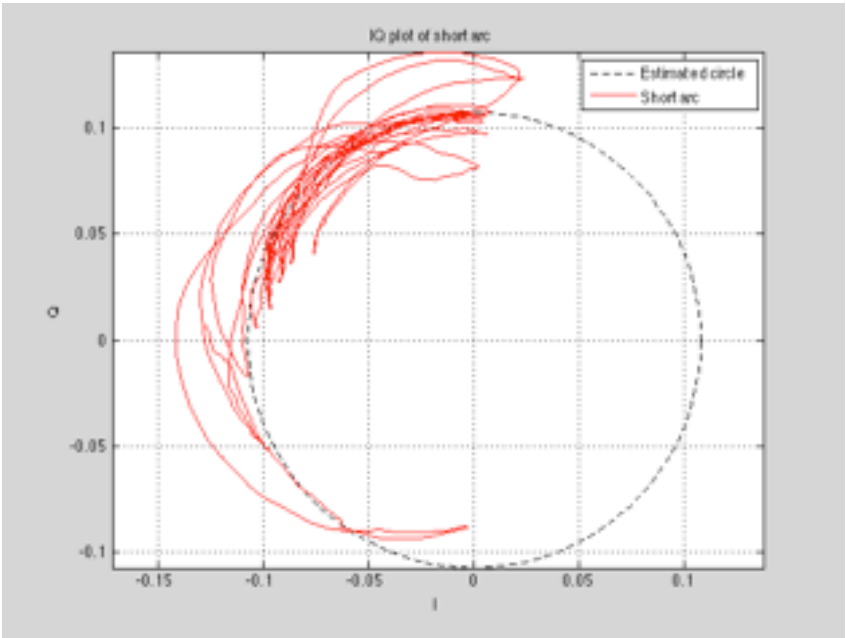

Figure 42. Circle fitted from average radius (~0.11) of arcs drawn on IQ plot during test 1 deep breathing measurements with radar.

From the IQ plots of test 1 for deep and shallow breathing it is clear that the radius is changing with breathing cycles. The displacement estimated with radar has been determined by the average radius of the entire test time and it introduces significant error as explained in [18]. If these transcribed arcs change shape because of variation in

breathing cycles or motion artifact, then these mis-centered arcs would subsequently propagate error to the estimated radius and displacement after circle fitting. In order to more accurately estimate the displacement with the radar data to compare with the sternum and abdomen markers, the radar data for deep breathing test 1 was segmented into 5.5 second intervals. For each interval, an arc was fitted to a circle using the same algorithm as before and the radius was calculated. Figure 43 shows how the radius is changing when test 1 deep breathing radar data is segmented into 10 cycles.

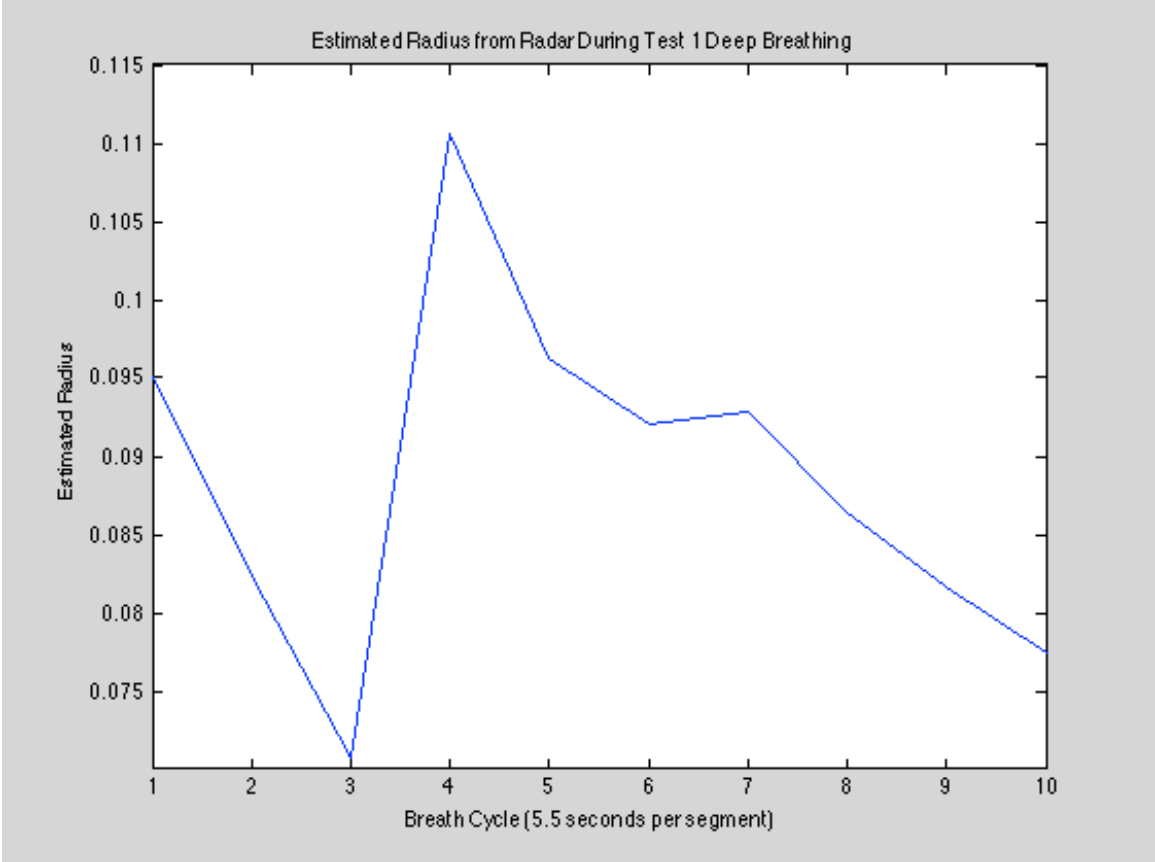

Figure 43. Test 1 deep breathing segmented into 5.5 second intervals and circle fitting run for each interval. The estimated radius varies from 0.07747 to 0.1105. Note that the radius estimated for the overall test time was approximately 0.11 for test 1 deep breathing.

The displacement estimated from the segmented radar data was then compared again with the sternum and abdomen IR markers. This is displayed in figure 44, where the displacement for each cycle is calculated for the IR markers in the same segment as the radar data.

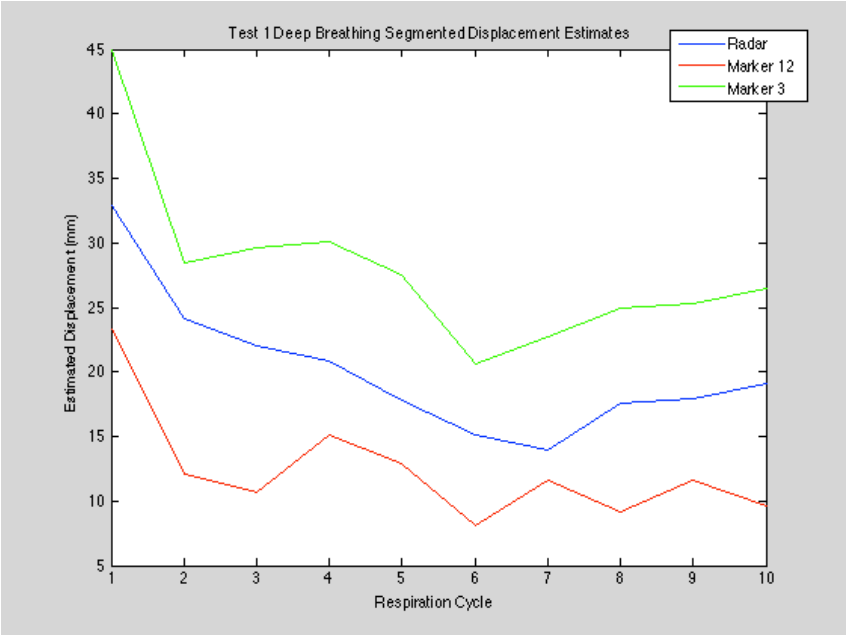

Figure 44. Segmented radar displacement estimation compared with abdomen (marker 3) and sternum (marker 12) markers for test 1 deep breathing. Will include a before and after displacement plot for radar in next draft.

After segmenting the test 1 deep breathing radar data and estimating displacement from the more accurate circles fitted to the arcs, the radar displacement was estimated to be closer to the abdomen marker displacement. The next step towards calculating RCS measurements was to determine what the contribution was from each area of displacement on the cardiopulmonary target. Starting with a theoretical model that simplifies the target to two general areas (sternum and abdomen) that move in phase (assuming no paradoxical breathing), but with different displacements, a mathematical proof starting from the baseband equations of the I and Q channel was used. The proof shows that it is possible to determine the exact values of contribution to the final RCS measurement of the radar data from each of the two areas. Figure 45 shows one of the possibilities where there is a small area with larger displacement and a larger area with small displacement.

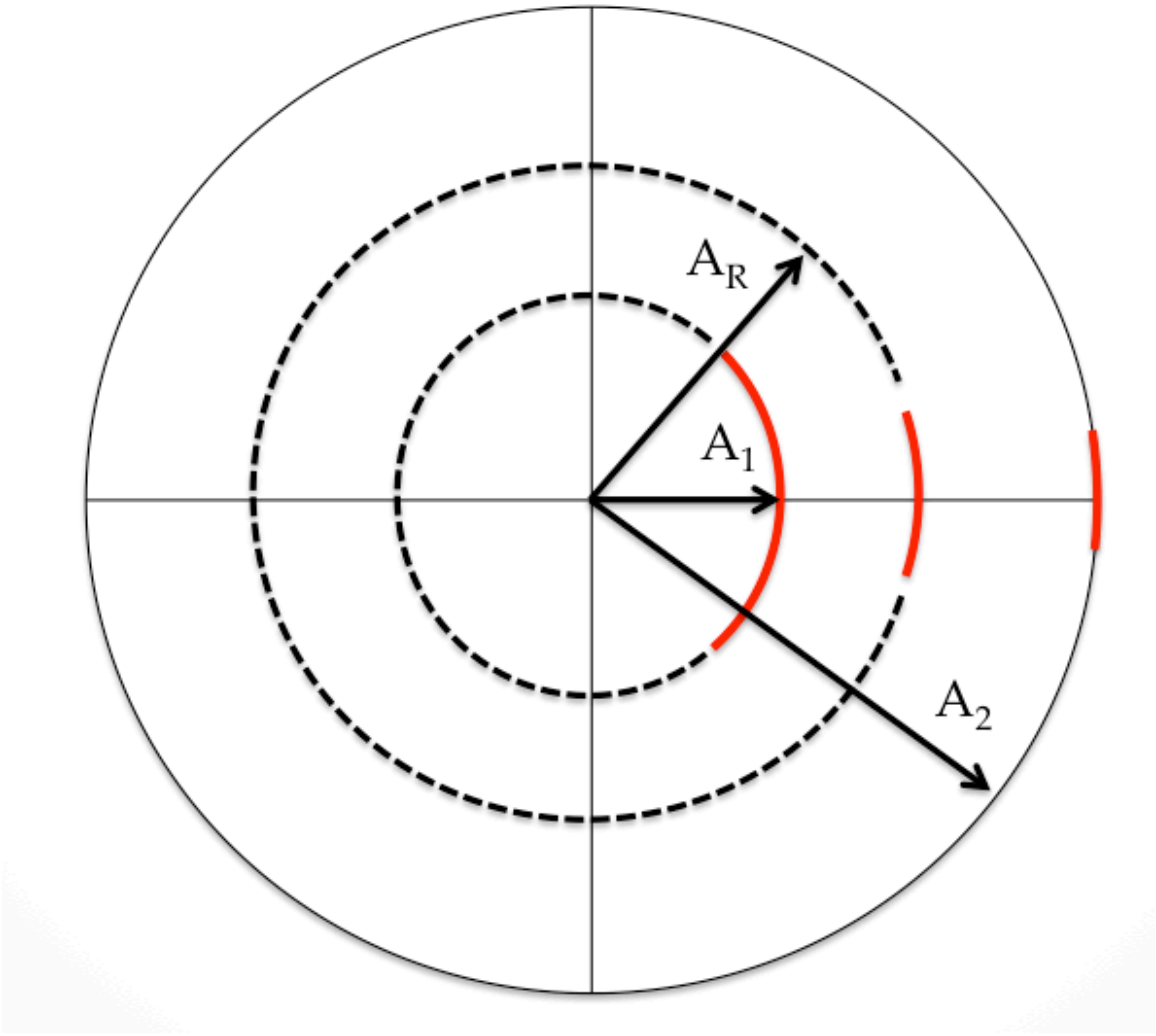

Figure 45. A_1 corresponds to the smaller area with a large displacement and A_2 corresponds to the larger area with smaller displacement. When these two areas contribute to the overall radar RCS, it is hypothesized that A_R is the resulting area that the radar sees. Note that this assumes both areas of the cardiopulmonary target (sternum and abdomen) are moving in phase, but with different displacement.

Using (4)-(7), the radius of each of the 10 segments was calculated for the sternum and abdomen markers. For each segment the radius estimated from the radar data is used to calculate the overall RCS for that segment and the contribution from each of the two areas (sternum and abdomen) is determined.

$$I_{BB} = A_1 \cos(wt + \varphi_1) + A_2 \cos(wt + \varphi_2)$$
$$Q_{BB} = A_1 \sin(wt + \varphi_1) + A_2 \sin(wt + \varphi_2) \quad (4)$$

$$B = A_1 \cos(\varphi_1 - \varphi_3) + A_2 \cos(\varphi_2 - \varphi_3) \quad (5)$$

$$B \sin(2\varphi_3) = A_1 \sin(\varphi_3 + \varphi_1) + A_2 \sin(\varphi_3 + \varphi_2) \quad (6)$$

$$A_2 = B \frac{\sin(\varphi_1 - \varphi_3)}{\sin(\varphi_1 - \varphi_2)}$$
$$A_1 = -B \frac{\sin(\varphi_2 - \varphi_3)}{\sin(\varphi_1 - \varphi_2)} \quad (7)$$

A_2 refers to the radius calculated from sternum marker displacement and A_1 refers to the radius calculated from abdomen marker displacement. The contribution to the RCS from each area's radius was calculated and plotted in comparison with the overall RCS in Figure 46 and 47 for shallow and deep breathing respectively.

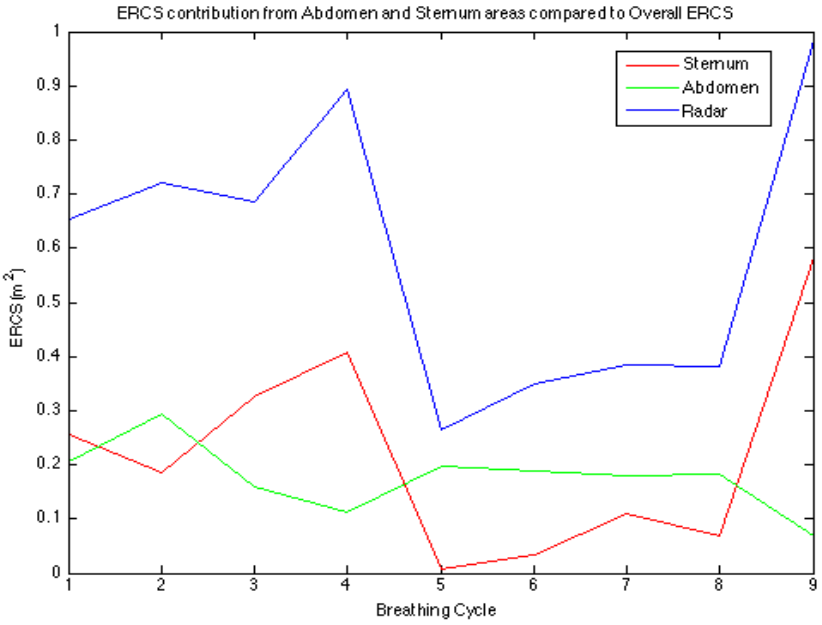

Figure 46. RCS contribution from sternum and abdomen areas compared to overall RCS for shallow breathing.

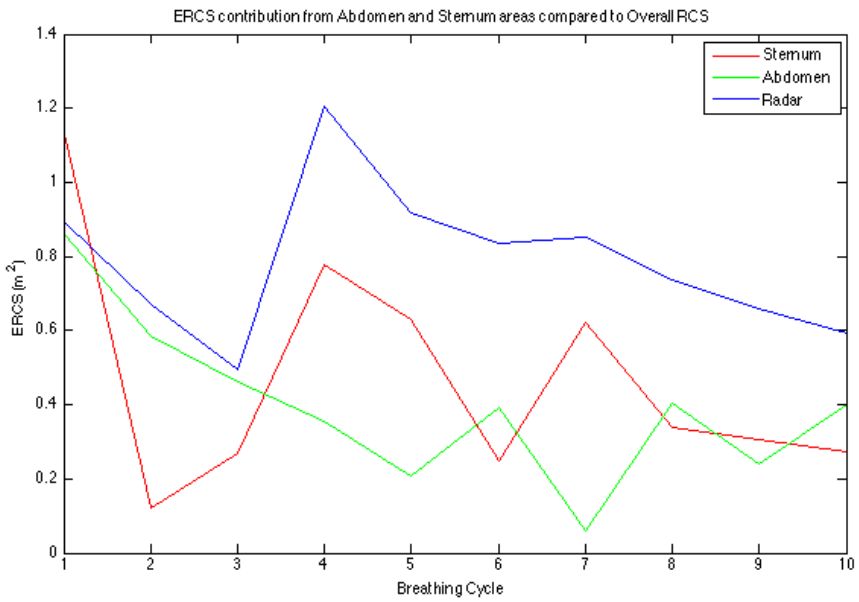

Figure 47. RCS contribution from sternum and abdomen areas compared to overall RCS for deep breathing.

Table 3. Estimated radius and displacement contributions from sternum and abdomen areas for Test 1 Deep Breathing after Segmentation of 5.5 second breathing cycles

Cycle	Estimated Radius (Radar)	Estimated Displacement (Radar) in mm	IR Marker (Sternum)	IR Marker (Abdomen)	A2 Radius (Sternum)	A1 Radius (Abdomen)
1	0.09512	32.86	23.34	44.98	0.10741	0.093447
2	0.08235	24.08	12.07	28.44	0.03485	0.076951
3	0.07072	21.98	10.56	29.68	0.05224	0.06825
4	0.1105	20.81	15.09	30.11	0.08878	0.059957
5	0.0963	17.85	12.94	27.56	0.07996	0.045676
6	0.09201	15.13	8.042	20.59	0.05026	0.063011
7	0.09281	13.98	11.57	22.77	0.07940	0.024609
8	0.08638	17.54	9.183	24.99	0.05856	0.064076
9	0.08158	17.95	11.62	25.25	0.05559	0.049320
10	0.07748	19.12	9.565	26.49	0.05245	0.063741

Chapter 6. Conclusion

6.1. Challenges

The main challenge of designing a practical and feasible wearable armband sensor device is to cancel out motion artifact from daily movements. Another challenge is the issue of powering the device without the need for constant charging with wires. Inductive charging could be a possibility or other means of harvesting energy might be used such as solar or RF backscatter. Although respiratory and heartbeat signals are useful, it is more important to develop a way to use this information to determine blood pressure from the arm through pulse transit time and pulse wave variability.

With regard to the RCS measurements on human subjects with varying respiration depth and motion artifact, the main challenge remains to be how to resolve the issue of motion artifact. Another challenge is to determine how to practically apply these results to clinical patients in hospitals or rehabilitation and obtain useful diagnostic results.

6.2. Summary

A wearable elastomeric based sensor device was designed and it was shown that both respiratory and heart rate were capable of being measured on the left upper arm. Testing on three human subjects with the device supports the theory that vital signs can be measured with an elastomeric method of sensing on the upper arm.

RCS measurements were done with an IR marker on the sternum to determine whether there were RCS changes during respiration depth variation. It was first noted that the radius estimated with radar did not match the IR marker displacement on the sternum. A calibration to determine the radius based on the marker displacement was done and the RCS associated with the sternum area was calculated. From this preliminary experiment, the question about what displacement the radar was measuring naturally followed. This led to a 13 IR marker configuration for testing with radar during deep and shallow breathing. It was found that the sternum and the abdomen had large differences in displacement measured. The radar displacement was first estimated using the overall average radius, but the IQ plot showed that the arcs were changing shape between breathing cycles. This change in arc shapes was recognized as a source of error for estimating the RCS and displacement. When the radar and IR camera data was segmented based on the breathing cycles, the results showed that the radar displacement

was closer to the abdomen marker displacement than previously calculated. The contribution from the sternum and abdomen area towards the overall RCS were then calculated from a mathematical proof derived from the I and Q baseband equations.

6.3. Future Work

Future work for the elastomeric sensor device, include adding wireless capabilities and energy harvesting to make the device practical for daily use. Another study could be done to determine what optimal elastomeric material to use and what conductive particles injected, are most suitable for the armband sensor. Lastly, for the armband device, a very important need in clinical settings, is a way to measure blood pressure continuously without cutting off blood flow in the arteries. A pulse wave variability algorithm or pulse transit time could be used with two elastomeric sensors (in one armband device) on the arm to determine blood pressure during exercise.

RCS future work includes testing human subjects at 5.8GHz frequency to investigate whether the same results occur as seen with 2.4GHz. Different types of breathing should also be tested with human subjects at the 2.4GHz frequency to investigate whether an algorithm could be designed to calculate the contribution of the abdomen and sternum to the overall RCS without needing the IR marker references. Unique identification of subjects using RCS changes as a feature is also a possible area of future study. If the radar system were able to process each segment of breathing cycles by adapting to the respiratory rate and continuously calculating the radius based on the changing arc shapes, it could be used to more accurately determine unique patterns of breathing based on these changes.

Appendix A. Bio-impedance Analysis Human Testing Protocol

A.1. CHS #19176 Research Protocol

Title of Project: **Respiratory Effort Sensing and Harvesting**

Principal Investigator: Olga Boric-Lubecke; Ph.D.; Electrical Engineering Department
Co-Principal Investigator: Jia Xu; Electrical Engineering Department

Abstract

Unobtrusive sensing of respiratory effort and heartbeat can be valuable for continuous medical monitoring. Our research group is developing low-cost zero-net energy wearable biosensors for unobtrusive, continuous, respiratory effort and heart beat sensing and harvesting. The goal is to produce self-powered unobtrusive sensors suitable for continues (24/7) health monitoring. The advantages of this technique is that first; the patient is not wired to monitoring equipment, and second; there is no battery to be replaced or disposed. A large sample of human subjects is needed to better understand how variations in the population affect the performance of our biosensors. The objectives of our project and the proposed experiment methods on human subjects are elaborated below.

1. Specific Aims

The objectives of this project are to develop and implement zero-net energy wearable biosensors that can sense and harvest energy from respiratory effort. The goal is to produce self-powered unobtrusive sensors suitable for continuous (24/7), unobtrusive health monitoring. Our system consists of three components, 1) physiological sensing/harvesting module, 2) local module that will condition and store harvested potentials, and extract physiological data, and communicate this information to the third part of the system which is 3) a remote module, via a short range, low data rate wireless link.

However, a good understanding of how variations in the population affect the performance of our systems is needed, thus we propose to conduct human testing for better understanding and improvement of our works. The experiment requires a human subject wearing a shirt with our embedded system. The system detects his/her respiratory rhythm and heart beat data and harvests the energy from his/her breathing and heart beat. Then the harvested energy will be conditioned and stored to be distributed to other parts of the system when needed and sends the physiological data to the wireless link. Wireless link then collects the data and sends it via a low data rate wireless link to a remote

computer to be further processed and analyzed. Each experiment will be done in a human performance laboratory and is expected to be two one-hour sessions.

2. Background and Significance

Human energy harvesting for wearable and portable electronics was proposed in the mid 1990's [1]. While a number of potential human energy sources were identified in [1], human energy harvesting has mostly been focused on kinetic energy [2-4], and more recently on thermal energy [5]. Primary self-powered electronic devices have included self winding wrist watches and more recently laptops with hand cranks and foot pedals [1-2]. The recent efforts to scavenge human kinetic energy using piezoelectric sensors and electromagnetic generators placed in shoes, and backpacks with spring-loaded straps have shown promise [2-3]. Also it has been demonstrated that electromagnetic scavenging is more efficient than piezoelectric [3, 6].

Perhaps the most readily available form of human power is respiration, yet no significant work has been done on energy harvesting from movement of the chest walls due to respiratory effort. Similarly, human electrical signals have been identified as a potential energy source [1, 7], with no published efforts to date. On the other hand; wearable biosensors have been investigated for remote health and fitness monitoring, including applications ranging from wound healing to athletic training [8]. Wearable sensors have included ring, ear, and body sensors [8-11]. To power these systems, simple batteries and proximity RF power scavenging [12] have been used. Our approach is to use self-powered biosensors, through sensing and harvesting methods for respiratory effort, and electro-cardiogram (ECG) potentials.

Movements of the chest due to quiet unforced respiration are mostly determined by movements of the rib cage and the abdominal wall. Studies have found that average chest wall displacement due to respiratory effort is on the order of cm [13]. Since respiratory effort itself is a valuable physiological parameter, the method that combines sensing and energy harvesting would enable efficient biosensing.

Our break-through approach is to concurrently harvest and sense physiological signals by reusing the hardware components to perform both functions, managed through a highly efficient control and communication protocol.

3. Preliminary Studies

Our recent work [14-16] to implement self-powered biosensors includes applying a method to detect and harvest respiration signals. However, we do not have a good understanding of how variations in the population affect the performance of our systems, thus we propose the experiments on a large number of subjects for better understanding and improvement of our works.

4. Research Design and Methods

The research experiments consist of measuring and categorizing data from our self-powered wearable biosensor system design. Each experiment will be done in the human performance laboratory located in the Kinesiology Department and is expected to be two one-hour sessions. The list of experimental instruments can be found in Table A.1.

5. Experimental Methods:

5.1 Human Subjects Involvement

Participants for the pilot will be 100 healthy, physically active adults 18 to 85 years of age recruited from the University of Hawaii (UH) student population and the Oahu community. Experimental protocol will include one on-site session. Participants will be instructed to report to the University of Hawaii Human Performance Laboratory in a well-hydrated state. Participants will complete health history and exercise questionnaires and sign the approved informed consent form. A healthcare professional (BOC Certified Athletic Trainer) will review each questionnaire and identify exclusion criteria. The subject's weight, height, and thorax dimensions will be measured. Thorax dimensions will be measured both at full inhale and full exhale – including waist circumference, chest circumference, chest breadth, and chest depth.

Inclusion criteria for all participants includes classification as low risk (ACSM Risk Stratification Categories) for exercise testing and free from any cardiovascular, coronary artery, pulmonary, or metabolic diseases (Mahler DA, Froelicher VF, Miller NH, York TD. ACSM's *Guidelines for Exercise Testing and Prescription*. 7th ed. Baltimore: Lippincott Williams and Wilkins; 2009.). Also being pregnant will exclude the participants from experiment.

Changes to the current protocol do not significantly increase participant risk and qualify as eligible for expedited review since the procedures being added would qualify for expedited review within any new IRB applications.

Participants will be informed of potential risks and that involvement is voluntary. Participants will also be informed they may refuse to participate at any time prior to or during the study without penalty.

5.2 Testing Protocol

Prior to test initiation, participants will be fitted with a heart rate monitor; 2 self-powered wearable respiratory effort sensors (one worn around the chest, and one worn around the stomach), a piezoelectric belt as a chest motion reference, headgear, and breathing mask to assess respiratory gas exchange throughout the test. Participants will breathe through the mask throughout the duration of the test which is connected to a metabolic cart through ventilation tubes. The metabolic cart will be used to determine oxygen consumption (VO2) and respiratory exchange ratio (RER).

Testing conditions will include a range of respiratory effort in order to determine if any effect of biosensor application is consistent across the activity range. Surface EMG electrode placements will be in pairs in the seventh or eighth intercostal space on the

right side of the body at the midclavicular line to record the activity of the diaphragm and in the 2nd or 3rd intercostal space at the midclavicular line for the external intercostals muscles.

Testing will begin in the resting condition, followed by assessment during a hyperventilatory condition. The hyperventilatory condition will include forced hyperventilation at a prescribed respiratory rate between 75-100% above resting respiratory rate for a period of less than one minute in each state. Increases in the metabolic cost of the hyperventilatory condition above the resting condition represent the respiratory effort. This condition will be followed by a 10-minute rest before completing the final condition. The final condition will include metabolic and EMG analysis during a submaximal exercise ramp protocol on a cycle ergometer. Subjects will complete 3-minute stages with increasing workloads of 50 Watts per stage until reaching 70% age-predicted-maximum heart rate (=191.5-(0.007*age)). Cycle ergometer testing is expected to last 9-12 minutes for each subject. The headgear and breathing mask will be removed at this time.

Variables of interest between the "control" and "scavenger application" state will include VO2, RER, KCAL expenditure, metabolic efficiency, ratings of perceived exertion (RPE), changes in respiratory muscle activation and indices of breathing economy (e.g. tidal volume, inspiratory time, etc.). For each condition, the control vs. sensor application state will be implemented using a counterbalanced design to determine which state the subject will complete first. Subject testing will include two one-hour sessions. During each session, each subject will be tested in both states for the resting and hyperventilatory condition. The changes between states will be determined as the average of the 2 sessions. The exercise protocol will be conducted in only one state (control or sensor application) per testing session based on a counterbalanced design.

5.3 Outcome Measures

- Cardiovascular responses will be collected via standard open circuit spirometry. Inspired ventilation was measured with a previously calibrated dry gas meter (Rayfield RAM-9200) fitted with a potentiometer.
- Expired ventilation will be channeled through Hans Rudolf high velocity valve through low resistance plastic tubing into a 5-liter mixing chamber.
- The concentrations of oxygen and carbon dioxide will be continuously sampled with an Applied Electrochemistry Oxygen analyzer S-3A/1, Oxygen sensor N-22M, carbon dioxide analyzer CD-3A, and a carbon dioxide sensor P-61B which will be calibrated with commercially available primary standard grade gases.
- Heart rate will be measured via Model Q710 electrocardiogram (Quinton Instrument Co., Bothell, Washington).
- Respiratory rate and tidal volume will be measured by both spirometry and the self-powered respiratory sensor during all stages.
- Participants will use the 6-20 point Borg Scale (attached) at the end of each stage by pointing to the appropriate RPE value while continuing to exercise.

Table A.1 The experiments consist of the following equipment

Type of Equipment	Equipment Name	Amount
Heart Rate/Respiratory Rate Sensors	Piezoelectric chest belt	1
(incorporated into shirt/belt/upper arm cuff/wrist cuff modules)	Electrocardiogram Quinton Instrument Co Model Q710	1
	Inductive plethysmography sensor	1
	Impedance plethysmography sensor	1
	Resistive elastomers	1
	Photometry sensor	1
	Acoustic (impedance-matched) microphone	1
	Galvanic skin response sensor	**1**
	Customized low voltage rectifier	1
Data Processing and Transmission	TI CC430 Wireless link Texas Instruments	1
Module	6-20 point Borg Scale	1
RPE reference	Hans Rudolf high velocity valve	1
	Low resistance plastic tubing	1
Velocity Valve	5-liter mixing chamber	1
	Electrochemistry Oxygen analyzer S-3A/1	1
Electrochemistry Oxygen analyzer	Oxygen sensor N-22M	1
	Carbon dioxide analyzer CD-3A	1
Oxygen sensor	Carbon dioxide sensor P-61B	1
Carbon dioxide analyzer	Spirometer	1
Carbon dioxide sensor	Polar wear link chest belt	1
References		

5.4 Risk and hazardous evaluations:

If you have a pacemaker or defibrillator, or have health issues which requires that you wear electronics of any sort, avoid using magnet generators. To be on the safe side we would advise pregnant women to avoid any exposure to magnetic fields. So if you are sexually active you should be in a birth control program in order to be in this study.

6. Data and Safety Monitoring Plan

1. All experiments will be logged.
2. All complaints from the participants will be logged and reported to the PI and CHS.
3. All unanticipated adverse events will be logged and reported to the PI and CHS.

7. Literature Cited

[1] Jansen, A.J.; Stevels, A.L.N., "Human power, a sustainable option for electronics," *Proceedings of the 1999 IEEE International Symposium on Electronics and the Environment*, ISEE 1999.11-13 May 1999 Page(s):215–218.

[2] J. Kymisis, C. Kendall, J. Paradiso, and N. Gershenfeld, "Parasitic Power Harvesting in Shoes, *Second International Conference on Wearable Computing*, 1998.

[3] L. C. Rome, L. Flynn, E. M. Goldman, and T.D. Yoo, "Generating electricity while walking with loads," *Science*, Vol. 309, Sept. 2005, Page(s): 1725-1728.

[4] C.R. Saha, T. O'Donnell, N.Wang, P. McCloskey, "Electromagnetic generator for harvesting energy from human motion" *Elsevier Sensors and Actuators A: Physical* Vol. 147, Issue 1, 15 Sep. 2008, pp: 248-253.

[5] V. Leonov, T. Torfs, P. Fiorini, and C. Van Hoof, "Thermoelectric Converters of Human Warmth for Self-Powered Wireless Sensor Nodes," *IEEE Sensors Journal*, Vol. 7, No. 5, May 2007.

[6] www.numetrex.com

[7] T. Starner and J. Paradiso, "Human Generated Power for Mobile Electronics," in *Low Power Electronics Design*, CRS Press, Fall 2004.

[8] Morris, Deirdre; Schazmann, Benjamin; Wu, Yangzhe; Coyle, Shirley; Brady, Sarah; Fay, Cormac; Hayes, Jer; Lau, King Tong; Wallace, Gordon; Diamond, Dermot; , "Wearable technology for biochemical analysis of body fluids during exercise," *Engineering in Medicine and Biology Society, EMBS. 30th Annual International Conference of the IEEE* , vol., no., pp.5741-5744, 2025 Aug. 2008.

[9] Asada, H.H.; Shaltis, P.; Reisner, A.; Sokwoo Rhee; Hutchinson, R.C.; , "Mobile monitoring with wearable photoplethysmographic biosensors," *Engineering in Medicine and Biology Magazine, IEEE*, vol.22, no.3, pp. 28-40, May-June 2003.

[10] Ming-Zher Poh; Swenson, N.C.; Picard, R.W.; , "Motion-Tolerant Magnetic Earring Sensor and Wireless Earpiece for Wearable Photoplethysmography," *Information Technology in Biomedicine, IEEE Transactions on* , vol.14, no.3, pp.786-794, May 2010

[11] J. Yoo, L. Yan, S. Lee, Y. Kim, and H. J. Yoo, "A 5.2 mW Self-Configured Wearable Body Sensor Network Controller and a 12uW Wirelessly Powered Sensor for a Continuous Monitoring System," *IEEE Journal of Solid State Circuits*, Vol. 45, No. 1, January 2010, pp. 178-188.

[12] C.R. Saha, T. O'Donnell, N.Wang, P. McCloskey, "Electromagnetic

generator for harvesting energy from human motion" *Elsevier Sensors and Actuators A: Physical* Vol. 147, Issue 1, 15 Sep. 2008, pp: 248-253.
[13]T. Kondo, T. Uhlig, P. Pemberton, P. D. Sly, "Laser monitoring of chest wall displacement," *EurRespir J.* 1997; 10: 1865-9.
[14]O. Boric-Lubecke, V. Lubecke, I. Mostafanezhad, and E. Shahhaidar, "Zero-Net Energy Wearable Biosensors," *ISCA25th International Conference on Computers and Their Applications (CATA- 2010)*, April 2010.
[15]E. Shahhaidar, M. Wolfe, R. Ghorbani, and O. B. Lubecke, "Electromagnetic Generator as Respiratory Effort Energy Harvester," *IEEE Power and Energy Conference*, Urbana-Champaign, Illinois, February 2011.
[16]B. Padasdao, O. B. Lubecke, "Respiratory Rate Detection Using a Wearable Electromagnetic Generator ", *EMBC 2011*.

A.2. CHS #19176 Consent Form

UNIVERSITY OF HAWAI`I

INFORMED CONSENT AND PRIVACY AUTHORIZATION TO TAKE PART IN A RESEARCH STUDY

Study Title: *Respiratory Effort Sensing and Harvesting*

Principal Investigator (PI):
Name: Dr. Olga Boric-Lubecke
Institutional Affiliation: Electrical Engineering Department, University of Hawaii at Manoa
Address: POST 205K, 1680 East-West Rd Honolulu, HI 96822
Phone Number: (808) 956-9648

Sponsor: REIS
Sponsor Name: Anthony Kuh
Sponsor Address: 2540 Dole Street, Honolulu, Hawaii, 96822

Sponsor: Archinoetics DoD SBIR Phase II subaward
Sponsor Name: Alan Furuno
Sponsor Address: Bldg. 1054 Patchel Street, Fort Detrick, Maryland 21702-5012
Voice: 808-433-3602, E-mail: alan.s.furuno.civ@mail.mil

Abbreviations Used:

UH: University of Hawaii
RA: Research Assistant
BOC: Board of Certification
ECG: Electrocardiogram
EMG: Electromyogram

Before you decide whether or not you would like to take part in this study, you should understand its purpose, how it may help, any risks, and what you will be asked to do. This process is called informed consent. If you agree to take part in the study, you will be asked to sign this consent form.

Before you learn about the study, it is important that you know the following:

- Taking part in this study is completely voluntary.
- If you decide to take part in the study, you can change your mind at any time and withdraw from the study.

What is the purpose of this study?

The objective of this project is to develop and verify self-powered unobtrusive wearable

biosensors, in the form of a belt and a shirt, that can sense and harvest energy from breathing and/or heartbeat.

Department of Defense (DoD) is the study sponsor, and the representatives of the DoD will have access to research records as they are the study sponsor.

Why are you being asked to participate in this study?

You are being asked to participate in this study because you are above 18 years old and do not have any significant medical problems.

Researchers plan to enroll a total of 100 participants from Hawaii.

How long will the study take and what procedures will be performed on you?

Each experiment will be done in the human performance laboratory in the Stan Sheriff Center at UH, and is expected to be two sessions, one hour each.

First, participants will undergo the consent process which provides participants time to read the consent form and ask questions. Then, if they agree to participate, participants will sign the consent form.

Next, participants will fill out a health history questionnaire and an exercise questionnaire. The questionnaire will be reviewed by a healthcare professional (BOC certified athletic trainer) to make sure you are healthy enough to participate.

Then the participant's weight, height, and thorax (the part of the human body between the neck and the diaphragm, partially encased by the ribs and containing the heart and lungs; the chest) dimensions will be measured. The thorax dimensions will be measured both at full inhale and full exhale including waist circumference, chest circumference, chest breadth, and chest depth.

Prior to test initiation, participants will be fitted with a heart rate monitor, a sensing module (incorporated into a shirt belt, upper arm cuff, and wrist cuff) comprising heart rate (ECG) and respiratory rate sensors, headgear, and breathing masks to assess respiratory gas exchange throughout the test. Participants will breathe through the mask throughout the duration of the test which is connected to a metabolic cart through ventilation tubes. The metabolic cart will be used to determine oxygen consumption and respiratory exchange ratio.
Testing conditions will include a range of breathing rates in order to determine if any effect of using sensors is observed for all activities. Participants will breathe through the mask throughout the duration of the test to measure parameters of respiration. Surface EMG electrode placements on the chest will be used to monitors muscle movement related to breathing.

Testing will begin in the resting condition, followed by assessment during exercise. The

exercise condition will include heavier breathing for a period of less than one minute in each state. This condition will be followed by a 10 minute rest before completing the final condition. The final condition will include walking on an exercise ramp. This testing is expected to last 9-12 minutes for each subject.

What are the risks and discomforts that you may experience?

If you have a pacemaker or defibrillator, or have health issues which require that you wear electronics of any sort, you should not participate in this study.

We would advise pregnant women to not participate in this study. If you are sexually active, you should be in a birth control program if you want to participate in this study.

People who are uncomfortable in confined spaces, have a tendency to be claustrophobic, or who might have a stress reaction to wearing the head gear and mask should not participate in this study.

How will your information be used?

There may not be direct benefit to the participants. However, the results from this project will help better identify and address the issues with respiratory effort sensing and harvesting. Mainly the researchers will look into the differences of the attainable energy from different people of various ages, gender, and physical characteristics.

Representatives of the DoD will have access to research records as they are the study sponsor.

How will my study data be kept confidential?

Research data will be confidential to the extent allowed by law. Agencies with research oversight, such as the UH Human Studies Program, have the authority to review research data. All research records will be stored on a password-protected computer in a locked room in the primary investigator's lab for the duration of the research project, and will be destroyed upon completion of the project.

The results of this research may be presented at meetings or in publications; however, you will not be identified.

Will you be given the results of the study?

The study PI or research assistant will not provide any individual study results to you or any member of your family, other doctors involved in your care, your insurance

company, or your employer.

How will this study benefit you?

It is unlikely that you will benefit directly from participating in this study.

Are there costs or payments involved in this study?

There will be no costs or payments for your examination and tests in this study.

Can you revoke your consent for your participation in this study?

If you enter the study and you later change your mind, you can revoke (take away) your consent at any time, and there will be no penalty for you. This means that you can leave the study at any point as you are a voluntary research participant.

The study RA will decide if it is not possible or appropriate for you to continue to participate in this study due to unexpected health concerns or reactions to the experiment. If the study RA observes or believes that you are experiencing significant discomfort or fatigue, and that continuation of the study would be detrimental to your health and safety, your participation in the study will be immediately discontinued.

Will you learn about new findings about risks of this study?

You will be told of any new information learned during the study that may change your willingness to continue in this study. At that time, you will be able to decide whether to continue your participation in this research study.

If you have any questions about this study, whom do you contact?

If you feel that you have been injured as a result of taking part in this study, or if you have any questions about the study, you should call the study PI, [Dr.Olga Boric-Lubecke], at [(808) 956-9648*]*.

If you have questions about your rights as a research participant in this study, you should contact the University of Hawaii Human Studies Program at 808.956.5007 or by email at uhirb@hawaii.edu

Authorization to Use and Disclose (Release) Personal Health Information

The federal government has created a "Privacy Rule" under the Health Insurance Portability and Accountability Act (HIPAA). This Rule gives you the right to decide who can use and release your personal health information (also called "protected health information" or "PHI") for the purposes of research.

PHI is health information about study participants that could be linked to their identity. But we will not use your PHI in this study.

What happens if you do not sign this authorization?

Signing this authorization form is voluntary. If you do not sign this form, you will not take part in this research study.

Consent for You to Take Part in this Research Study

My signature indicates that I have read and understand this research consent/authorization form and that my questions have been satisfactorily answered. I understand that if at any time I have other questions, I can contact the study PI listed on page 1 and page 4 of this form. I further understand that I will be given a copy of this signed consent/authorization form for my records.

_____
Name of the Participant

_____ _____
Signature of the Participant Date

A.3. CHS #19176 Approval Letter

Office of Research Compliance
Human Studies Program

UNIVERSITY of HAWAI'I® MĀNOA

MEMORANDUM
CR

December 2, 2015

TO: Olga Boric-Lubecke, Ph.D.
Principal Investigator
Electrical Engineering

FROM: Denise A. Lin-DeShetler, MPH, MA
Director

SUBJECT: CHS #19176- "A Pilot Study for Respiratory Effort Sensing and Harvesting"

Under an expedited review procedure, the research project identified above was approved for one year on November 27, 2015 by the University of Hawaii (UH) Human Studies Program. The application qualified for expedited review under CFR 46.110 and 21 CFR 56.110, Category (7).

This memorandum is your record of the Human Studies Program approval of this study. Please maintain it with your study records.

The Human Studies Program approval for this project will expire on November 26, 2016. If you expect your project to continue beyond this date, you must submit an application for renewal of this Human Studies Program approval. The Human Studies Program approval must be maintained for the entire term of your project.

If, during the course of your project, you intend to make changes to this study, you must obtain approval from the Human Studies Program prior to implementing any changes. If an Unanticipated Problem occurs during the course of the study, you must notify the Human Studies Program within 24 hours of knowledge of the problem. A formal report must be submitted to the Human Studies Program within 10 days. The definition of "Unanticipated Problem" may be found at: http://hawaii.edu/irb/download/documents/SOPP_101_UP_Reporting.pdf, and the report form may be downloaded here: http://hawaii.edu/irb/download/forms/App_UP_Report.doc.

You are required to maintain complete records pertaining to the use of humans as participants in your research. This includes all information or materials conveyed to and received from participants as well as signed consent forms, data, analyses, and results. These records must be maintained for at least three years following project completion or termination, and they are subject to inspection and review by the Human Studies Program and other authorized agencies.

1960 East-West Road
Biomedical Sciences Building B104
Honolulu, Hawai'i 96822
Telephone: (808) 956-5007
Fax: (808) 956-8683

Appendix B. CHS #14884 Research Protocol Proposal

Title of Project:	**Remote Sensing of Physiological Motion Using Doppler Radar**
Principal Investigator:	Olga Boric-Lubecke; Ph.D.; Electrical Engineering Department
Co-Principal Investigator:	Shuhei Yamada; Xiaomeng Gao; Ehsan Yavari; Electrical Engineering Department

Abstract

Cardiopulmonary and respiratory motions can be detected by Doppler radar techniques. Our research group has applied this concept and developed a low-cost microwave Doppler radar system. The radar system has demonstrated ability and limitation on remote sensing of physiological motions. A larger sample of human subjects is needed to better understand how variations in the population affect the performance of our radar system. This protocol outlines the objectives of our project and the proposed experiment methods on human.

A.1. Specific Aims

The objectives of this project are to develop and verify Doppler radar systems that can perform remote sensing of human physiological measurement. In order to identify the person from other sources of motion in the environment, we also propose the use of a passive Radio Frequency sensor on the subject. A low-cost Doppler radar system, a computerized data acquisition system, a low power passive radiofrequency tag and algorithms for automatic rate detection have been developed for this project. In addition of using signal generator, a Texas Instrument RF transceiver microcontroller evaluation board is also used to generate the signal. It has the intermittent transmission capability. The radio developed using intermittent signal transmission can cost less power. Furthermore, a pulse radar is developed with coaxial component for intermittent transmission for better signal to noise ration and enhancing receiver performance. We introduced a set of IR optical tracking system, a passive RF harmonic tag, liner variable differential transformer (LVDT), strain gauge-based digital scale, and load cell to the study for displacement estimation, and may be further developed for chest motion detection. A load cell may be used to detect the force from respiration applied to the chest belts. The Leviton OSC10-M0W multi-technology hybrid occupancy sensor is used as common occupancy sensor which is equipped with both infrared and ultrasonic sensors for occupancy detection based on respiration signal.

However, a good understanding of how variations in the population affect the performance of our systems is needed, thus we propose the experiments on a large

number of subjects for better understanding and improvement of our work. The experiment requires a human sitting and lying down in front of the radar system. The radar system detects his/her heartbeat and respiratory rhythm data. The computer then collects these data to be processed and analyzed. In the case when the tag is put on a human subject, the experiment would only require a human sitting in front of the radar. The tag would be put above the clothing of the human subject. Each experiment will be done in a laboratory and is expected to take less than ninety minutes. It is important to note that the passive RF tag will not emit any radiation by itself. It just modulates the incoming frequency and reflects the modulated information. The reflected power level is less than 0.1 mW. The length of the tag is 15.7 cm and the width is 1 cm.

A.2. Background and Significance

The use of Doppler radar was demonstrated for detection of respiratory rate in 1975 [1], and heart rate in 1979 [2]. By detecting the associated Doppler shift in a radio signal reflected by the body, cardiopulmonary related movement could be discerned without physical contact. Additional benefits of microwave Doppler radar include the versatile ability to function at a distance through clothing, walls, or debris. The remote sensing of physiological motion could prove a powerful tool for health care monitoring, emergency medical response, and surveillance applications. Such unobtrusive sensing could benefit patients with conditions that may be perturbed or worsened by contact sensors, as when monitoring for sleep disorders [3], SIDS prevention, and burn victim care. It would also be of value in emergency scenarios where first responders can benefit from any additional data for triage decisions, in disaster areas where victims could not easily be located, and in security screening situations where subjects must be detected and/or monitored and often do not/cannot cooperate.

A.3. Preliminary Studies

Our recent works [4-10] to implement this concept include applying existing wireless terminals to detect heart and respiration signals, implementing dedicated low-cost microwave Doppler radar, and developing related software for automated rate detection. However, we do not have a good understanding of how variations in the population affect the performance of our systems, thus we propose the experiments on a large number of subjects for better understanding and improvement of our works. We have also noticed that any external motion around the radar affects the received information quality. We want to improve radar performance by the inclusion of the tag.

A.4. Research Design and Methods

The research experiments consist of measuring and categorizing data from our Doppler radar system design. Each experiment will be done in the laboratory on the fourth floor of POST building (POST 417) or in the classroom on the third floor of Holmes Hall (H388) and is expected to be no longer than sixty minutes. The list of

experimental instruments can be found in Table I. This renewal includes measurements at 900MHz and 5.8 GHz, in addition to measurements at 2.4GHz.

Experimental Methods:
The administrator of the measurement will perform the followings:

1. Inform subject about the research and obtain his/her consent form.
2. Ask the subject his/her age and gender.
3. Ask the subject whether
   a. he/she has any diseases or disorders relating to or affecting the heart or respiratory system.
   b. he/she has a pacemaker or neurostimulator.
   c. she is pregnant. If the subject answered yes to any of these questions, he/she would have been excluded from the study.
4. Measure the subject's weight, height, and thorax dimensions. Thorax dimensions will be measured both at full inhale and full exhale – including waist circumference, chest circumference, chest breadth, and chest depth.
5. Place ECG electrodes, on the subject's left and right upper arms and left ankle, if desired.
6. Place piezoelectric respiratory effort belts on the subject's abdomen and chest.
7. Place accelerometer on the chest and abdomen of the patient.
8. Place RF harmonic tag on the apex of the chest area of the subject.
9. Place IR optical tracking system in front of the subject, with the retro-reflective markers attached on the surface of the chest.
10. Place piezoelectric finger pulse sensor on the subject's left index.
11. Place chest band including LVDT or stain gauge on the chest if desired
12. Place load cell chest belt on chest if desired
13. Place blood pressure cuff, pulse oximeter, nasal airflow sensor and thermometer, if desired.
14. Select type of measurements:
    a. 5-minute seated at distance of 0.5m to 2m from antennas, measured from four sides of the body, transmitter frequency is 900MHz, 2.4GHz, or 5.8GHz, ask the subject to breathe normally
    b. 5-minute supine at distances of 0.5m to 2m from antennas, measured from four sides of the body, transmitter frequency is 900MHz, 2.4GHz, or 5.8GHz, ask the subject to breathe normally
    c. Same as (7) and (8) but ask subject to breathe through the transducer
    d. Ask the subject to sit in a chair or lie down on a stretcher for the measurements accordingly. If the experiment is (9), place the transducer and the disposable mouth piece in front of the subject to breathe comfortably.
15. Adjust the transmitting antenna height to be approximately level with the subject's sternum.
16. Ask the subject to remain still, to refrain from scratching, talking, and any other motion for the duration of each measurement if possible.
17. Ask the subject to perform reading, walking or jumping in front of the antenna

and reference sensor.

18. Perform two measurements.
19. When the measurements are completed, instruct the subject to remove the reference sensors.
20. 1 to 5-minute seated at distance of 1 m measured from the front, transmitter frequency is 2.45 GHz. The tag is placed on the respiratory belt and then the belt is appropriately placed on the subject's chest. The subject is asked to breathe normally.

The experiments consist of the following equipment:

Figure B.1 Equipment list

Type of Equipment	Equipment Name	Amount
Doppler Radar System	E4433B Agilent signal generator or equivalent	1
	HP 83640B signal generator	1
	HP 33120A signal generator	1
	SR560 Standford Research low noise amplifier or equivalent	8
	CC2530EM with SmartRF05EB Texas Instrument RF transceiver	1
	ZFSC-2-2500 Minicircuits 0° power splitter or equivalent	7
	4033C 90° Narda power splitter or equivalent	4
	ZX10Q-2-12 Minicircuits 90^{o} power splitter or equivalent	1
	ZFSC-2-10G Minicircuits 0° power splitter or equivalent	4
	ZFM-4212 Minicircuits mixer or equivalent	8
	ZX05-10L Minicircuits mixer or equivalent	2
	ZX05-83 Minicircuits mixer or equivalent	2
	ZX60-542LN-S+ Minicircuits Amplifier or equivalent	2
		2
	ZX05-14-S+ Minicircuits mixer or equivalent	4
	VHF-3500 Minicircuits High Pass filter	
	ASPPT2988 Antenna Specialists antenna or equivalent	5
	CM248 Cellphone-Mate Dual-Band Panel antenna or equivalent	2
	Indoor directional Wi-Fi antenna or equivalent	2
	PE2058 90^{o} hybrid or equivalent	1
	Custom made antenna board	1
Data Acquisition System	PC with MATLAB and LabVIEW	1
	PC with GalilTools	1
	PC with DTrack softwarePC with PyCharm	1
	PCI-6259 National Instruments data acquisition card	1
	SHC68-68-EPM National Instruments shield	2

Type of Equipment	Equipment Name	Amount
	cable	
	16-bit National Instruments terminal block	2
	14-bit National Instruments terminal block or equivalent	1
Reference	PC with Biopac MP150WSW	1
	Opitcal Isolator	1
	Strain-gauge based digital scale	1
	Measuring tape	1
	01440 Lafayette chest depth calipers	1
	3-lead ECG electrodes	1
	ECG100C Biopac Amplifier	1
	DA100C Biopac Amplifier	4
	TSD117 Biopac pneumotach respiratory transducer	1
	Dymedix Airflow Sensor	
	- Model 4912 Dymedix Electronic	1
	Filtration Module FM-4912 1.5 mm	1
	- Model 2400 Dymedix Small Airflow	1
	Sensors	1
	- Model 2401 Dymedix Medium Airflow Sensors	
	- Model 2402 Dymedix Large Airflow Sensors	
	Pneumotrace piezoresistor chest belts	2
	Pneumotrace piezoresistor finger pulse sensor	1
	3-Axis Accelerometer, Model: Phidget 1059 with USB cable connection	2
	Thera- Elastic Band, model: Yellow 6mils light resistance	2
	3-Axis Accelerometer : ADXL327 analog devices	1
	Load cell xlus88 from Deltametrics	1
	Displacement sensor LVDT SE750-2000 from microsensors	1
	Blood pressure monitor	
	Pulse oximeter	1
	Griffin Motion Precision Linear Motion Platform, Model: MLS-050-BS-A-F-S-0-00	1
	Galil Motion Control CDS-3310 controller	1
	Digital thermometer	1
	Griffin Motion Precision Linear Motion Platform, Model: LNS-100-BS-A-F-P-0-00	1
	Galil Motion Control CDS-3310 controller	1
	Infrared optical tracking system and retro-reflective markers	1 1

Type of Equipment	Equipment Name	Amount
	Leviton OSC10-M0W multi-technology hybrid occupancy sensor which is equipped with both infrared and ultrasonic sensors	

Risk and hazardous evaluations:

The Doppler radar system operates at 900 MHz, 2.4 GHz, or 5.8 GHz frequency and radiates power similar to or lower than that used in many wireless consumer electronics products operating in this frequency band – including wireless network cards, cordless telephones, cellular phones, and video infant monitors, and well below the FCC limit for consumer electronics devices in this band.

A.5. Human Subjects

1. Up to hundred healthy people will be recruited for the experiments. The subjects' ages range from 21-70. All BMI's are acceptable. Women and minorities are encouraged to participate.
2. Research data will be confidential to the extent allowed by law. Agencies with research oversight, such as the UH Committee on Human Studies, have the authority to review research data. All research records will be stored on a computer in a locked room in the primary investigator's lab for the duration of the research project, and will be destroyed upon completion of the project
3. Posters will be placed on the bulletin boards around campus for recruitment. The subject can participate upon understanding and signing the consent form.
4. We believe there is little or no risk involved in participating. The frequency and power of the radar system used in according to FCC regulations.
5. There may not be direct benefit to the participants. However, the results from this project will help the biomedical application research better identify and address the issues with Doppler radar sensing vital signs.

A.6. Data and Safety Monitoring Plan

1. All experiments will be logged.
2. All complaints from the participants will be logged and reported to the PI and CHS.
3. All unanticipated adverse events will be logged and reported to the PI and CHS .

A.7. Literature Cited

[1] J. C. Lin, Non-invasive microwave measurement of respiration, *Proc. IEEE*, vol. 63, p1530, 1975.

[2] J. C. Lin, Microwave apexcardiography*, IEEE Transactions MTT*, vol. 27, pp. 618-620, 1979.

[3] M. F. Hilton, R. A. Bates, K. R. Godfrey, et al., Frequency Spectral Analysis of Heart Rate Variability as a Diagnostic Marker of the Sleep Apnea Syndrome,*Med. Biol. Eng. Comput*., 37, (6), pp. 760-769, Nov. 1999.

[4] V.M. Lubecke, O. Boric-Lubecke, G. Awater, P.-W. Ong, P. Gammel, R.-H. Yan, J.C. Lin, *World Congress on Medical Physics and Biomedical Engineering (WC2000)*, Chicago IL, July 2000.
[5] V.M. Lubecke, O. Boric-Lubecke, and E. Beck, "A compact low-cost add-on module for Doppler radar sensing of vital signs using a wireless communications terminal," *IEEE MTT-S International Microwave Symposium*, Seattle, WA, USA, June 2002.
[6] A. D. Droitcour, V. M. Lubecke, J. Lin, and O. Boric-Lubecke, Doppler radar sensing of vital signs,*IEEE MTT-S IMS2001 Digest* (student paper competition honorable mention), Phoenix, AZ, vol. 1, pp. 175-178, May 2001.
[7] A. D. Droitcour, O. Boric-Lubecke, V. M. Lubecke, and J. Lin, mm CMOS and BiCMOS single chip direct conversion Doppler radars for remote sensing of vital signs,*IEEE ISSCC Digest of Technical Papers*, pp. 348-349, February 2002.
[8] A. D. Droitcour, O. Boric-Lubecke, V. M. Lubecke, J. Lin and G. T. A. Kovacs, Correlation Effect on ISM Band I/Q CMOS Radar for Non-Contact Sensing of Vital Signs, *IEEE MTT-S IMS2003 Digest* (student paper competition first place), vol. 3, pp. 1945-1948, Philadelphia, PA, June 2003.
[9] B. Lohman, O. Boric-Lubecke, V. M. Lubecke, P. W. Ong, and M. M. Sondhi, signal processor for Doppler radar sensing of vital signs, *IEEE Engineering in Medicine and Biology Conf*. (student paper competition third place), Istanbul, Turkey, October 2001.
[10]Byung-Kwon Park; Yamada, S.; Boric-Lubecke, O.; Lubecke, V., Single-channel receiver limitations in Doppler radar measurements of periodic motion, Radio and Wireless Symposium, 2006 IEEE, pp.99 – 102, Jan. 2006
[11]http://recco.com/system/reflectors_info.asp

Date 2015/01/22
Version 7.0

CHS #14884 Consent Form

Agreement to Participate in
"A Pilot Study of Remote Sensing of Physiological Motion Using Doppler Radar"

Olga Boric-Lubecke, Primary Investigator (PI), olgabl@hawaii.edu
Shuhei Yamada, Xiaomeng Gao, Ehsan Yavari, Co-PI's,
y_shuhei@hotmail.com, gaoxiaom@hawaii.edu, ehsan@hawaii.edu
Department of Electrical Engineering, University of Hawaii at Manoa, HI 96822, (808) 956-9648

This experiment is being done as a part of our research project to measure human breathing and heart rate with Doppler radar. Approximately 100 people will participate in the study. Persons of various physical characteristics and age from 21-70 are being invited.

Participation in the experiment will consist of filling out a form on background information, measuring body type (weight, height, and upper-body dimensions) and staying in a room for Doppler radar measurement. The measurement will focus on recording your breathing and heart rates and the torso/chest displacement due to breathing. The heart rate will be measured using up to three methods: Doppler radar system, three electrocardiogram (ECG) leads, and a finger pulse sensor. The breathing rate will be measured using up three of the following four methods: Doppler radar system, two chest belt sensors, accelerometer and a pneumotach respiratory transducer. In two experiments, you may be asked to breathe through the transducer. You will also be asked to perform reading, walking or jumping in front of the radar. The sagittal and/or circumferential displacement of the chest will be measured by up to five methods: Doppler radar system, two chest belt sensors, IR optical tracking systems, linear variable differential transformer (LVDT) or strain gauge-based digital scale. The chest belt sensors will be placed around your upper and/or lower torso. The finger pulse sensor will be placed around your index finger. The three ECG leads will be placed on your left hand, right hand, and left foot. The blood pressure monitor, pulse oximeter, and digital thermometer may be used during the measurements. The Doppler radar system will be located several feet away from you. For certain measurements with accelerometer measuring respiration rate, the subject will be required to wear an elastic belt around upper chest or abdomen. Measurements with IR optical tracking system will require a set of retro-reflective markers attached to the surface of the subject's chest. In displacement measurement experiments there will be a non-flexible spring-attached belt including LVDT, or strain gauge which is going to be placed around the chest as well. No personal identifying information will be included with the research results. Before running any experiment the subjects must read and sign consent forms completely. Completion of the form containing background data should take no more than 5 minutes. Measurements may be taken at 900 MHz, 2.4 GHz, and at 5.8 GHz at the distances of 0.5-2 meters in supine and seated positions, with the power levels adjusted to produce the same power incident on the human body. Each subject will be measured from the four sides of the body, and each measurement will take no more than 5 minutes. Each experiment is expected to be no longer than ninety minutes.

The investigators believe there is little risk to subjects participating in this experiment. The radio signal from Doppler radar is the same frequency used in various cellular phones and wireless cards on computers. The power levels of the radio signal used in this experiment is less than of those in consumer electronic devices in compliance with FCC regulations.

Participating in this research may be of no direct benefit to you. It is believed, however, the results from this project will help the biomedical application research better identify

and address the issues with Doppler radar sensing vital signs. The remote sensing of physiological motion could prove a powerful tool for health care monitoring, emergency medical response, and surveillance applications. Such unobtrusive sensing could benefit patients with conditions that may be perturbed or worsened by contact sensors, as when monitoring for sleep disorders and burn victim care.

Research data will be confidential to the extent allowed by law. Agencies with research oversight, such as the UH Committee on Human Studies, have the authority to review research data. All research records will be stripped of any identification and stored on a computer in a locked room in the primary investigator's lab for the duration of the research project.

Participation in this research project is completely voluntary. We appreciate your time and patience. You are free to withdraw from participation at any time during the duration of the project with no penalty, or loss of benefit to which you would otherwise be entitled. There will be no compensation for participating. In the unfortunate event should you be injured during the study, we may not be responsible for the cost of treating your injury.

If you have any questions regarding this research project, please contact the primary investigator, Olga Boric-Lubecke, at (808) 956-9648.

If you have any questions regarding your rights as a research participant, please contact the UH Committee on Human Studies at (808) 956-5007.

Agreement to Participate in
"A Pilot Study of Remote Sensing of Physiological Motion Using Doppler Radar"

Participant:

"I certify that I have read and that I understand the foregoing, that I have been given satisfactory answers to my inquiries concerning project procedures and other matters and that I have been advised that I am free to withdraw my consent and to discontinue participation in the project at any time without prejudice. I understand that if I am injured in the course of this research procedure, I alone may be responsible for the costs of treating my injuries.

I herewith give my consent to participate in this project with the understanding that such consent does not waive any of my legal rights, nor does it release the Principal Investigator or the institution or any employee or agent thereof from liability for negligence."

_____
Name (printed)

_____ _____
Signature Date

CHS #14884 Approval Letter

Office of Research Compliance
Human Studies Program

UNIVERSITY of HAWAI'I® MĀNOA

MEMORANDUM
CR

February 18, 2016

TO: Olga Boric-Lubecke, Ph.D.
Principal Investigator
Electrical Engineering

FROM: Denise A. Lin-DeShetler, MPH, MA
Director

SUBJECT: CHS #14884- "Remote Sensing of Physiological Motion Using Doppler Radar"

Your research project identified above, including the informed consent/privacy authorization form, was approved for one year by the University of Hawaii (UH) Human Studies Program at its IRB meeting on February 17, 2016.

This memorandum is your record of the Human Studies Program approval of this study. Please maintain it with your study records.

The Human Studies Program approval for this project will expire on February 16, 2017. If you expect your project to continue beyond this date, you must submit an application for renewal of this Human Studies Program approval. Human Studies Program approval must be maintained for the entire term of your project.

If, during the course of your project, you intend to make changes to this study, you must obtain approval from the Human Studies Program prior to implementing any changes. If an Unanticipated Problem occurs during the course of the study, you must notify the Human Studies Program within 24 hours of knowledge of the problem. A formal report must be submitted to the Human Studies Program within 10 days. The definition of "Unanticipated Problem" may be found at: http://hawaii.edu/irb/download/documents/SOPP_101_UP_Reporting.pdf, and the report form may be downloaded here: http://hawaii.edu/irb/download/forms/App_UP_Report.doc.

You are required to maintain complete records pertaining to the use of humans as participants in your research. This includes all information or materials conveyed to and received from participants as well as signed consent forms, data, analyses, and results. These records must be maintained for at least three years following project completion or termination, and they are subject to inspection and review by the Human Studies Program and other authorized agencies.

Please notify this office when your project is completed. Upon notification, we will close our files pertaining to your project. Reactivation of the Human Studies Program approval will require a new Human Studies Program application.

Please contact this office if you have any questions or require assistance. We appreciate your cooperation, and wish you success with your research.

1960 East-West Road
Biomedical Sciences Building B104
Honolulu, Hawai'i 96822
Telephone: (808) 956-5007
Fax: (808) 956-8683

Appendix C. Matlab Code

Code #1.

```
%%%%%%%%%%%%%%%%%%%%%%%%%%%%%%%%%%%%%%%%%%%%%%%%%%%%%%%%%%%%%%%%%%%%%%%%
% Radar data processing

% This code processes I/Q channel radar data with circle fitting
method,
% in the purpose of getting the following parameters:
% - Estimated radius error rate R%
% - Estimated displacement error rate D%
% - Displacement profile correlation coefficient to ideal target motion
RR
% Method used:
% LM circle fitting directly applied on original short arc



% Created by Xiaomeng Gao
% UH Manoa
% 2017/02/09 rev.01
%%%%%%%%%%%%%%%%%%%%%%%%%%%%%%%%%%%%%%%%%%%%%%%%%%%%%%%%%%%%%%%%%%%%%%%%
clc;
%close all;
clear all;
%%%%%%%%%%%%%%%%%%%%%%%%%%%%%%%%%%%%%%%%%%%%%%%%%%%%%%%%%%%%%%%%%%%%%%%%
% radar conf and data import
%%%%%%%%%%%%%%%%%%%%%%%%%%%%%%%%%%%%%%%%%%%%%%%%%%%%%%%%%%%%%%%%%%%%%%%%
stamp = 1;
fs=1000;                                            % Sampling frequency
f = 2.4e9;                                          % Carrier frequency
LAMBDA = 3e8/f;                                     % Wavelength at 2.4GHz

% importfile('10dBM_DST2m_G200_10HzLP_DeepAL1.txt');
% importfile('10dBM_DST2m_G200_10HzLP_ShallowAL1.txt');

% importfile('10dBM_DST2m_G200_10HzLP_DeepAL2.txt');
% importfile('10dBM_DST2m_G200_10HzLP_ShallowAL2.txt');
%
% importfile('10dBM_DST2m_G200_10HzLP_DeepAL3.txt');
% importfile('10dBM_DST2m_G200_10HzLP_ShallowAL3.txt');
%
% importfile('10dBM_DST2m_G200_10HzLP_DeepXM3.txt');
% importfile('10dBM_DST2m_G200_10HzLP_ShallowXM3.txt');

% importfile('10dBM_DST2m_G200_10HzLP_DeepXM2.txt');
% importfile('10dBM_DST2m_G200_10HzLP_ShallowXM2.txt');

importfile('10dBM_DST2m_G200_10HzLP_ShallowXM1.txt');
% importfile('10dBM_DST2m_G200_10HzLP_ShallowXM1.txt');



% Bi_ro = data(time*fs:time*fs*2,2);
% Bq_ro = data(time*fs:time*fs*2,4);
Bi_ro = data(10000:end-2000,2);  %4549
```

```
Bq_ro = data(10000:end-2000,4);
% Bi_ro = data(1:end-10000,2);
% Bq_ro = data(1:end-10000,4);
% Bi_ro = data(15000:end,2);
% Bq_ro = data(15000:end,4);

figure;
plot(Bi_ro, Bq_ro,'r');
title('Raw IQ plot of short arcs')
xlabel('I');
ylabel('Q');
axis equal;
grid on;
hold off;
% Bi_r1 = downsample(Bi_r1, 10, 9);
% Bq_r1 = downsample(Bq_r1, 10, 9);
% Bi_r2 = downsample(Bi_r2, 10, 9);
% Bq_r2 = downsample(Bq_r2, 10, 9);
%%%%%%%%%%%%%%%%%%%%%%%%%%%%%%%%%%%%%%%%%%%%%%%%%%%%%%%%%%%%%%%%%%%%%%%%%%%
% Filtering with FIR filter
%%%%%%%%%%%%%%%%%%%%%%%%%%%%%%%%%%%%%%%%%%%%%%%%%%%%%%%%%%%%%%%%%%%%%%%%%%%
Wn=10/(fs/2);                                          % Wn*(sampling
frequency/2)= LPF stop ferq
BI_filtered_o=filtering(Bi_ro, Wn);
BQ_filtered_o=filtering(Bq_ro, Wn);

figure;
plot(BI_filtered_o, BQ_filtered_o,'r');
title('Filtered IQ plot of three arcs')
xlabel('I');
ylabel('Q');
axis equal;
grid on;
hold off;

%% %%%%%%%%%%%%%%%%%%%%%%%%%%%%%%%%%%%%%%%%%%%%%%%%%%%%%%%%%%%%%%%%%%%%%%%%%
% #1 Short arc + LM
%%%%%%%%%%%%%%%%%%%%%%%%%%%%%%%%%%%%%%%%%%%%%%%%%%%%%%%%%%%%%%%%%%%%%%%%%%%
% Imbalance compensation with known imbalance factors
% amp = 0.9654;                                         % Amplitude imbalance
% 3.1, 3.2, 4.1
% phase = 5.3886;                                       % Phase imbalance
% amp = 0.9565;                                         % Amplitude imbalance

%2nd 1 marker tests
amp=1.0186
phase=-16.3223

%13 marker tests
%  amp=1.06113
%  phase=-12.26839

[BI_o, BQ_o] = imbCali(phase, amp, BI_filtered_o, BQ_filtered_o);
result_s = BI_o + sqrt(-1)*BQ_o;
% BI_o = BI_filtered_o;
% BQ_o = BQ_filtered_o;
% result_s = BI_filtered_o + sqrt(-1)*BQ_filtered_o;
```

```
[Ctr_a, Ctr_b, arc_radius] = Circle_Fit_LM_Radius (BI_o,BQ_o);
Short_arc_a = Ctr_a
Short_arc_b = Ctr_b                                % output circle
centers
I_result_o = BI_o - Short_arc_a;
Q_result_o = BQ_o - Short_arc_b;
Radius_short = arc_radius                          % output estimated
radius
result_o = I_result_o + sqrt(-1)*Q_result_o;

% Plotting estimated circle on short arc with its center at origin
th = 0:pi/50:2*pi;
x_origin_est_short = Radius_short * cos(th);
y_origin_est_short = Radius_short * sin(th);
figure;
plot(x_origin_est_short, y_origin_est_short,'k--');
hold on;
plot(I_result_o , Q_result_o,'b');
title('IQ plot of short arc')
xlabel('I');
ylabel('Q');
legend('Estimated circle','Short arc');
axis equal;
grid on;
hold off;

[x_estimate, ave_disp] = Arctangent_demod(result_o,LAMBDA,fs);
Disp_Short_LM_cm = ave_disp*100
% title('Short arc vs. nominal motion (LM on short arc)');
% x_est_1 = x_estimate;
x_est_1 = x_estimate;
time=0:1:(length(x_est_1)-1);
t=time/1000;
x=x_est_1*-1000;
```

Code #2

```
function Par = LM(XY,ParIni,LambdaIni)

%-------------------------------------------------------------------------
----
%
%     Geometric circle fit (minimizing orthogonal distances)
%     based on the standard Levenberg-Marquardt scheme
%        in the full (a,b,R) parameter space
%     This is perhaps the best geometric circle fit
%
%     Input:  XY(n,2) is the array of coordinates of n points
x(i)=XY(i,1), y(i)=XY(i,2)
%             ParIni = [a b R] is the initial guess (supplied by user)
%             LambdaIni is initial value for the correction factor
lambda
%               (this is optional; if it is missing, LM sets it to 1)
%
%     Output: Par = [a b R] is the fitting circle:
%                           center (a,b) and radius R
%
%-------------------------------------------------------------------------
----

if (nargin < 3), LambdaIni = 1; end;  % if Lambda(initial) is not
supplied, set it to one

epsilon=0.000001;    % tolerance (small threshold)

IterMAX = 50;      % maximal number of (main) iterations; usually 10-20
suffice

lambda_sqrt = sqrt(LambdaIni);   %  sqrt(Lambda) is actually used by
the code

Par = ParIni;     % starting with the given initial guess

[J,g,F] = CurrentIteration(Par,XY);    % compute objective function and
its derivatives

for iter=1:IterMAX         %  main loop, each run is one (main)
iteration

    while (1)         %  secondary loop - adjusting Lambda (no limit on
cycles)

        DelPar = [J; lambda_sqrt*eye(3)]\[g; zeros(3,1)];   % step
candidate
        progress = norm(DelPar)/(norm(Par)+epsilon);
        if (progress < epsilon)  break;  end;               % stopping
rule
        ParTemp = Par - DelPar';
        [JTemp,gTemp,FTemp] = CurrentIteration(ParTemp,XY);  %
objective function + derivatives
```

```
        if (FTemp < F && ParTemp(3)>0)        %   yes, improvement
           lambda_sqrt = lambda_sqrt/2;   % reduce lambda, move to next
iteration
           break;
        else                                  %   no improvement
           lambda_sqrt = lambda_sqrt*2; % increase lambda, recompute
the step
           continue;
        end
    end   %   while (1), the end of the secondary loop
%    fprintf(1,'   %d     %.8f   %.8f   %.8f\n',iter,Par);
    if (progress < epsilon)  break;  end;             % stopping rule
    Par = ParTemp;  J = JTemp;  g = gTemp;  F = FTemp;  % update the
iteration
end    %  the end of the main loop (over iterations)
end    %    LM

%================ function CurrentIteration ================

function [J,g,F] = CurrentIteration(Par,XY)

%    computes the objective function F and its derivatives at the
current point Par

Dx = XY(:,1) - Par(1);
Dy = XY(:,2) - Par(2);
D = sqrt(Dx.*Dx + Dy.*Dy);
J = [-Dx./D, -Dy./D,  -ones(size(XY,1),1)];
g = D - Par(3);
F = norm(g)^2;

end  %  CurrentIteration
```

Code #3

```
function output = filtering(input, Wn)

B=fir1(500,Wn);% low pass filter with order 500 and fc=0.02 Hz
output1=filter(B,1,input);


[fdd xx]=grpdelay(B);
fd = length(fdd);
output=output1(fd+1:length(output1),1);

% save('output')

%% Person Product-moment Correlation Coefficient (PMCC)
% determin the PMCC coefficient (correlation coefficient) between two
datasets
function [r_xy]= PMCC_disp(vec1,vec2)

x = vec1;
y = vec2;
% % % figure;
% % % plot(x,'r*');
% % % hold on;
% % % plot(y,'b+');
% % % xlabel('Samples');
% % % ylabel('Displacement [cm]');
% % % title('Displacement comparison between preset and estimation');
% % % legend('predefined movement','estimated movement');
% % % grid on;

% PMCC
ux = mean(x);
uy = mean(y);
n = length(x);
std_x = std(x);
std_y = std(y);

for i=1:length(x)
    rxy_d(i) = (x(i)-ux)*(y(i)-uy);
end
r_xy = sum(rxy_d)/((n-1)*std_x*std_y);

function [rc,phi,k,C]=cest(r)
% CEST      Find center of circle.
%           Input
%           r: complex measured data
%           Output
%  rc=r-k
%  phi=rotated arc angle
%  k=median of center
%  C=covariance matrix

Nmax=3000;

r=r(:); N=length(r);
```

```
% subtract mean
mm=mean(r);%Step 1
r=r-mm;%Step 2

% rotate data to be parallel with y axis
rr=[real(r),imag(r)];
[U,S,V]=svd(rr,'econ');
C=V(1,2)-1i*V(2,2);
r=r*C;%Step 3-rotate data

%estimate center of circle

rx=r(1:min(N,Nmax));
ra=reshape(repmat(rx.',length(rx),1),length(rx)^2,1);
rb=reshape(repmat(rx,length(rx),1),length(rx)^2,1);
idx=find(ra-rb~=0);
s=(abs(ra(idx)).^2-abs(rb(idx)).^2)./real(ra(idx)-rb(idx))/2;%-
estimation of k
% k=median(s);%Step 4.1-get median of k
k=nanmedian(s);
if k>0; % possible mirror image in y-axis
    C=-C;
    r=-r;
    k=-k;
end;

%customerize center value k (Vector Mode)
% k=-0.0127; %5.0cm data
% k=-0.0281; %4.5cm data
% k=-0.0397; %4.0cm data
% k=-0.0713; %3.5cm data
% k=-0.0819; %3.0cm data
% k=-0.0886; %2.5cm data
% k=-0.0932; %2.0cm data
% k=-0.0988; %1.5cm data
% k=-0.1002; %1.0cm data
% k=-0.0986; %0.5cm data



% customerize center value k (Position Tracking)
% k=-0.0021; %5.0cm data
% k=-0.0281; %4.5cm data
% k=-0.0397; %4.0cm data
% k=-0.0175; %3.5cm data
% k=-0.0222; %3.0cm data
% k=-0.0408; %2.5cm data
% k=-0.0334; %2.0cm data
% k=-0.0417; %1.5cm data
% k=-0.0573; %1.0cm data
% k=; %0.5cm data



rc=r-k; %Step4.2-substract k

phi=angle(rc); %calculate angle from rotated arc, but for arctan we
```

```
don't need this info
% save('s_index.mat','s','k','rc','phi')
% figure;plot(s);
%%%%%%%%%%%%%%%%%%%%%%%%%%%%%%%%%%%%%%%%%%%%%%%%%%%%%%%%%%%%%%%%%%%%%%%
%this cest.m estimate the universal parameters for center estimation
%which 1)mean r1, 2)minus mean(r1), 3)multiply C, 4)minus k
%%%%%%%%%%%%%%%%%%%%%%%%%%%%%%%%%%%%%%%%%%%%%%%%%%%%%%%%%%%%%%%%%%%%%%%



%%%%%%%%%%%%%%%%%%%%%%%%%%%%%%%%%%%%%%%%%%%%%%%%%%%%%%%%%%%%%%%%%%%%%%%
% Arctangent demodulation for displacement measurement and correlation
%%%%%%%%%%%%%%%%%%%%%%%%%%%%%%%%%%%%%%%%%%%%%%%%%%%%%%%%%%%%%%%%%%%%%%%

function [x_estimate, ave_disp] = Arctangent_demod(result,LAMBDA,fs);

%%%%%%%%%%%%%%%%%%%%%%%%%%%%%%%%%%%%%%%%%%%%%%%%%%%%%%%%%%%%%%%%%%%%%%%
%%%
% Arctangent function for phase extraction
%%%%%%%%%%%%%%%%%%%%%%%%%%%%%%%%%%%%%%%%%%%%%%%%%%%%%%%%%%%%%%%%%%%%%%%
%%%
output=atan2(imag(result),real(result));%this completes arctangent
demodulation
output_unwrap_signal=unwrap(output);
out2=output_unwrap_signal; % This is what we want for deducing disp

deviation_length = (out2*LAMBDA)/(4*pi); %converting phase to length
% Displacement estimation
t_est =1:length(deviation_length);
x_est = deviation_length-mean(deviation_length);

%%%%%%%%%%%%%%%%%%%%%%%%%%%%%%%%%%%%%%%%%%%%%%%%%%%%%%%%%%%%%%%%%%%%%%%
%%%
% Peak detection and average displacement estimation_adapted from Ehsan
%%%%%%%%%%%%%%%%%%%%%%%%%%%%%%%%%%%%%%%%%%%%%%%%%%%%%%%%%%%%%%%%%%%%%%%
%%%
t1 = 0:(1/fs):(length(x_est)-1)/fs;
x1 = x_est;

figure; plot(t1,x1);grid on;
title('Displacement Estimation with Short Arc')
xlabel('Time [s]')
ylabel('Displacement[m]')
[maxtab, mintab] = peakdet(x1, 0.001, t1);% set threshold
hold on; plot(mintab(:,1), mintab(:,2), 'g*');
plot(maxtab(:,1), maxtab(:,2), 'r*');
ave_max=sum(maxtab(2:end,2))/numel(maxtab(2:end,2));
ave_min=sum(mintab(2:end,2))/numel(mintab(2:end,2));
ave_disp=ave_max-ave_min;
x_estimate = x_est;
% disp_error_rate = abs(ave_disp - Preset_disp_m)/Preset_disp_m*100;

%%%%%%%%%%%%%%%%%%%%%%%%%%%%%%%%%%%%%%%%%%%%%%%%%%%%%%%%%%%%%%%%%%%%%%%
%%%
% Correlation coefficient calculation (PMCC)
%%%%%%%%%%%%%%%%%%%%%%%%%%%%%%%%%%%%%%%%%%%%%%%%%%%%%%%%%%%%%%%%%%%%%%%
%%%
% x_est_trunk = x_est(maxtab(2,1)*1000:end);
```

```
% l_same = min(length(x_est_trunk),length(x_pre));
%
%     x_original = x_pre(1:l_same);
%     x_estimate = x_est_trunk(1:l_same);
%
%
% figure;
% t1 = 0:(1/fs):(l_same-1)/fs;
% plot(t1, x_original,'r');
% hold on;
% plot(t1, x_estimate,'b');
% xlabel('Time [s]');
% ylabel('Amplitude [V]');
% legend('Original Target Motion','Estimated Target Motion');
% title('Comparison of Estimated and Original Target Motion');
% hold off;
% [r_xy]= PMCC_disp(x_original,x_estimate);
% correlation = r_xy;

%%%%%%%%%%%%%%%%%%%%%%%%%%%%%%%%%%%%%%%%%%%%%%%%%%%%%%%%%%%%%%%%%%%%%%%%%%%%%%%
%
% Circle fitting algorithm based on LM method

% Input: I and Q channel data(quadrature data sets)
% Output: Center, Radius
% Create by Xiaomeng Gao, based on Chernov's code
% UH-Manoa
% 11/16/2016
%%%%%%%%%%%%%%%%%%%%%%%%%%%%%%%%%%%%%%%%%%%%%%%%%%%%%%%%%%%%%%%%%%%%%%%%%%%%%%%
%
function [Ctr_a, Ctr_b, arc_radius] = Circle_Fit_LM_Radius (I2,Q2)
%LM method
% [Ir, Qr] = rotate(I2'+ sqrt(-1)*Q2');  % rotate
XY(:,1) = I2;
XY(:,2) = Q2;
xdata = I2;
ydata = Q2;
a = mean(xdata);
b = mean(ydata);
R = 1./length(xdata) .* sum( sqrt( (xdata-a).^2 + (ydata-b).^2 ) );
ParIni = [a b R];
LambdaIni = 1;
Par  = LM(XY,ParIni,LambdaIni);
a = Par(1);
b = Par(2);
r = Par(3);

arc_radius = r;
Ctr_a = a;
Ctr_b = b;
```

Code #4

```
function [I2, Q2] = imbCali(phase, amp, I1, Q1)
% I1=real(r1);% New denotation for filter IQ data
% Q1=imag(r1);

phie = (real(phase)/180)*pi;%for phase imbalance it's always RADIAN in
calculation
% but the phase_imb output is in degree
Ae = real(amp);


orig =[I1;Q1];
conv=[1 0;-tan(phie) 1/(Ae*cos(phie))];
for j=1:length(I1);
    I2(j)=I1(j);
    Q2(j) =-1*tan(phie)*I1(j)+Q1(j)/(Ae*cos(phie));
end

% r2 = I2+ sqrt(-1)*Q2;

save('I2', 'Q2')

clc
clear all

%% __Importing data from drf file


%Importing data

%fileID = fopen('normal_13marker_2.drf');

%Read data into sepereate cells
        %[1 marker/s]
%             C = textscan(fileID,'%*s %*s %*s %7*s %s %s %7s');

        %[13 marker/s normal_2]
            %C = textscan(fileID,'%*s %*s %*s %7*s %s %s %5s %*s %*s
%7*s %s %s %6s %*s %*s %7*s %s %s %5s %*s %*s %7*s %s %s %5s %*s %*s
%7*s %s %s %5s %*s %*s %7*s %s %s %5s %*s %*s %7*s %s %s %6s %*s %*s
%7*s %s %s %6s %*s %*s %7*s %s %s %6s %*s %*s %7*s %s %s %6s %*s %*s
%7*s %s %s %6s %*s %*s %7*s %s %s %6s %*s %*s %7*s %s %s %6s');
                                  %-------------------------%----------
-----------%----------------------%----------------------%----------
----------%----------------------%----------------------%-------------
--------%----------------------%----------------------%---------------
------%----------------------%----------------------%


%           % 'normal_13marker_3.drf'
%                       fileID = fopen('normal_13marker_3.drf');
%                       C = textscan(fileID,'%*s %*s %*s %7*s %s %s %6s
%*s %*s %7*s %s %s %6s %*s %*s %7*s %s %s %5s %*s %*s %7*s %s %s %7s
%*s %*s %7*s %s %s %5s %*s %*s %7*s %s %s %6s %*s %*s %7*s %s %s %6s
%*s %*s %7*s %s %s %7s %*s %*s %7*s %s %s %6s %*s %*s %7*s %s %s %6s
```

```
%*s %*s %7*s %s %s %6s %*s %*s %7*s %s %s %6s %*s %*s %7*s %s %s %6s');
%

%           % 'deep_13marker_3.drf'
%                       fileID = fopen('deep_13marker_3.drf');
%                       C = textscan(fileID,'%*s %*s %*s %7*s %s %s %6s
%*s %*s %7*s %s %s %6s %*s %*s %7*s %s %s %5s %*s %*s %7*s %s %s %7s
%*s %*s %7*s %s %s %5s %*s %*s %7*s %s %s %6s %*s %*s %7*s %s %s %6s
%*s %*s %7*s %s %s %7s %*s %*s %7*s %s %s %6s %*s %*s %7*s %s %s %6s
%*s %*s %7*s %s %s %6s %*s %*s %7*s %s %s %6s %*s %*s %7*s %s %s %6s');
%

%           % 'normal_13marker_2.drf'
%                     fileID = fopen('normal_13marker_2.drf');
%                     C = textscan(fileID,'%*s %*s %*s %7*s %s %s %5s
%*s %*s %7*s %s %s %6s %*s %*s %7*s %s %s %5s %*s %*s %7*s %s %s %5s
%*s %*s %7*s %s %s %5s %*s %*s %7*s %s %s %5s %*s %*s %7*s %s %s %6s
%*s %*s %7*s %s %s %6s %*s %*s %7*s %s %s %6s %*s %*s %7*s %s %s %6s
%*s %*s %7*s %s %s %6s %*s %*s %7*s %s %s %6s %*s %*s %7*s %s %s %6s');


%           % 'deep_13marker_2.drf'
%
%                     fileID = fopen('deep_13marker_2.drf');
%                   C = textscan(fileID,'%*s %*s %*s %7*s %s %s %5s %*s
%*s %7*s %s %s %6s %*s %*s %7*s %s %s %5s %*s %*s %7*s %s %s %6s %*s
%*s %7*s %s %s %5s %*s %*s %7*s %s %s %5s %*s %*s %7*s %s %s %6s %*s
%*s %7*s %s %s %6s %*s %*s %7*s %s %s %6s %*s %*s %7*s %s %s %6s %*s
%*s %7*s %s %s %6s %*s %*s %7*s %s %s %6s %*s %*s %7*s %s %s %6s');


%             % 'normal_13marker_1.drf'
%                       fileID = fopen('normal_13marker_1.drf');
%                       C = textscan(fileID,'%*s %*s %*s %7*s %s %s %6s
%*s %*s %7*s %s %s %6s %*s %*s %7*s %s %s %5s %*s %*s %7*s %s %s %6s
%*s %*s %7*s %s %s %5s %*s %*s %7*s %s %s %5s %*s %*s %7*s %s %s %6s
%*s %*s %7*s %s %s %6s %*s %*s %7*s %s %s %6s %*s %*s %7*s %s %s %6s
%*s %*s %7*s %s %s %6s %*s %*s %7*s %s %s %6s %*s %*s %7*s %s %s %6s');
%




           % 'deep_13marker_1.drf'
                     fileID = fopen('deep_13marker_1.drf');
                     C = textscan(fileID,'%*s %*s %*s %7*s %s %s %6s
%*s %*s %7*s %s %s %6s %*s %*s %7*s %s %s %5s %*s %*s %7*s %s %s %7s
%*s %*s %7*s %s %s %5s %*s %*s %7*s %s %s %5s %*s %*s %7*s %s %s %6s
%*s %*s %7*s %s %s %7s %*s %*s %7*s %s %s %6s %*s %*s %7*s %s %s %6s
%*s %*s %7*s %s %s %6s %*s %*s %7*s %s %s %6s %*s %*s %7*s %s %s %6s');



%number of markers
num_markers = 13;
% num_markers = 1;
```

```
% % %% __Extracting cell and converting to num type
% %     i = 1;
% %     for i = 1:1:(num_markers*3);
% %         X(:,1) = str2num(cell2mat(C{1,i}));
% %         Y(:,1) = str2num(cell2mat(C{1,i+1}));
% %         Z(:,1) = str2num(cell2mat(C{1,i+2}));
% %     i = i+1;
% %     end
% %
% % %
% __Extracting cell and converting to num type_JR_EE496
    n = 1;
    for i = 1:3:(num_markers*3);
        X(:,n) = str2num(cell2mat(C{1,i}(1614:4:end,1)));
        Y(:,n) = str2num(char(C{1,i+1}(1614:4:end,1)));
        Z(:,n) = str2num(cell2mat(C{1,i+2}(1614:4:end,1)));
    n = n+1;
    end

%% Creating time vector normalized to the amount of data points taken
persecond
    format long

% !!!!!!!!!!MUST CHANGE VALUES MANUALY!!!!!
% test_time = (76461.281100-76430.734809);
%
%     length_x = length(X(:,1)); % number of data points taken
%         data_per_sec = length_x/test_time; % amount of data taken per
second
%     time = 0:1:(length_x-1); % dt = unit
%
%     t = (time/data_per_sec)'; % final time vector normalized to
amount of data taken per second

%% 2D plots of marker movement vs time

    % Centering amplitude data at 0
    n = 1;
    for i = 1:num_markers;
            XYZ_2dplot(:,n) = X(:,i) - mean(X(:,i));
            XYZ_2dplot(:,n+1) = Y(:,i) - mean(Y(:,i));
            XYZ_2dplot(:,n+2) = Z(:,i) - mean(Z(:,i));
    n = n+3;
    end

    % graphing XYZ movement of each marker (seperate figures)
    n = 1;
    for i = 1:3:3*num_markers
        figure(2);
        Yplot(:,n)=XYZ_2dplot(:,i+1);
        %plot(t,XYZ_2dplot(:,i:i+2));
            ylabel('Distance (mm)');
            xlabel('time (sec)');
            %legend('x_plot','Y_plot','Z_plot');
            n = n+1;
```

```
    end
    Yplot=Yplot(end-282:end,1:13);  %120:end-303
    time=0:1:length(Yplot)-1;
    t=time/60;
    plot(t,Yplot(:,1:13));
    ylabel('Distance (mm)');
    xlabel('time (sec)');

        %   figure(1),plot(t,XYZ_2dplot(:,1:3)),ylabel('Distance
(mm)'),xlabel('time (sec)'),title('MARKER
1'),legend('x_plot','Y_plot','Z_plot','XYZ_plot')
        %   figure(2),plot(t,XYZ_2dplot(:,4:6)),ylabel('Distance
(mm)'),xlabel('time (sec)'),title('MARKER
2'),legend('x_plot','Y_plot','Z_plot','XYZ_plot')
        %   figure(3),plot(t,XYZ_2dplot(:,7:9)),ylabel('Distance
(mm)'),xlabel('time (sec)'),title('MARKER
3'),legend('x_plot','Y_plot','Z_plot','XYZ_plot')
        %   figure(4),plot(t,XYZ_2dplot(:,10:12)),ylabel('Distance
(mm)'),xlabel('time (sec)'),title('MARKER
4'),legend('x_plot','Y_plot','Z_plot','XYZ_plot')
        %   figure(5),plot(t,XYZ_2dplot(:,13:15)),ylabel('Distance
(mm)'),xlabel('time (sec)'),title('MARKER
5'),legend('x_plot','Y_plot','Z_plot','XYZ_plot')
        %   figure(6),plot(t,XYZ_2dplot(:,16:18)),ylabel('Distance
(mm)'),xlabel('time (sec)'),title('MARKER
5'),legend('x_plot','Y_plot','Z_plot','XYZ_plot')
%% total marker displacement calculation (avg. precision)
    % detects maxs and mins, finds the mean of maxs and mins
    % finds displacement in each coordinate and total displacement
    for i = 1:1:3*num_markers;

[max min] = peakdet(XYZ_2dplot(:,i),0.5);
            x_max_avg_mm = mean(max(2:length(max)-1,2));
            x_min_avg_mm = mean(min(2:length(min)-1,2));
        total_x_displacement_mm = x_max_avg_mm - x_min_avg_mm;

[max min] = peakdet(XYZ_2dplot(:,i+1),2);
            Y_max_avg_mm = mean(max(2:length(max)-1,2));
            Y_min_avg_mm = mean(min(2:length(min)-1,2));
        total_Y_displacement_mm = Y_max_avg_mm - Y_min_avg_mm;

[max min] = peakdet(XYZ_2dplot(:,i+2),2);
            Z_max_avg_mm = mean(max(2:length(max)-1,2));
            Z_min_avg_mm = mean(min(2:length(min)-1,2));
        total_Z_displacement_mm = Z_max_avg_mm - Z_min_avg_mm;
    end
    total_XYZ_displacement_marker = sqrt((total_Y_displacement_mm)^2 +
(total_x_displacement_mm)^2 + (total_Z_displacement_mm)^2);

%% 3D plotting with the marker1 pinned down

    % "test3_6mark_jas.drf" markers track weirdly, I don't know why
    % A1 = X(:,1); B1 = Y(:,1); C1 = Z(:,1); X1 = X(:,6); Y1 = Y(:,6);
Z1 = Z(:,6); X6 = X(:,4); Y6 = Y(:,4); Z6 = Z(:,4); % X4 = X(:,3); Y4 =
Y(:,3); Z4 = Z(:,3); X3 = X(:,5); Y3 = Y(:,5); Z3 = Z(:,5); X5 = A1, Y5
= B1, Z5 = C1
    % X10 = X1; Y10 = Y1; Z10 = Z1; X1 = X1 - X10; Y1 = Y1 - Y10; Z1 =
```

```
Z1 - Z10; X2 = X(:,2) - X10; Y2 = Y(:,2) - Y10; Z2 = Z(:,2) - Z10; X3 =
X3 - X10; Y3 = Y3 - Y10; Z3 = Z3 - Z10; X4 = X4 - X10; Y4 = Y4 - Y10;
Z4 = Z4 - Z10; X5 = X5 - X10; Y5 = Y5 - Y10; Z5 = Z5 - Z10; X6 = X6 -
X10; Y6 = Y6 - Y10; Z6 = Z6 - Z10;

    % pinning the model down at marker 1.
    X10 = X(:,1);
    Y10 = Y(:,1);
    Z10 = Z(:,1);
        for i = 1:6
            X_0(:,i) = X(:,i) - X10;
            Y_0(:,i) = Y(:,i) - Y10;
            Z_0(:,i) = Z(:,i) - Z10;
        end
    % 3D plotting for easier visualization
    figure(1)
    plot3(X_0(:,1:6),Y_0(:,1:6),Z_0(:,1:6))
        xlabel('X');
        ylabel('Y');
        zlabel('Z');
        title('3D-plot of markers');

,legend('Marker_1','Marker_2','Marker_3','Marker_4','Marker_5','Marker_
6'),axis equal,grid on

    % calculating the angle of displacement (needs to be redone)
        for i = 2:6
            angle_a(:,i) = atand(Z_0(:,i)./Y_0(:,i));
            angle_b(:,i) = angle_a(:,i) - mean(angle_a(:,i));
        end
    figure(2),plot(t,angle_a(:,2:6))
        ,xlabel('Time (s)'),ylabel('Angle of Displacement (deg)')
        ,legend('Marker_2','Marker_3','Marker_4','Marker_5','Marker_6')
        ,title('Angle of Displacement')
    figure(3),plot(t,angle_b(:,2:6))
        ,xlabel('Time (s)'),ylabel('Angle of Displacement (deg)')
        ,legend('Marker_2','Marker_3','Marker_4','Marker_5','Marker_6')
        ,title('Angle of Displacement')


%IR Marker Segmentation Code

clc
clear all
%close all

%           % 'normal_13marker_3.drf'
%                       fileID = fopen('normal_13marker_3.drf');
%                       C = textscan(fileID,'%*s %*s %*s %7*s %s %s %6s
%*s %*s %7*s %s %s %6s %*s %*s %7*s %s %s %5s %*s %*s %7*s %s %s %7s
%*s %*s %7*s %s %s %5s %*s %*s %7*s %s %s %6s %*s %*s %7*s %s %s %6s
%*s %*s %7*s %s %s %7s %*s %*s %7*s %s %s %6s %*s %*s %7*s %s %s %6s
%*s %*s %7*s %s %s %6s %*s %*s %7*s %s %s %6s %*s %*s %7*s %s %s %6s');
%

%           % 'deep_13marker_3.drf'
%                       fileID = fopen('deep_13marker_3.drf');
```

```
%                        C = textscan(fileID,'%*s %*s %*s %7*s %s %s %6s
%*s %*s %7*s %s %s %6s %*s %*s %7*s %s %s %5s %*s %*s %7*s %s %s %7s
%*s %*s %7*s %s %s %5s %*s %*s %7*s %s %s %6s %*s %*s %7*s %s %s %6s
%*s %*s %7*s %s %s %7s %*s %*s %7*s %s %s %6s %*s %*s %7*s %s %s %6s
%*s %*s %7*s %s %s %6s %*s %*s %7*s %s %s %6s %*s %*s %7*s %s %s %6s');
%

%           % 'normal_13marker_2.drf'
%                     fileID = fopen('normal_13marker_2.drf');
%                     C = textscan(fileID,'%*s %*s %*s %7*s %s %s %5s
%*s %*s %7*s %s %s %6s %*s %*s %7*s %s %s %5s %*s %*s %7*s %s %s %5s
%*s %*s %7*s %s %s %5s %*s %*s %7*s %s %s %5s %*s %*s %7*s %s %s %6s
%*s %*s %7*s %s %s %6s %*s %*s %7*s %s %s %6s %*s %*s %7*s %s %s %6s
%*s %*s %7*s %s %s %6s %*s %*s %7*s %s %s %6s %*s %*s %7*s %s %s %6s');


%           % 'deep_13marker_2.drf'
%
%                     fileID = fopen('deep_13marker_2.drf');
%                   C = textscan(fileID,'%*s %*s %*s %7*s %s %s %5s %*s
%*s %7*s %s %s %6s %*s %*s %7*s %s %s %5s %*s %*s %7*s %s %s %6s %*s
%*s %7*s %s %s %5s %*s %*s %7*s %s %s %5s %*s %*s %7*s %s %s %6s %*s
%*s %7*s %s %s %6s %*s %*s %7*s %s %s %6s %*s %*s %7*s %s %s %6s %*s
%*s %7*s %s %s %6s %*s %*s %7*s %s %s %6s %*s %*s %7*s %s %s %6s');


           % 'normal_13marker_1.drf'
%                      fileID = fopen('normal_13marker_1.drf');
%                      C = textscan(fileID,'%*s %*s %*s %7*s %s %s %6s
%*s %*s %7*s %s %s %6s %*s %*s %7*s %s %s %5s %*s %*s %7*s %s %s %6s
%*s %*s %7*s %s %s %5s %*s %*s %7*s %s %s %5s %*s %*s %7*s %s %s %6s
%*s %*s %7*s %s %s %6s %*s %*s %7*s %s %s %6s %*s %*s %7*s %s %s %6s
%*s %*s %7*s %s %s %6s %*s %*s %7*s %s %s %6s %*s %*s %7*s %s %s %6s');
%




%             % 'deep_13marker_1.drf'
                    fileID = fopen('deep_13marker_1.drf');
                    C = textscan(fileID,'%*s %*s %*s %7*s %s %s %6s
%*s %*s %7*s %s %s %6s %*s %*s %7*s %s %s %5s %*s %*s %7*s %s %s %7s
%*s %*s %7*s %s %s %5s %*s %*s %7*s %s %s %5s %*s %*s %7*s %s %s %6s
%*s %*s %7*s %s %s %7s %*s %*s %7*s %s %s %6s %*s %*s %7*s %s %s %6s
%*s %*s %7*s %s %s %6s %*s %*s %7*s %s %s %6s %*s %*s %7*s %s %s %6s');
num_markers = 13;
fs=60;
n = 1;
    for i = 1:3:(num_markers*3);
        X(:,n) = str2num(cell2mat(C{1,i}(1614:4:end,1)));
        Y(:,n) = str2num(char(C{1,i+1}(1614:4:end,1)));
        Z(:,n) = str2num(cell2mat(C{1,i+2}(1614:4:end,1)));
    n = n+1;
    end

    format long
```

```
n = 1;
    for i = 1:num_markers;
            XYZ_2dplot(:,n) = X(:,i) - mean(X(:,i));
            XYZ_2dplot(:,n+1) = Y(:,i) - mean(Y(:,i));
            XYZ_2dplot(:,n+2) = Z(:,i) - mean(Z(:,i));
    n = n+3;
    end

n = 1;
    for i = 1:3:3*num_markers

        Yplot(:,n)=XYZ_2dplot(:,i+1);
            n = n+1;
    end
%     Test 1 Deep
    start=120;
    segment=330;
%     Test 1 Normal
%         start=120;
%         segment=180;
    for i=1:10

    Yplott=Yplot(start:start+(segment-1),1:13);  %120:end-303
    time=0:1:length(Yplott)-1;
    t=time/60;
    figure(i)
    plot(t,Yplott(:,12));
    ylabel('Distance (mm)');
    xlabel('time (sec)');
    hold on
    plot(t,Yplott(:,3),'g');
    hold off
    t1 = 0:(1/fs):(length(Yplott)-1)/fs;
    y12 = Yplott(:,12);
    y3 = Yplott(:,3);

    [maxtab,mintab]=peakdet(y12,0.001,t1);
    IRdisp(1,i)=max(maxtab(:,2))-min(mintab(:,2));

    figure(i);
    hold on

    [min12,minloc12]=min(mintab);
    plot(mintab(minloc12(1,2),1),min12(1,2),'r*');
    [max12,maxloc12]=max(maxtab);
    plot(maxtab(maxloc12(1,2),1),max12(1,2),'g*');

    [maxtab2,mintab2]=peakdet(y3,0.001,t1);
    IRdisp(2,i)=max(maxtab2(:,2))-min(mintab2(:,2));

    [min3,minloc3]=min(mintab2);
    plot(mintab2(minloc3(1,2),1),min3(1,2),'r*');
    [max3,maxloc3]=max(maxtab2);
    plot(maxtab2(maxloc3(1,2),1),max3(1,2),'g*');
    hold off
```

```
    start=start+segment;
    end


%Calculating Contribution of RCS from Two Areas
clc
clear all
syms A1 A2

q1=2.649;  %In Radians
q2=0.9565;
q3=1.912;
B=0.07748;

A2=B*(sin(q1-q3))/(sin(q1-q2))
A1=-B*(sin(q2-q3))/(sin(q1-q2))
```

References

[1] Prathyusha, B., T. Sreekanth Rao, and D. Asha. "Extraction of respiratory rate from ppg signals using pca and emd." *International Journal of Research in Engineering and Technology* 1.2 (2012): 164---184

[2] Cernat, Roxana Alexandra, et al. "Real---time extraction of the respiratory rate from photoplethysmographic signals using wearable devices." (2014).

[3] Murphy, J., G. Manoharan, and A. A. J. Adgey. "EFFECT OF RESPIRATION ON PULSE WAVE VELOCITY MEASUREMENTS IN THE ARM: PP. 8.314."Journal *of Hypertension* 28 (2010): e144

[4] Yamada, Shuhei, Olga Boric-Lubecke, and Victor M. Lubecke. "Cancellation techniques for LO leakage and dc offset in direct conversion systems."*Microwave Symposium Digest, 2008 IEEE MTT-S International*. IEEE, 2008.

[5] Huang, Xinping, and Mario Caron. "Gain/phase imbalance and DC offset compensation in quadrature modulators." *Circuits and Systems, 2002. ISCAS 2002. IEEE International Symposium on*. Vol. 4. IEEE, 2002.

[6] Gu, Changzhan, et al. "Doppler radar vital sign detection with random body movement cancellation based on adaptive phase compensation." *Microwave Symposium Digest (IMS), 2013 IEEE MTT-S International*. IEEE, 2013.

[7] Gu, Changzhan, et al. "A hybrid radar-camera sensing system with phase compensation for random body movement cancellation in Doppler vital sign detection." *IEEE Transactions on Microwave Theory and Techniques* 61.12 (2013): 4678-4688.

[8] Lee, Yee Siong, and Pubudu N. Pathirana. "Motion artefact separation in single channel Doppler radar respiration measurement." *Bioelectronics and Bioinformatics (ISBB), 2015 International Symposium on*. IEEE, 2015.

[9] Ren, Lingyun, et al. "Noncontact multiple heartbeats detection and subject localization using UWB impulse Doppler radar." *IEEE Microwave and Wireless Components Letters* 25.10 (2015): 690-692.

[10] Li, Yiran, Ranadip Pal, and Changzhi Li. "Non-contact multi-radar smart probing of body orientation based on micro-Doppler signatures." *Engineering in Medicine and Biology Society (EMBC), 2014 36th Annual International Conference of the IEEE*. IEEE, 2014.

[11] Kiriazi, John E., Olga Boric-Lubecke, and Victor M. Lubecke. "Radar cross section of human cardiopulmonary activity for recumbent subject."*Engineering in Medicine and Biology Society, 2009. EMBC 2009. Annual International Conference of the IEEE*. IEEE, 2009.

[12] Rahman, Ashikur, et al. "Noncontact Doppler radar unique identification system using neural network classifier on life signs." *Biomedical Wireless Technologies, Networks, and Sensing Systems (BioWireleSS), 2016 IEEE Topical Conference on*. IEEE, 2016.

[13] Atalay, Ozgur, and William Richard Kennon. "Knitted strain sensors: impact of design parameters on sensing properties." *Sensors* 14.3 (2014): 4712-4730.

[14] Trung, Tran Quang, and Nae-Eung Lee. "Flexible and Stretchable Physical Sensor Integrated Platforms for Wearable Human-Activity Monitoring and Personal Healthcare." *Advanced materials* (2016).

[15]Marani, Roberto, Gennaro Gelao, and Anna Gina Perri. "A New system for continuous monitoring of breathing and kinetic activity." *Journal of Sensors* 2010 (2010).

[16] Li, Changzhi, et al. "A review on recent advances in Doppler radar sensors for noncontact healthcare monitoring." *IEEE Transactions on microwave theory and techniques* 61.5 (2013): 2046-2060.

[17] Xu, Jia, et al. "Estimation of physiological sub-millimeter displacement with CW Doppler radar." *Engineering in Medicine and Biology Society (EMBC), 2015 37th Annual International Conference of the IEEE*. IEEE, 2015.

[18] Gao, Xiaomeng, and Olga Boric-Lubecke. "Radius Correction Technique for Doppler Radar Noncontact Periodic Displacement Measurement." *IEEE Transactions on Microwave Theory and Techniques* (2016).

[19] Piuzzi, Emanuele, et al. "Complex radar cross section measurements of the human body for breath activity monitoring applications." *IEEE Transactions on Instrumentation and Measurement* 64.8 (2015): 2247-2258.

[20] Cavagnaro, Marta, Erika Pittella, and Stefano Pisa. "Numerical Evaluation of the Radar Cross Section of Human Breathing Models." *Applied Computational Electromagnetics Society Journal* 30.12 (2015).

[21] Kiriazi, John E., Olga Boric-Lubecke, and Victor M. Lubecke. "Radar cross section of human cardiopulmonary activity for recumbent subject."*Engineering in Medicine and Biology Society, 2009. EMBC 2009. Annual International Conference of the IEEE*. IEEE, 2009.

[22] J.E. Kiriazi, “Human Cardiopulmonary Recognition Using Close-range Doppler Radar,” Ph.D. dissertation, Dept. Elect. Eng., Univ. of Hawaii, Honolulu, HI, 2010.
[23] Yeo, Joo Chuan, and Chwee Teck Lim. "Emerging flexible and wearable physical sensing platforms for healthcare and biomedical applications."*Microsystems & Nanoengineering* 2 (2016): 16043.
[24] Wikipedia contributors. "Conductive elastomer." *Wikipedia, The Free Encyclopedia*. Wikipedia, The Free Encyclopedia, 3 Dec. 2016. Web. 17 Mar. 2017.
[25] Murphy, J., G. Manoharan, and A. A. J. Adgey. "EFFECT OF RESPIRATION ON PULSE WAVE VELOCITYMEASUREMENTS IN THE ARM: PP. 8.314."Journal *of Hypertension* 28 (2010): e144